CHEMICAL REVIEWS

REVIEW

pubs.acs.org/CR

Hybrid Resonant Organic–Inorganic Nanostructures for Optoelectronic Applications

V. M. Agranovich,[*,†,‡] Yu. N. Gartstein,[§] and M. Litinskaya[‡,∥]

[†]NanoTech Institute, Chemistry Department, The University of Texas at Dallas, Richardson, Texas 75083, United States
[‡]Institute of Spectroscopy, Russian Academy of Science, Troitsk, Moscow Region 142190, Russia
[§]Department of Physics, The University of Texas at Dallas, P.O. Box 830688, EC36, Richardson, Texas 75083, United States
[∥]Department of Chemistry, University of British Columbia, Vancouver, British Columbia V6T 1Z1, Canada

CONTENTS

1. INTRODUCTION

The majority of modern commercial optoelectronic devices (such as LEDs, solar cells, and nonlinear-optical devices) are built on the basis of traditional inorganic semiconductors. Over the last couple of decades, however, a lot of progress has been made in producing devices based on organic electronic materials, which, for many applications, may become less expensive

Received: May 22, 2010
Published: July 25, 2011

   dx.doi.org/10.1021/cr100156x | *Chem. Rev.* 2011, 111, 5179–5214

alternatives to inorganic counterparts. Various organic compounds (such as small molecules, conjugated polymers, carbon nanotubes) have been shown to be of high interest and utility in electronic applications. Advances have been reported on a variety of device types: from OLEDs to organic lasers (see, e.g., refs 1−3), to devices of nonlinear optics, molecular-scale transistors, etc. Especially impressive have been successes in organic LED development, making them a real player in a commercial arena.

The current development prospects of organic materials are however mostly limited in their scope to relatively low-performance areas. One of the reasons for this is, for instance, a low mobility of charge carriers in molecular materials. Already in early studies of Pope et al.[4] on organic electroluminescence, it was established that this process requires the injection of electrons from one electrode and holes from the other, transport of one or both charges, capture of oppositely charged carriers on the same molecule (or recombination center), and radiative decay of the resulting excited electron−hole state. For inorganic semiconductors, where the recombining electron−hole state may be a Wannier−Mott exciton, all of the above-mentioned processes are investigated and well documented.[5] In organic materials, one can be faced with many problems in the use of electroluminescence to make devices conceptually similar to what has been done with inorganic semiconductor materials. Besides low mobilities of charge carriers, frequently also manifest are strong chemical interactions between organic molecules and metal electrodes, which can suppress the injection of carriers into organic materials. Because of the low mobility of charge carriers in organic materials, the current can also be bulk-limited, principally through the built-up of a space charge.

A qualitatively different way of using organic electronic compounds can be via exploiting resonant interactions in organic−inorganic hybrid structures.[6−8] In this work, we will review some optoelectronic properties of hybrid organic−inorganic nanostructures consisting of inorganic and organic semiconductor components possessing nearly equal energies (hence "resonant") of neutral electronic excitations (excitons). We will argue that such structures with properly selected materials for organic and inorganic components may find a suitable place in the development of organics-based material science. They are interesting from the point of view of basic science as well as for applications in optoelectronics. Within the same hybrid structure, one could combine high conductivity of the inorganic semiconductor component (important for electrical pumping) with the strong light−matter interaction of the organic component. In this way, the desirable properties of both the organic and the inorganic materials can be synergistically exploited to overcome their limitations when used separately. The resonant coupling between Frenkel excitons of the organic molecules and Wannier−Mott excitons of the inorganic semiconductor may lead, in hybrid structures, to simultaneously high oscillator strength typical of many organic materials and enhanced optical nonlinearity typical of inorganic semiconductor quantum wells. Very important for applications can be efficient nonradiative Förster energy transfer between inorganic quantum wells and organic materials. These effects could make resonant hybrid nanocomposites a versatile platform for the development of a variety of devices, such as in light-emitting, photovoltaic, nonlinear-optical, and sensing applications. Quoting from ref 9, "In the future, the combination of both materials systems will allow the rules that apply to matter and light to be further stretched, potentially seeding a new paradigm in optoelectronic devices." This sentiment substantiated by already obtained experimental data calls for an intense research effort. Theoretical and experimental work that has been done in support of the ideas around resonant heterostructures suggests that judicious combinations of organic and inorganic materials could likely lead to both qualitatively new physical effects and new devices on their basis. A growing realization of the promise offered by this area of research is reflected in the appearance of dedicated funding initiatives, including a recent call from the European Commission on "Organic-inorganic hybrids for electronics and photonics". Such programs are expected to stimulate further advances in the study of this class of nanomaterials.

1.1. Strong and Weak Coupling Regimes in Hybrid Nanostructures

The manifestations of the resonance interaction of excited states of the system components are significantly affected by the dissipation of these states. At the resonance of two states, a familiar quantum-mechanical mixing and energy level splitting can actually take place only if the dissipative widths of these resonating states are smaller than the magnitude of the energy splitting. This limiting case of the strong-coupling regime in the hybrid structures has been the subject of consideration in ref 6. As a result of the strong coupling of excitations in the components of the hybrid system, hybrid Frenkel−Wannier−Mott excitons can be formed whose unusual properties may lead to new effects. A striking example of such an effect is a strong enhancement of the resonance all-optical nonlinearity that can be exhibited by hybrid excitations. This nonlinearity would be principally limited[10] in either class of materials but can be increased by 2 orders of magnitude due to hybrid excitations.[11]

In organic materials, however, the dissipative width of excited electronic states is frequently large, and the opposite limiting case of the weak coupling is more typical. In the weak-coupling regime, the interaction of the components results in nonradiative energy transfer between them. It was particularly found[7,12] that this nonradiative excitation energy transfer from an inorganic quantum well (QW) to organic materials can be very fast and efficient. For this reason, weakly coupled hybrid structures have been suggested to be used as a conceptual basis for novel light emitting devices, where the electrical pumping of excitations in the semiconductor QW would efficiently turn on the organic material luminescence.[7,13] Such devices could exploit organic materials with a high photoluminescence yield across the visible spectrum.[14] In fact, the high rate of energy transfer from QWs to organics might diminish the role of defects and surface states in QWs that would otherwise be responsible for small quantum yield of the stand-alone QW fluorescence.

It is interesting to note that already in 1997 two different groups[15,16] proposed and built GaN-based "hybrid" light-emitting diodes where the organic thin-film part and GaN semiconductor layer are spatially separated and where the organic thin-film radiates after absorbing the electroluminescence of the GaN semiconductor layer. In those devices, however, the spatial separations between the components were large enough for energy transfer pumping the organic material to be radiative rather than nonradiative as discussed above. Using AlInGaN materials, various light-emitting diodes based on radiative energy transfer were produced. A detailed comparison of different light emitting devices using either radiative energy transfer through reabsorption of the electroluminescence of a GaN semiconductor

layer or contact nonradiative Förster-like energy transfer from inorganic QWs to organics can be found in ref 17. As one should expect, with the same components in a nanostructure, radiative energy transfer is generally much less efficient than nonradiative Förster transfer.[9,18]

Hybrid heterostructures can also be created in microcavity configurations,[8] including microcavities with spatially separated organic and inorganic components. In microcavities with an embedded organic material having a large excitonic oscillator strength, cavity photons strongly interact with excitons forming cavity polaritons, which may exhibit a large gap (the polariton splitting) in their spectrum. As discussed in section 3, this modification of the spectrum leads to significant changes in the kinetics of relaxation and luminescence and modifies the conditions of polariton−polariton scattering, bimolecular quenching, typical for excitons in organics, and condensation. The studies of organic microcavities are driven, as stressed in ref 19, by the potential for revolutionary optoelectronic devices such as ultrafast optical amplifiers and switches, structures with enhanced nonlinear optical properties, and coherent polariton light emitters, known as polariton lasers. While being very important, the wide knowledge accumulated in the field of polaritons in inorganic materials cannot be directly transferred to the case of organic systems. Organic materials exhibit small-radius Frenkel excitons, which typically interact much stronger with phonons and disorder. The spectrum of excitations in organic microcavities may show substantially different properties, and, as a result, some processes with the participation of exciton-polaritons in organic cavities may differ even qualitatively from the corresponding processes in inorganic semiconductors.

In this work, we review both stand-alone hybrid nanostructures and structures in microcavity configuration. We focus mostly on important qualitative features of hybrid structures and recent experimental studies of various resonant hybrids. As the theory of hybrid structures involves notions and approaches developed for both organic and inorganic materials, some discussion of the corresponding basics is provided. This discussion is however understandably limited; we go into more technical detail when we feel this would benefit prospective readers with different backgrounds. This particularly concerns the case of structures in microcavities. Extended theoretical treatments available, for example, in refs 20−22 should also be helpful.

1.2. Excitons in Inorganic and Organic Materials

Before proceeding with the physical properties of hybrid structures and their excitations, it is useful to briefly recall some features of excitons in organic and inorganic materials. Neutral electronic excitations known as excitons play a fundamental role in the optical properties of dielectric solids. They correspond to a bound state of one electron and one hole and can be created by light or can appear as a result of relaxation processes for free electrons and holes, which, for example, may be injected electrically. There are three models conventionally used to classify excitons: the small-radius Frenkel and charge-transfer exciton models and the large-radius Wannier−Mott (W−M) exciton model. Below, we will discuss only the structures with Frenkel and W−M excitons.

The internal structure of W−M excitons can be represented by hydrogen-like wave functions. Such a representation results from the two-particle Coulombically bound electron−hole (e−h) states in a crystalline periodic potential. The mean electron−hole distance for this type of excitons is typically large (in comparison with the lattice constant a). On the other hand, the Frenkel exciton is represented as an excited electronic state of a crystal in which an electron and a hole are placed on the same molecule. We can say that Frenkel excitons in organic crystals have radii a_F comparable to the lattice constant a: $a_F \approx a \approx 5$ Å. In contrast, weakly bound W−M excitons in semiconductor QWs have large Bohr radii ($a_B \approx 100$ Å in III−V materials and $a_B \approx 30$ Å in II−VI ones; in both cases, $a_B \gg a$).

The oscillator strength of a Frenkel exciton is close to a molecular oscillator strength F and, due to a substantial overlap of electron and hole wave functions in a molecule, can become very large (on the order of unity). The oscillator strength f of a W−M exciton, on the other hand, is usually much weaker: in a QW, for instance, $f \approx (a^3 a_B^{-2} L^{-1})F$, where L is the QW width ($a_B > L > a$). The small front factor in this expression for the W−M oscillator strength reflects the small probability of electron and hole to be in the same unit cell.

In high-quality semiconductors as well as in organic crystalline materials, the optical properties near and below the band gap are dominated by the exciton transitions. The same situation takes place also for organic and inorganic QWs, wires, and dots. The excitonic optical nonlinearities in semiconductor QWs can be large because the ideal bosonic-like picture of W−M excitons breaks down as soon as they start to overlap with each other, that is, when their 2D density n becomes comparable to the saturation density n_S. This value $n_S \approx 1/(\pi a_B^2)$ is rather small (typically, n_S is on the order of 10^{12} cm^{-2}) because the Bohr radius is large. As pointed out by Schmitt−Rink et al.,[23] the nonlinear changes per photoexcited e−h pair at low temperatures are independent of dimensionality (apart from geometrical and lifetime factors) and similar to those of the underlying atomic transition. This was demonstrated by considering the form of the nonlinear optical susceptibility $\chi = \chi_0(1 - n/n_s)$. Thus, the so-called all-optical resonance nonlinearity $\chi^{(3)}$ is proportional to the ratio n/n_S and can be large at relatively small concentrations n of excitons (that is, at relatively small pumping I_P). Because of the phase space filling, exchange, and collisional broadening, the exciton resonance is bleached. The generic figure of merit for all optical nonlinearities scales like $I_P^{-1}(\Delta\chi/\chi)$, where $\Delta\chi$ is the nonlinear part in the susceptibility in the presence of the pump of intensity I_P. As $\Delta\chi/\chi \approx n/n_S \approx n a_B^2$ and $n \propto f I_P \propto a_B^{-2} I_P$, such a figure of merit of resonance nonlinearity becomes nearly independent of the exciton Bohr radius.[10]

For organic materials, where the electron−hole distance in the excited molecule is on the order of lattice constant a, the respective saturation density would be on the order of the density of molecules in the crystal, $n_s \simeq 1/a^3$. The molecular crystals with high concentration of excitations n (on the order of n_s) are however unstable, which prevents the application of the results of the above consideration in semiconductor QWs to thin organic layers. It is in fact known that the main contributions to the optical nonlinearity in organic materials arise not due to exciton−exciton interactions but due to the optical nonlinearity of isolated molecules.[24] This is described as due to transitions via virtual molecular states and taking into account the population of the first state in each sequence of virtual transitions[25] (see also section 2.1.4).

The situation can change drastically in hybrid structures. In the resonant hybrids featuring traits of excitations of both classes, new possibilities open up for the resonant all-optical nonlinearity. Particularly, the saturation density of Frenkel−Wannier−Mott hybrid excitons should be on the order of saturation density in

semiconductor QWs, while their oscillator strength is largely determined by the Frenkel component. Hence, the enhancement of the resonant nonlinearity can be achieved at exciton densities much smaller than the saturation density of pure Frenkel excitons.

1.3. Electric Interactions in Donor−Acceptor Nanostructures

To discuss the interaction of (spatially extended) excitations in hybrid structures, it is useful to first recall how the electric interaction takes place between two closely spaced small molecules ("donor" and "acceptor"). The latter, more familiar, case is at the heart of the basic process of nonradiative Förster resonant energy transfer (FRET) from the excited molecule (donor) to the molecule in the ground electronic state (acceptor). For small molecules, the approximation of point transition dipole moments is valid, and we respectively use $\mathbf{P}_d$ to denote the polarization of the donor species and $\mathbf{P}_a$ of the acceptor. The oscillations of the electric dipole polarization $\mathbf{P}_d$ in the excited donor create the standard electric field:

$$\mathbf{E} = \frac{\mathbf{P}_d - 3(\mathbf{P}_d \cdot \mathbf{s})\mathbf{s}}{\varepsilon R^3} \quad (1)$$

at the position of the acceptor (here, the unit vector in the donor−acceptor direction $\mathbf{s} = \mathbf{R}/R$, R being the distance between them and ε the dielectric constant of the medium). The electrostatic-like field eq 1 is responsible for the resulting nonradiative donor−acceptor interaction:

$$\hat{H}_{int} = -\mathbf{E} \cdot \mathbf{P}_a \quad (2)$$

and the corresponding energy transfer with the rate of

$$\Phi(R) = \frac{1}{\tau}\left(\frac{R_F}{R}\right)^6 \quad (3)$$

where R_F is the so-called Förster radius and τ is the lifetime of the excited state of the donor. The theory of such energy transfer assumes that spectra of the donor fluorescence and acceptor absorption are overlapping and wide (the weak-coupling regime). If the energies of excited states in the donor and acceptor coincide and their widths are very narrow, then donor−acceptor interaction eq 2 would result in the splitting of the energy levels and the appearance of two hybrid dimer donor−acceptor excited states (the strong-coupling regime).

In the treatment of the resonant interaction of excitations in hybrid nanostructures, we have some conceptional analogy with the resonant interaction of two molecules. In both cases, the relevant spatial sizes are small in comparison with the light wavelength, and, hence, one can neglect the retardation effects in the calculation of the electric field. The substantial difference, however, is that for the spatially extended excitonic states (such as W−M excitons in semiconductors), the approximation of the point dipole eq 1 used in the derivation of Förster formula eq 3 becomes invalid. One should also be aware that different layers of hybrid structures can have different dielectric constants. These distinctions need to be taken into account in the evaluation of the electric field that drives the interaction.

For the extended states, instead of the total transition dipole moment, one deals with the spatially dependent excitonic polarization $\mathbf{P}(\mathbf{r})$, the corresponding transitional charge density being

$$\rho(\mathbf{r}) = -\nabla \cdot \mathbf{P}(\mathbf{r}) \quad (4)$$

The polarization in the semiconductor QW, for example, can be found using the quantum theory of electronic states and transitions in the well.[26,27] The charge density eq 4 is then used in the Poisson equation to determine the resulting electric field $\mathbf{E}$. Being a typical electrostatic problem, the standard electric potential $\varphi(\mathbf{r})$ formulation applies: $\mathbf{E}(\mathbf{r}) = -\nabla\varphi(\mathbf{r})$ and

$$\nabla \cdot (\varepsilon(\mathbf{r})\nabla\varphi(\mathbf{r})) = -4\pi\rho(\mathbf{r}) \quad (5)$$

In eq 5, we used the isotropic position-dependent dielectric function $\varepsilon(\mathbf{r})$; it can be easily rewritten for anisotropic dielectric properties as well. Poisson equation eq 5 has to be solved taking into account the appropriate boundary conditions for the potential $\varphi(\mathbf{r})$ at surfaces and interfaces of the hybrid structure under consideration. We exemplify this approach below for specific examples of the hybrid structures in the weak and strong coupling regimes.

2. RESONANT HYBRID STRUCTURES

2.1. Weak Coupling in Hybrid Nanostructures

2.1.1. Förster-like Energy Transfer. The probability of Förster resonant energy transfer from an excited molecule (donor) to another molecule (acceptor) is proportional to the overlap of the fluorescence spectrum of the donor and the absorption spectrum of the acceptor, these spectra being determined in the absence of the donor−acceptor interaction. Förster energy transfer between different dye molecules in solid solutions has been explored in numerous studies including, in particular, with the purpose of achieving light amplification in optically pumped organic thin films.[28] For organic materials, Förster radius R_F is usually about several nanometers and strongly depends on the magnitude of the overlap of the spectra. In eq 3 for the rate of FRET, any explicit footprints of the dissipation are absent because this expression is actually correct only in the limit of a very strong dissipation in the acceptor. Thus, in applications of the Förster mechanism of energy transfer between molecules, we assume that the dissipation in the acceptor is much faster than the time of energy transfer in the reverse direction, from the acceptor to the donor (for a more detailed discussion, see ref 29). This physical picture can also be valid for neighboring resonant nanostructures when they are in the weak-coupling regime, including hybrid nanostructures as well. In this case, the dissipation of the excited state in the organic (or another type) acceptor component of the nanostructure should be sufficiently strong. In other words, the energy of the resonance Coulomb coupling between the semiconductor and organic components is not strong enough to produce a stable coherent superposition of the excited states of both components.

The dependence of energy transfer on the distance between components of the nanostructure strongly depends on its geometry and is different for quantum wells, wires, and dots. One can however expect that this dependence may be similar to the Förster result eq 3 for energy transfer between small enough quantum dots or between a quantum dot and an organic molecule. In this regard, we mention that theoretical studies of the Förster energy transfer from an excited semiconductor quantum dot to an organic material surrounding the dot were performed in refs 30,31. These papers treated both limiting cases of strong and weak exciton confinement[30] as well as intermediate dot sizes variationally[31] (the exciton confinement here refers to the relationship between the dot size and the Bohr radius of the bulk exciton). A quantum-mechanical microscopic description of a Wannier−Mott exciton in a quantum dot was employed along with a macroscopic description of the organic medium.

The calculations showed that for II−VI semiconductors energy transfer can occur on a time scale of tens of picoseconds, which is much shorter than the lifetime of an excitation in a quantum dot in the absence of the transfer. The same conclusion on the relationship between lifetime of excitations and time to transfer energy nonradiatively holds for III−V semiconductor quantum dots. Therefore, just as for quantum well structures, nonradiative energy transfer mechanism was shown to be a prospectively quite efficient means for pumping organic sources of radiation.

One of the interesting examples of hybrid structures was demonstrated in the studies of energy transport in CdSe nanocrystals assembled with molecular wires.[32] Recently, however, more attention was attracted to studies of resonant energy transfer from amorphous organic materials to quantum dots in quantum dot/organic composite. The interest in such structures is evidently due to their potential application in optoelectronic devices. In these systems, the efficiency of energy transfer depends on the spectral overlap between the components and on the spatial distances between quantum dots and molecules in an amorphous or ordered organic material. As discussed above, the geometry of this case allows calculations to be based on Förster theory (see ref 33 and references therein).

In what follows, we illustrate a general discussion by more detailed results for the specific case of planar geometries, such as when a semiconductor QW interfaces an organic overlayer and when the relationship of eq 3 for energy transfer rate does not apply.

2.1.2. Exciton Energy Transfer as Joule Losses. The electric field $\mathbf{E}(\omega)$ created by oscillations of the quantum well polarization penetrates into an organic component of the hybrid nanostructure and dissipates its energy via the excitation of organic molecules if the transitional frequency ω is close to the molecular resonance. Nonradiative energy transfer rate in the case of the weak coupling can be evaluated in a particularly simple and transparent way because it essentially corresponds to Joule losses of the electromagnetic field in the acceptor material. In other words, one can use a semiclassical approach[7,12,34] and characterize the acceptor overlayer (whether organic or another material) as some medium with its frequency ω-dependent complex dielectric tensor $\varepsilon_{ij}(\omega) = \varepsilon_{ij}'(\omega) + i\varepsilon_{ij}''(\omega)$.

As discussed in section 1.3, the polarization $\mathbf{P}(\omega,\mathbf{r})$ of the semiconductor quantum well at the transition frequency ω can be calculated within the framework of the microscopic exciton theory. The related transitional charge density $\rho(\mathbf{r})$ would then follow from eq 4 and the resulting spatial behavior of the electric potential $\varphi(\mathbf{r})$ from Poisson equation eq 5 with appropriate boundary conditions. This way one finds the spatial distribution of the electric field $\mathbf{E}(\mathbf{r})$ induced by by the exciton polarization at the donor transition frequency, including in the region of the acceptor overlayer.

Knowing the electric field $\mathbf{E}$ and the dielectric tensor (function) $\varepsilon_{ij}(\omega)$ of the overlayer material enables one to calculate the Joule losses in the overlayer by using standard expressions from the electrodynamics of continuous media.[35] For the time-averaged rate of the energy dissipation of the monochromatic electromagnetic field, $\mathbf{E}(\mathbf{r},t) = \mathbf{E}(\mathbf{r})e^{-i\omega t} + \mathbf{E}^*(\mathbf{r})e^{i\omega t}$, one has

$$Q(\omega) = \frac{\omega}{2\pi}\int \varepsilon''_{ij}(\mathbf{r},\omega)E_i(\mathbf{r})E_j^*(\mathbf{r})\,\mathrm{d}\mathbf{r} \qquad (6)$$

where the integration is over the volume of the overlayer. In the isotropic medium, $\varepsilon_{ij} = \varepsilon\delta_{ij}$ and eq 6 reduces to

$$Q(\omega) = \frac{\omega}{2\pi}\int \varepsilon''(\mathbf{r},\omega)|\mathbf{E}(\mathbf{r})|^2\mathrm{d}\mathbf{r} \qquad (7)$$

The corresponding transfer time τ for the exciton of energy $\hbar\omega_{\mathrm{exc}}$ from the semiconductor quantum well to the overlayer can now be found from the relationship:

$$\tau = \hbar\omega_{\mathrm{exc}}/Q(\omega_{\mathrm{exc}}) \qquad (8)$$

These expressions for $Q(\omega)$ and τ can be starting points for further considerations (see also ref 7).

The macroscopic description of the acceptor (organic) medium is valid as long as the electric field created by the oscillations of quantum well polarization is slowly varying in space on the molecular scale. This condition is usually fulfilled in all cases, because the typical wave vectors of free or localized excitons as well as e−h pairs in the quantum well are small as compared to the inverse distance between neighboring molecules. It can also be shown that the semiclassical calculational procedure described above exactly corresponds to results that would be obtained within consistent microscopic quantum-mechanical derivations of the transfer rate using Fermi's Golden Rule. Needless to say that this approach can be applied to evaluate energy transfer rate in the weak-coupling regime for other geometries such as of quantum wires or quantum dots. As the overlayer material is described here only by its dielectric function, the approach is equally applicable if another material is used in the role of an acceptor as long as it possesses fast relaxation times and a broad spectrum in the spectral region of the resonance with the exciton transition in the donor. As an experimentally relevant example, this, for example, can be energy transfer from a quantum well to proximal layers of semiconductor wires or nanocrystals. Depending on the relative magnitude of the excitation energies in components of the hybrid nanostructure, energy transfer can preferentially take place in either direction. It should be evident that energy transfer becomes truly consequential for overall kinetics of the excitation if the transfer time eq 8 is shorter than the lifetime of the excitation in the absence of the transfer.

2.1.2.1. Calculations of Energy Transfer Time. Here, we present an example of calculations[12,34] of energy transfer time τ from free excitons in a QW in a planar structure of the type shown in Figure 1. Pumping of the QW could be be either optical or electrical. In Figure 1 the electrical pumping is assumed, which can be important for practical hybrid LEDs. Note that numerical evaluations of τ from eq 8 were performed in refs 12,34 for the infinitely thick overlayer of organic molecules; the obtained results however are correct with a rather high accuracy even for layers with thickness on the order of 10 nm.

To specify the geometry of the problem, consider a symmetric structure, consisting of a semiconductor QW of thickness L_w between two barriers of thickness L_b each, the whole semiconductor structure being surrounded by thick slabs of an organic material. In the frequency region of interest, the background dielectric constant of the semiconductor ε_b is real (the same value for the well and the barrier), while that of the organic material $\tilde{\varepsilon}$ is complex. For simplicity, the organic material is considered to be isotropic (generalization to the anisotropic case is straightforward). Thus, the dielectric functions to be

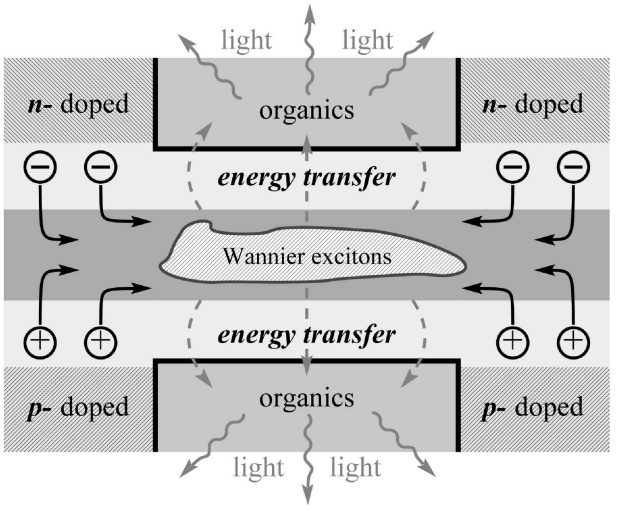

Figure 1. A sketch of the planar structure that could be used for an energy-transfer-based LED.

used in eqs 7 and 5 are specified as

$$\varepsilon_{ij}(\mathbf{r}) = \begin{cases} \varepsilon_b \delta_{ij}, |z| < L_w/2 + L_b \\ \tilde{\varepsilon}\delta_{ij}, |z| > L_w/2 + L_b \end{cases} \quad (9)$$

The polarization **P** corresponding to the excitonic transition in the QW is proportional to the electric dipole transition moment $\mathbf{d}^{vc}$ between the conduction and valence bands of the semiconductor material that appears, for example, in standard treatments[26] of optical transitions. For details of the corresponding calculations, we refer the reader to Appendix A.1 of this Review. The electric field penetrating the organic material is then found from eq 43 for the solution of the potential problem as

$$\mathbf{E}(\mathbf{r}) = [-i\mathbf{k} + k\hat{\mathbf{z}}]\varphi(z)e^{i\mathbf{k}\mathbf{r}_\parallel} \quad (10)$$

Evaluating eq 8 with this electric field, we obtain the exciton decay rate due to energy transfer as

$$\frac{1}{\tau} = \frac{2Im\,\tilde{\varepsilon}}{\pi^2\hbar}\frac{|d^{vc}|^2}{a_B^2}\frac{k|C_k|^2}{L_w^4} \quad (11)$$

Numerical evaluations of τ were performed with parameters representative of II−VI semiconductor (e.g., ZnSe/ZnCdSe) quantum wells:[36] $\varepsilon_b \approx 6$, $d^{vc} \approx 0.1ea_B$ (about 12 D for the Bohr radius of 25 Å), and of organic condensed media such as metallophthalocyanines:[37] ($\tilde{\varepsilon} \approx 4 + 3i$). Both exciton polarizations have been considered: within the quantum well plane, $\mathbf{kd}^{vc}$ (L-excitons), and perpendicular to it, $\mathbf{k}\perp\mathbf{d}^{vc}$ (Z-excitons). Shown in Figure 2a and b are numerical results for τ_L and τ_Z as functions of $k = |\mathbf{k}|$ for two sets of parameters and geometrical dimensions of $L_w = 60$ Å and $L_b = 40$ Å. It was found that the lifetime does not depend drastically on the polarization and the real parts of dielectric constants and that the dependence on L_w is also weak. The dependence on the barrier width L_b features an obvious exponential falloff factor (clearly seen from the hyperbolic functions in the denominators of expressions for $C_k^{X,Z}$ in Appendix A.1).

Quite interesting is the resulting dependence of τ on the in-plane wavenumber k of the W−M exciton. As displayed in Figure 2, τ exhibits a minimum at $k_{min} \leq 1/L_b$. While dependent on many parameters, for the case presented in Figure 2 it is

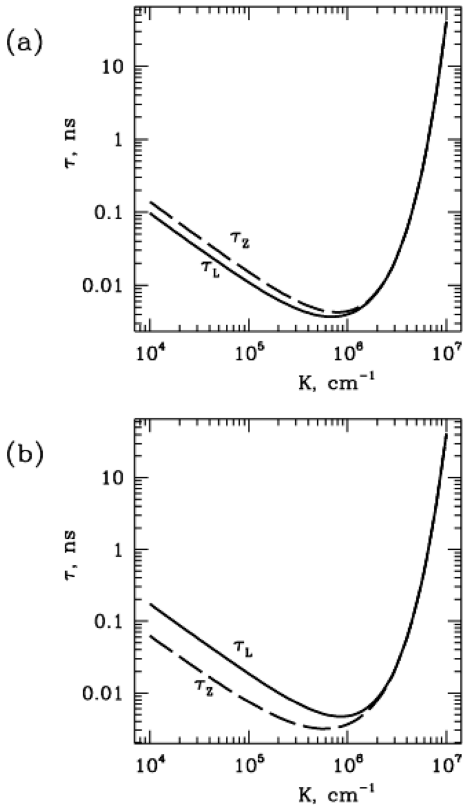

Figure 2. Free L-exciton (solid line) and Z-exciton (dashed line) lifetime τ (ns) with respect to energy transfer as functions of the in-plane wavenumber k (cm^{-1}). (a) $d^{vc} = 0.1ea_B$, $L_w = 60$ Å, $L_b = 40$ Å, $\varepsilon_b = 6$, $\tilde{\varepsilon} = 4 + 3i$; (b) the same, but $\varepsilon_b = 4$, $\tilde{\varepsilon} = 6 + 3i$.

approximately 8×10^5 cm^{-1} corresponding to the penetration length ~10 nm. For a broad range of wave numbers, lifetime is in tens of picoseconds or less, which is much shorter than the exciton recombination lifetime, the latter being about 200 ps in II−VI semiconductor QWs, as reported by different authors (see ref 36 and references therein, ref 38). Thus, the nonradiative energy transfer mechanism proves to be efficient enough to quench a large fraction of the semiconductor excitons, thereby activating the organic medium luminescence.

Analogous calculations (energy transfer time versus the wavenumber k for several values of the width L_w of the QW) were also performed for the case of III−V semiconductor materials. With $\varepsilon_b \approx 11$, $d^{vc} \approx 0.05ea_B$, and other parameters as for the II−VI structures above, it was found that for the III−V materials the energy transfer lifetime is longer by about an order of magnitude (as caused by the larger values of a_B and ε_b). However, the energy transfer rate is still efficient enough because the effective exciton recombination time in III−V materials is also much longer (about 1 ns[39]). Clearly, nonradiative energy transfer becomes truly fast for hybrid structures where the width of barriers separating semiconductor QWs and organic materials is narrow enough.

The original Förster model and radius describe energy transfer between two point-dipole objects. In the semiconductor QW discussed in this chapter, the Wannier−Mott exciton properties depend on its wave vector **k**; as seen from Figure 2, the lifetime with respect to energy transfer is also a function of **k**. The minimum of this lifetime corresponds to the maximum of the

dx.doi.org/10.1021/cr100156x |*Chem. Rev.* 2011, 111, 5179–5214

transfer rate. As different excitons would have different **k**-vectors, it is necessary to average over those assuming, for instance, the Boltzmann distribution for the excitons. A similar averaging would be applied in the determination of the mean value of the spatial depth of energy transfer. It is expected to be on the order of 50−100 Å and would depend not only on the temperature but also on many other parameters such as the width of the QW, the width of the barriers, and the set of relevant dielectric constants.[7,12,20]

2.1.2.2. Energy Transfer from Local Exciton States. It is known that the QW width fluctuations, alloy disorder, or impurities lead to localization of 2D excitons (this situation is more frequent for the II−VI semiconductor QWs than for the III−V ones). In localized state, the wave function of the center-of-mass exciton motion $\mathbf{\Psi}(\mathbf{r})$ is no longer a plane wave ($\exp(i\mathbf{k}\eta_{\parallel})$ in eq 40), and the corresponding $\mathbf{P}(\mathbf{r})$ is also localized. A detailed analysis of energy transfer from localized excitons to an organic material[12] demonstrated, just as for free excitons, that energy transfer time can be much shorter than the lifetime of excitons in quantum well in the absence of such transfer.

In the limiting case of local states in thin semiconductor quantum wells ($L_b \gg L_w$), where the Bohr radius and the length of localization $L \approx a_B$ are less than the width of barrier L_b, energy transfer to the organic material can be estimated using the point dipole approximation (assuming, of course, that organic molecules are also enough small). This is the case where the interaction of the localized exciton with each molecule of organic material can be considered as satisfying Förster relation eq 3 with the subsequent summation over all molecules. As expected from such a picture, the rate of energy transfer in such hybrid structures $1/\tau \propto L_b^{-3}$.

In the next section of this Review, we survey recent experimental results on resonant hybrid structures. Nonradiative energy transfer in a hybrid structure with an organic overlayer has been first experimentally studied by the group of F. Henneberger[40] using ZnO quantum wells and by the group of D. Bradley[18] using InGaN quantum wells. In both mentioned papers, QWs were optically pumped. Studies of the electrically pumped structures employing different organic materials could enrich this field and lead to creation of new, hybrid, types of LEDs (potentially bright, inexpensive, and more variable in color).

Resonant hybrid structures can also be employed where the role of the acceptor molecules is played by nanocrystals. The hybrid nanostructures with the InGaN QW as a donor and a monolayer of quantum dots as an acceptor were first studied by the group of V. Klimov.[41] We also mention here another study[42] on similar structures, where the temperature dependence of exciton energy transfer was investigated. The authors observed the increase of the exciton transfer rate with temperature (at $T < 130$ K) and explained this effect as the result of a reduced degree of exciton localization, assuming the exciton transfer rate increases at the delocalization.[12] Note, however, that the efficiency and the temperature dependence of exciton energy transfer at nonresonant pumping to organic as well as to inorganic material can be also affected by the population of exciton states, or, in more general words, by the dynamics of quasi-particles (electrons, holes, and excitons) created in the QW by pumping. The fast processes of energy transfer from quantum well excitons to organics and depopulation of some exciton states can influence the dynamics of all quasi-particles appearing in the well. This interesting problem deserves to be addressed in the future. This dynamics is dependent on temperature and can be different

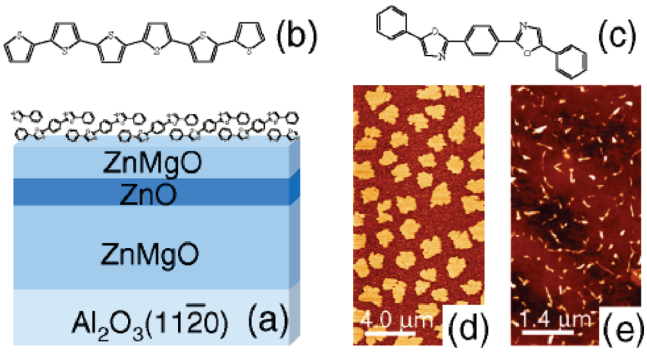

Figure 3. Sketch of the hybrid nanostructure. The 4 nm wide ZnO quantum well is situated on top of a 600 nm thick $Zn_{0.9}Mg_{0.10}O$ barrier layer grown on a $Al_2O_3(1120)$ substrate. The growth direction is along the wurtzite *c* axis. After being capped with a $Zn_{0.9}Mg_{0.10}O$ spacer of variable thickness (0−50 nm), the sample is transferred into the adjacent chamber where the organic layer is deposited. (b,c) Structures of 6T and POPOP. (d,e) AFM images of 6T and POPOP deposited on ZnO-(0001)(4 × 4) at a substrate temperature of 100 °C (6T) and 25 °C (POPOP), respectively, and a deposition rate of 1 Å/min. Reprinted with permission from ref 40. Copyright 2006 American Physical Society.

for various pumping regimes (resonance, nonresonance, or electrical) of hybrid nanostructure. For comparison, an analysis of such dynamics for the stand-alone semiconductor QW can be found in refs 43,44.

At their beginning now are also experimental and theoretical studies of energy transfer from semiconductor quantum dot to organic materials[30,31] including dendrimers.[45−47] Another recent example of such studies is ref 48 discussing results of the synthesis and optical spectroscopy of exciton energy transfer from semiconductor CdS quantum dots to dendrimer nanocomposites.

2.1.3. The Weak-Coupling Regime: Experimental Realizations. *2.1.3.1. ZnO Quantum Wells and an Organic Layer as an Acceptor.* The first paper published by the Henneberger group[40] had the title "Converting Wannier into Frenkel Excitons in an Inorganic/Organic Hybrid Semiconductor Nanostructure" directly emphasizing the essence of the effects we discussed above. It is interesting that this paper was published soon after the publication of ref 18 (see below) in which a GaInN-polymer structure was investigated yielding only indirect signatures of radiationless energy transfer conjectured from the temperature dependence of the emission yield. In the study of ref 40, to realize a resonant coupling between Frenkel and Wannier excitons, a hybrid layered nanostructure was used where a ZnO semiconductor quantum well confines the electronic excitations close to the inorganic surface covered by an organic overlayer (Figure 3a). For the organic component, thin layers were employed of either α-sexithiophene (6T) or 2,2-*p*-phenylenebis-(5-phenyloxazol) (POPOP). The structures of these molecules are depicted in Figure 3b and c, respectively. Unlike other semiconductors, for example, GaAs or Si, no passivation of the ZnO(0001) surface is required to allow for an unperturbed ordered growth of the organic overlayer. The formation of chemically inert interfaces through a stable bond reconstruction thus makes these materials especially well-suited candidates for the realization of electronically coupled organic/inorganic composites. A further motivation for the use of ZnO follows from its large band gap of 3.37 eV and the resultant potential for the fabrication of light emitters in the visible and ultraviolet spectral range. The spectrum of PL of quantum well ZnO strongly overlaps with the absorption curve

dx.doi.org/10.1021/cr100156x |*Chem. Rev.* 2011, 111, 5179–5214

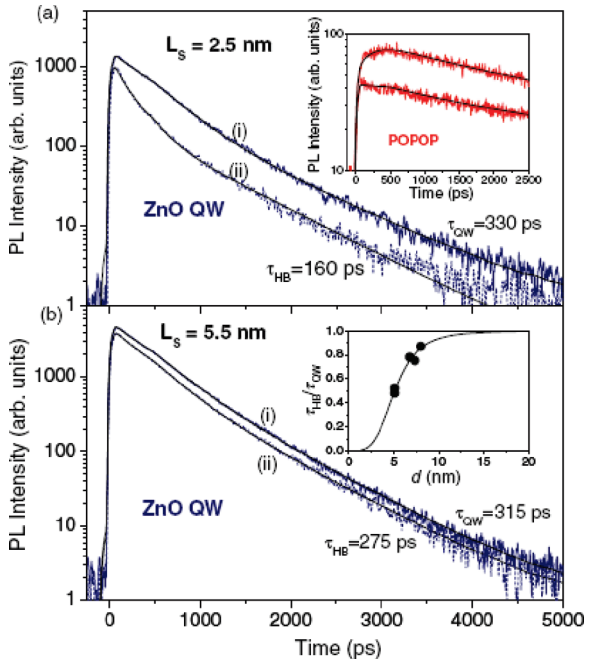

Figure 4. PL transients of the ZnO QW in (i) a ZnO/ZnMgO reference sample and in (ii) a POPOP/ZnO/ZnMgO hybrid structure: (a) L_S = 2.5 nm; (b) L_S = 5.5 nm. Excitation photon energy is 3.78 eV. Reprinted with permission from ref 40. Copyright 2006 American Physical Society.

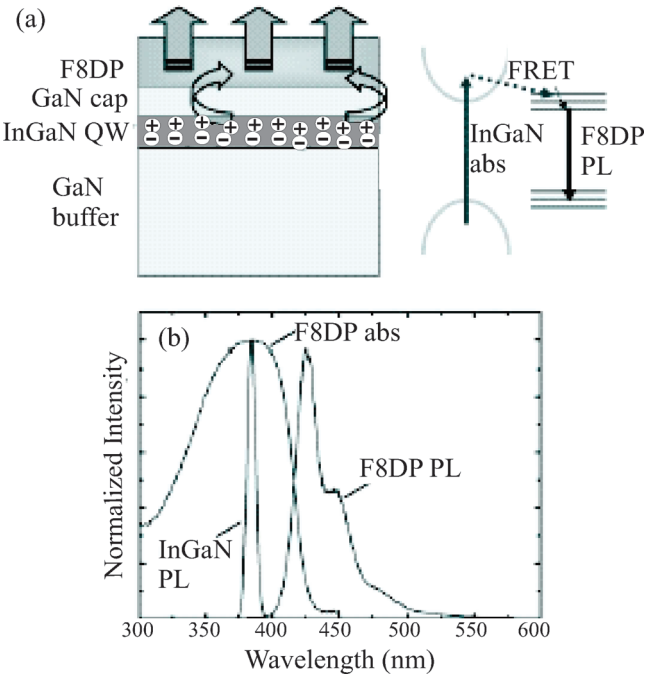

Figure 5. (a) Schematics of the hybrid inorganic/organic semiconductor heterostructures and a simplified energy-level diagram illustrating the proposed energy-transfer scheme: the excitations initially generated by absorption (ABS) in the QW layer (InGaN) can resonantly Förster transfer (FRET) their energy to the singlet excited states of the poly(9,9-dioctylfluoreneco-9,9-di(4-methoxy)phenylfluorene) (F8DP) polymer layer. Following internal conversion (vibrational relaxation), emission should then occur via radiative decay to the polymer ground state (photoluminescence, F8DP PL). (b) Absorption spectrum (labeled F8DP ABS) of F8DP and photoluminescence (labeled PL) emission spectra of the InGaN QW and the F8DP thin film. Reprinted with permission from ref 18. Copyright 2006 Wiley-VCH Verlag GmbH & Co. KGaA.

of the used organic materials, and the time scale of energy transfer between the inorganic quantum well and the organic overlayer was addressed in time-resolved photoluminescence (PL) measurements.

Figure 4 summarizes PL transients measured at 5 K by time-correlated single photon counting with a resolution of 10 ps. For a ZnO/ZnMgO quantum well without POPOP, the emission from the exciton ground state decays, to a good approximation, as a single exponent with a time constant of τ_{QW} = 330 ps (curve (i), Figure 4a). This value is in good agreement with the lifetime of the ZnO Wannier exciton of 322 ps. In a hybrid structure with a thin spacer (L_S = 2.5 nm), the lifetime shortens to τ_{HB} = 160 ps (curve (ii), Figure 4b) confirming that an additional decay channel due to energy transfer opens up. Increasing the spacer thickness, the lifetime shortening quickly disappears.

In a more recently published paper,[49] the Henneberger group demonstrated that organic molecules can be overgrown with ZnO employing epitaxial methods without degradation of their electronic structure. This observation opens possibilities for design of sandwich hybrid structures with advanced features. Excitonic coupling between the inorganic and organic components was fully maintained after overgrowth. The sandwich hybrid structures form planar waveguides, which improve organic laser action. The growth of ZnO on the amorphous SP6 layer used in this initial study was still polycrystalline. However, the authors believe that use of other organic assemblies may admit crystalline overgrowth. It can also be expected that in this way organic/inorganic superlattice structures with entirely new photonic properties would become feasible.

2.1.3.2. InGaN Quantum Wells and an Organic Layer as an Acceptor. In ref 18, the fabrication and study of a hybrid inorganic/organic semiconductor structure was reported, which employed an organic polyfluorene thin film that could be placed in a sufficiently close proximity to the underlying InGaN quantum well (PL maximum corresponds to about 385 nm). A schematic of the fabricated structures is shown in Figure 5. The UV light-emitting InGaN QW (2 nm thick) is spaced from the blue-light-emitting poly(9,9-dioctylfluorene-*co*-9,9-di(4-methoxy)phenylfluorene) film (5 nm thick) by GaN cap layers of variable thickness. Energetic alignment (as illustrated in the energy-level diagram of Figure 5) is thus needed to maximize the resonant coupling between the inorganic and organic excitations. Radiative or nonradiative decay of the latter should then result in light emission with the characteristic spectrum of the organic layer. Figure 5 shows the corresponding InGaN QW photoluminescence (PL) emission and the absorption and PL spectra of the organic film. The QW has a narrow PL band that peaks at 385 nm, coincident with the organic layer absorption maximum. The organic layer, in turn, emits blue light with a broad-structured PL band (vibronic features at 425, 450, and 480 nm). To investigate relative contributions of radiative and nonradiative energy transfer, three hybrid heterostructures were fabricated with different GaN cap thicknesses (15, 4, and 2.5 nm) between the QW and the organics. The variation in GaN cap-layer thickness allowed one to tune the strength of the resonant interaction between the QW and organics and, hence, to look for the expected improvement in organics emission efficiency (relative to the radiative transfer) due to nonradiative Förster-like energy

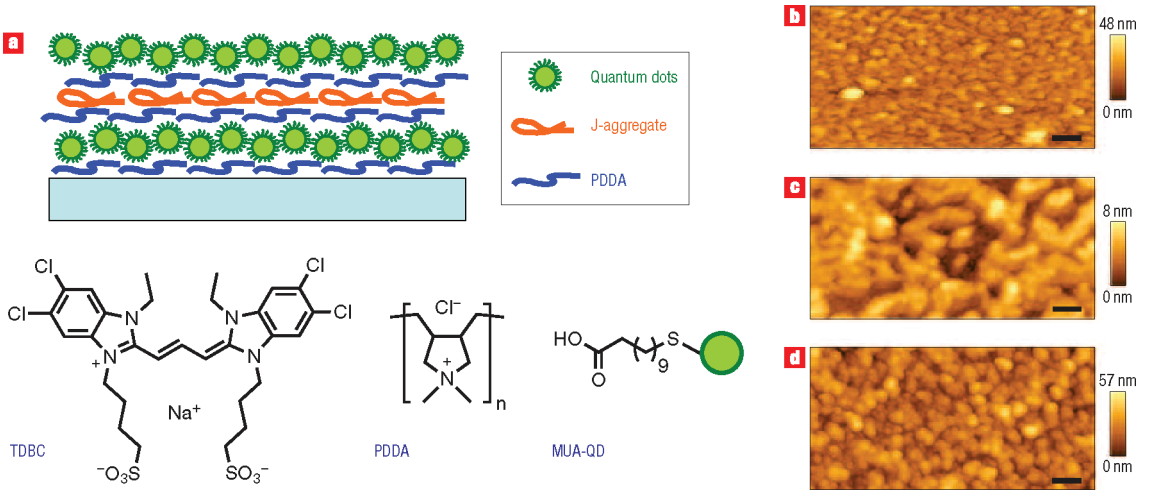

Figure 6. Hybrid organic−inorganic (J-aggregate/QD) multilayer film deposited by the LBL assembly. (a) Schematic of the hybrid film layer structure: a monolayer J-aggregate of 5,6-dichloro-2-[3-[5,6-dichloro-1-ethyl-3-(3-sulphopropyl)-2(3*H*)-benzimidazolidene]-1-propenyl]-1-ethyl-3-(3-sulphopropyl) benzimidazolium hydroxide (TDBC) is sandwiched between two monolayers of CdSe-ZnS QDs, joined by monolayers of poly(diallyldimethyl-ammonium chloride) (PDDA). Molecular structures of TDBC, PDDA, and MUA are illustrated in the lower panel. (b−d) AFM images of the LBL-grown films, consisting of a monolayer of NCs (λ_{em} = 653 nm) (PDDA/QD) (b), a monolayer of *J*-aggregate (PDDA/TDBC/PDDA) (c), and the hybrid film II (d). The scale bars in are 100 nm. Reprinted with permission from ref 52. Copyright 2007 Nature Publishing Group.

transfer from the QW to the organics at small separating distances. In concluding remarks, the authors stress that decreasing the separation between the inorganic and organic layers produces an intensity enhancement of the organic layer radiation by 20 times in comparison with the case of purely radiative transfer from the QW to organics. Such structures, as emphasized by the authors, should be able to take advantage of the complementary properties of organic and inorganic semiconductors, which may lead to devices with a highly efficient emission across the entire visible band of the electromagnetic spectrum. Further experimental work of the Bradley group can be found in refs 17,50. In ref 50, the authors studied the Förster resonant coupling between the Wannier−Mott and Frenkel excitons in hybrid structures comprising single (Ga,In)N quantum wells spaced from F8DP polymer overlayers with variable thickness GaN caps. By considering spectrally and time-resolved data, they found that the efficiency of energy transfer process can be of up to 43%.

A few words will now be spent on the efficiency of energy transfer in the hybrid structures.[13] In the case of the fast energy transfer from the semiconductor quantum well to the organic material, the nonradiative processes in quantum well with characteristic times larger than that of energy transfer will be inefficient. As a result, the overall quantum yield of the hybrid layered structure will be increased (in comparison with the quantum yield of an individual semiconductor quantum well), if the luminescent quantum yield of the emissive organic layer is high enough. This widens the choice of semiconductor quantum wells and organic materials to be used in the hybrid structures, provided that that they satisfy the condition of a large overlap of the donor photoluminescence and acceptor absorption spectra and high quantum yield of luminescence of organic molecules.

Note that this overlap may depend on the temperature. As an example, we can mention the temperature dependence of exciton energy transfer in hybrid single InGaN quantum well/colloidal CdS nanocrystals from ref 51. It was demonstrated in that paper that an optimum transfer energy efficiency of 65% can be observed at 60 K.

2.1.3.3. J-Aggregates−Nanocrystals Layered Nanostructure. Efficient nonradiative energy transfer from organics to semiconductor nanocrystal quantum dots (QDs) and in the opposite direction from semiconductor QDs to organics was demonstrated in ref 52. In this paper, the electronic energy transfer has been investigated using the multilayer structure presented in Figure 6.

The structure was obtained by the layer-by-layer (LBL) assembly approach. Figure 6a schematically shows the typical structure of the hybrid organic/inorganic (*J*-aggregate/QD) LBL films that was synthesized for the discussed study, along with the chemical structures of the constituents. In the hybrid film, a single monolayer of cyanine dye *J*-aggregates (TDBC) was sandwiched between two monolayers of CdSe−ZnS core−shell structured QDs, with polyelectrolyte (PDDA) acting as the ultrathin "molecular glue". Two types of hybrid films were considered in ref 52, one with QD emission centered at 548 nm (referred to as film I) and the other at 653 nm (referred to as film II), thus providing contrasting cases of excitation coupling with respect to the fixed *J*-aggregate emission at 594 nm. Representative atomic force microscopy images of hybrid film II and two additional QDs and *J*-aggregate reference films are shown in Figure 6b−d. It was found for films II that the resonance coupling of electronic excitations in *J*-aggregates with electronic excitations in the two monolayers of QDs can reach efficiencies of energy transfer from *J*-aggregates to QDs up to 98% at room temperature. The details of optical characterization of hybrid film can be found in ref 52. The demonstration in ref 52 of efficient energy transfer from organics to semiconductor nanostructures may have important implications for photovoltaics, as will be discussed later (see also refs 22,53).

Interesting optical properties of hybrid molecular-wire and semiconductor nanocrystal (NC) superstructures have been also found in ref 54. In that study, the organic substituent consisted of a conjugated acid with varying length between 1.9 and 3.3 nm, while the NCs (either CdS or PbS) had diameters in the range of 2.0−5.0 nm. The NCs were excited both via the molecular wires

dx.doi.org/10.1021/cr100156x |*Chem. Rev.* 2011, 111, 5179–5214

and directly into their quantized states. Simulation of the luminescence decay process suggested energy transfer between the organic acid and NCs by an exciton diffusion mechanism.[55] The studied superstructures exhibited typical quantum size effect properties of the NCs but also additional collective properties (exciton diffusion and the red-shifted exciton absorption) not encountered with individual NCs.

2.1.3.4. Triplet−Triplet Dexter Energy Transfer from Wannier−Mott Excitons to Naphthalene. Experiments described above demonstrated efficient Förster-like energy transfer from singlet excitons in inorganic quantum wells to singlet excitations in the organics. There, the spin of nanostructures in the ground as well as in the excited state is equal to zero and does not change. The efficiency of such transfer is proportional to the product of oscillator strengths of donor and acceptor and can be in some cases very large. However, there is another type of energy transfer mechanism called the Dexter type of energy transfer[56] (see also ref 57). Just as in the original Förster work, Dexter formulated his theory for two interacting molecules. In application to the case of two interacting nanostructures, the Dexter type of energy transfer from one nanostructure (donor) to another nanostructure (acceptor) implies that one or both nanostructures change the spin state. The majority of molecules, particularly molecules with saturated bonds, have a singlet ground state, and the qualification above means that, if the donor is initially in a singlet state, the acceptor, following Dexter energy transfer, has to be in a triplet final excited state. If the donor is initially in a triplet state, the acceptor, after energy transfer, can be in a singlet or triplet state.

The first experimental observation of Dexter-type energy transfer in organic/inorganic hybrid materials was published only recently.[58] In contrast to the Förster mechanism, which is rather long-range (so-called Förster radius for molecule-to-molecule energy transfer can be few nanometers), the Dexter mechanism is short-range and usually weak because its efficiency is proportional to the squared overlap of the wave functions of the donor and acceptor (which falls off exponentially with the increased separation of the donor and acceptor). Nevertheless, this mechanism was demonstrated in ref 58 to work. In that paper, an organic/inorganic hybrid quantum-well structure consisting of perovskite-type lead bromide well layers and naphthalene-linked ammonium barrier layers (see Figure 7) was used. It is a nearly ideal self-organized material where there is no stress and lattice mismatch at the interface. The well layers form monolayers without well-width fluctuations, and the interface between the well and the barrier is intrinsically flat. The authors of ref 58 demonstrated almost perfect Dexter-type energy transfer to the lowest triplet state in naphthalene incorporated layered perovskite-type quantum-well materials. It was found that the photoexcited energy is transferred from the lowest energy Wannier excitons in inorganic quantum wells to the lowest energy triplet state in naphthalene molecules in organic barrier layers. Using observations made in refs 59,60 and the time-resolved photoluminescence (PL) measurements, the authors have been able to describe the energy transfer mechanism as mainly the triplet−triplet Dexter-type transfer.

The layered perovskite-type quantum-well family $(C_nH_{2n+1}NH_3)_2PbX_4$ (X = I, Br, Cl) forms organic/inorganic hybrid quantum well systems, where inorganic well layers are composed of a two-dimensional network of corner sharing $[PbX_6]^{4-}$ octahedra between organic barrier layers of alkyl ammonium chains.[61,62] The schematic of the crystal structure of $(C_nH_{2n+1}NH_3)^2PbBr_4$ (further denoted as C_nPbBr_4) is shown in Figure 7a. Because of

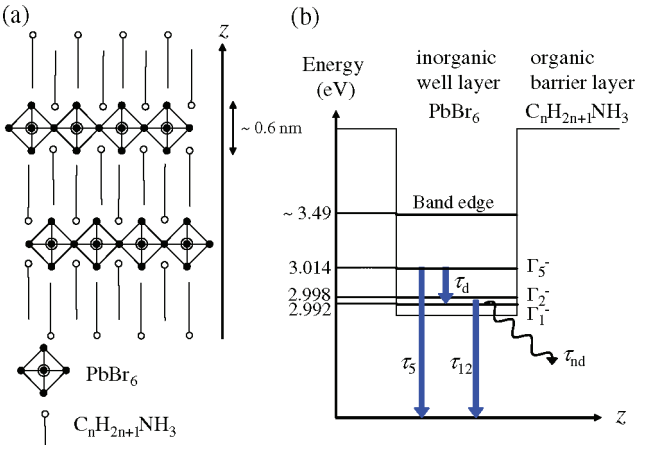

Figure 7. (a) Schematic of the crystal structure of C_4PbBr_4. (b) Energy diagram and decay dynamics of the excitons in the inorganic well. Reprinted with permission from ref 58. Copyright 2006 American Physical Society.

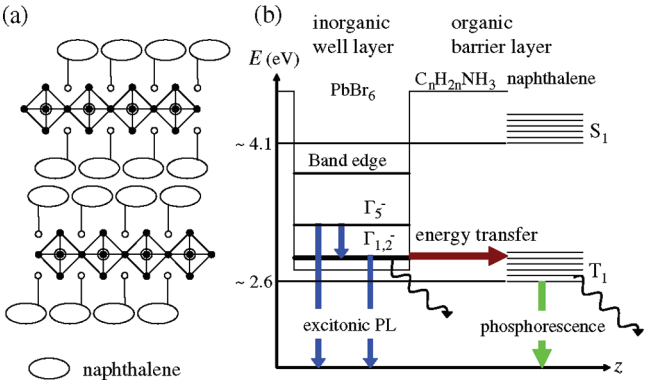

Figure 8. (a) Schematic of the crystal structure of N−Cn. (b) Energy diagram and decay dynamics of N−Cn. Reprinted with permission from ref 58. Copyright 2006 American Physical Society.

the quantum confinement and dielectric enhancement effects, the excitons are tightly confined in the inorganic well layers and form two-dimensional (2D) Wannier excitons.[59,62,63] Figure 7b shows the energy structure and decay dynamics of the excitons in C_4PbBr_4. Γ_5^- excitons are dipole-allowed singlet excitons, while Γ_2^- and Γ_1^- excitons are mainly composed of triplet excitons.[60] Optical excitation above the band gap of the inorganic well layer creates the Γ_5^- and $\Gamma_{1,2}^-$ excitons ($\Gamma_{1,2}^-$ denotes Γ_1^- or/and Γ_2^- excitons). However, the Γ_5^- excitons quickly relax to $\Gamma_{1,2}^-$ excitons due to the spin relaxation within several picoseconds, leaving relatively small populations at the Γ_5^- level. Because the $\Gamma_{1,2}^-$ excitons have a relatively long lifetime (1−10 ns), many excitons are accumulated in the $\Gamma_{1,2}^-$ levels. Therefore, the intensity of the singlet Γ_5^- emission is weaker than that of the $\Gamma_{1,2}^-$ emissions in the time-integrated PL measurements.

Figure 8a shows the schematic of the structure with naphthalene investigated in ref 58. In this new structure, the naphthalene molecules are linked to the alkyl chains. The excited singlet state of the naphthalene (S_1) as shown in Figure 8b is located above the band edge of the well layer, and the excited triplet state (T_1) is located at and below the exciton levels. The T_1 levels are widely distributed due to the molecular vibronic bands. When the

dx.doi.org/10.1021/cr100156x |Chem. Rev. 2011, 111, 5179–5214

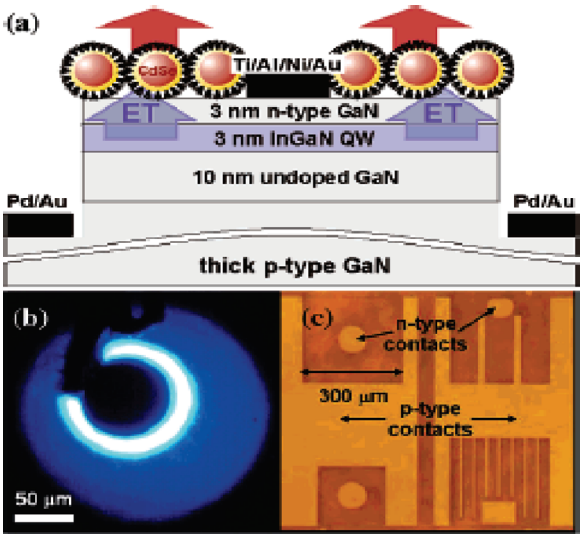

Figure 9. (a) Schematic cross-section of the ET-LED structure. The 10 nm undoped GaN layer below QW is a transition layer to provide a good interface for the QW growth. (b) ET-LED under electrical excitation. The white ring around the n-contact indicates strongest QW emission. (c) Contact geometry of a real device. Reprinted with permission from ref 64. Copyright 2006 American Chemical Society.

excitons are excited in the quantum well layer, energy transfer from the accumulated $\Gamma_{1,2}^{-}$ excitons to the naphthalene T_1 layer has efficiency[58] of 99%.

2.1.3.5. Electrical Pumping of a Quantum Well in a Hybrid Structure. Needless to say that for practical applications of light-emitting resonant organic/semiconductor devices, direct experimental evidence is required of the hybrid structures that can operate when driven by the electrical pumping of inorganic quantum wells. A first successful demonstration of such operation in hybrid structure was described in ref 64 where an example of an implementation of an electrically pumped light-emitting device was achieved in a hybrid structure using nonradiative energy transfer. Here, however, similar to the previous study in ref 41, a monolayer of CdSe quantum dots was used as an acceptor layer. To realize the electrical pumping, the structure presented in Figure 9a was used. In this structure, an InGaN quantum well on a top of thick, p-doped GaN barrier was grown and completed with a thin, n-type GaN cap layer (normally a quantum well is grown on the top of an n-type layer). This way the advantage of a much higher mobility of n-GaN as compared to p-GaN was exploited, which allows one to obtain a significant current spreading despite the small thickness of the electron-injection layer. By performing direct spatial mapping of the emission intensity (Figure 9b), the authors observed that the quantum well emission extends up to 80 μm from the edge of the n-contact. It was thus demonstrated that CdSe nanocrystals are excited by nonradiative energy transfer from the electrically driven InGaN/GaN quantum well. The nanocrystals act as efficient color converters of the quantum well emission. The measured color conversion efficiency was 13%, which is significantly higher than the values expected for a mechanism based on the emission−reabsorption.

By eliminating several intermediate steps of the traditional color-conversion scheme, the energy transfer mechanism can provide a significant reduction in losses during the color-conversion process. Another attractive feature of the energy transfer scheme is that it can also produce improved efficiencies as compared to stand-alone LEDs. Specifically, if the energy transfer rate is sufficiently high as compared to the rate of nonradiative losses in the quantum well, the majority of excitations can be "rescued" from nonradiative recombination by transferring them into the phosphor, which then efficiently converts them into photons (see also ref 13). This consideration implies that the energy transfer approach can produce high overall quantum efficiencies, even in the case of moderately efficient LEDs with thin quantum well barriers adjusted to optimize the energy transfer rate.

As technologies for synthesizing and fabricating semiconductor colloidal nanocrystals have matured over last years, the nanocrystals are becoming promising candidates for highly efficient multicolor lighting devices. As another example of recent successful applications of nanocrystals in hybrid structures, we mention ref 65, where a novel method for utilizing nonradiative energy transfer in color-conversion lighting by depositing bright colloidal nanocrystals on surface-patterned GaN-based LEDs was demonstrated. In this method, the energy of electrically injected carriers in the active layers of the deep-etched LED can be transferred to the adjacent nanocrystals by means of nonradiative energy transfer (see details in ref 65). The design of proposed electrically pumped hybrid structure is interesting and definitely will be used in future investigations. One of the important issues in evaluation of hybrid structures is the efficiency of the energy transformation. The optimization of the FRET mechanisms should lead to novel devices that combine favorable properties of donor and acceptor materials in a single hybrid structure. Such devices can have applications in solid state lighting, where an efficient down-conversion into the visible is required, and in hybrid lasers, where electrically driven semiconductor nanostructures can provide FRET-pumping of the gain media, whether organic or made with nanocrystals.

2.1.4. On Optical Nonlinearities in Weakly Coupled Hybrid Structures. A possibly substantial enhancement of the resonant optical $\chi^{(3)}$ nonlinearity can be achieved in strongly coupled hybrid structures as will be discussed below in section 2.3.2. Here, we address the issue of the optical nonlinearity in hybrid structures with weak coupling.[66] We will argue that an enhancement of the resonance $\chi^{(3)}$ nonlinearity of the semiconductor QW could take place in this case as well. These systems may also provide a possibility to vary the nonlinearity optically by changing the pumping of the organic material.

Indeed, the resonance optical nonlinearity $\chi^{(3)}$ of the QW is proportional to the concentration of excitons in the well.[23] This concentration (and subsequently $\chi^{(3)}$) can be increased in the hybrid structure due to the absorption of incident light by the organic component followed by energy transfer from the organic layer to the QW. Such energy transfer is realized if the light produces Frenkel excitons in the organic layer with energies larger than the exciton energy in the semiconductor quantum well as, for instance, occurred in experiments of ref 52. The overall light absorption in the organic component of the hybrid structure can be much larger than the direct absorption by a thin QW so that the organic component plays in this case the role of the concentrator of pumping radiation energy. Under the influence of this radiation, the QW in the hybrid structure can therefore be converted into the state with the increased resonant $\chi^{(3)}$. The increase of the optical nonlinearity, however, would be happening only for the second beam of light that is actually resonant with exciton transitions in the QW. As this beam can

have the light frequency appreciably lower than the Frenkel exciton frequency, it would not be absorbed in the organic part of the hybrid structure. Variations in the pumping of the organic component would produce, via energy transfer, variations in the concentration of the Wannier−Mott excitons in the QW. The hybrid structure, thus, could act as a kind of an optical switch.

We will add here a few words on the nonlinearity at the nonresonant pumping. The nonlinear optical susceptibility in this case can be calculated in terms of virtual transitions between various levels of the system.[24,25,67] Such an analysis shows that the enhancement of the nonlinearity in a hybrid structure could be taking place if the semiconductor component would "borrow" the oscillator strength from strong transitions of neighboring organic molecules.

The experimental studies of optical nonlinearities in hybrid nanostructures are only in the very beginning. We can mention here that some enhancement of the two-photon absorption was reported in experiments of refs 68,69 on semiconductor quantum dot arrays embedded in an organic matrix. Of course, this first observation needs a more detailed analysis because it is not clear what type of coupling was responsible for that rather small enhancement and what type of electronic excitations (localized or coherent) can be realized in that structure.

The second-order optical nonlinearity $\chi^{(2)}$ in hybrid structures is another interesting subject. The situation here may be complicated due to the parity selection rule: if the donor−acceptor structure has an inversion symmetry, the second-order nonlinearity would vanish. In the absence of the inversion symmetry, the factors that determine the enhancement are similar to those found for the $\chi^{(3)}$ nonlinearity. Another possibility here is to consider the coupling of the dipole and quadrupole transitions that change the selection rules and the intensity for the corresponding transition. For the case of the strongly coupled structures, such an effect was discussed in ref 70.

2.2. Energy-Transfer-Based Hybrids for Solar Cells

2.2.1. Hybrid Structures and an Earlier Paper by Dexter.

In the bulk of our discussion above of the weakly coupled hybrid nanostructures, the focus has been on energy transfer from the semiconductor component to an organic overlayer with possible applications in light-emitting devices. The fast and efficient nonradiative (Förster-like) energy transfer between nanostructures takes place due to purely electrostatic coupling of their electronic transitions. Energy transfer in this case is a long-range process in comparison with a short-range direct charge-transfer process and requires only a reasonable energy overlap between excitons in the participating components of the hybird structure. In this section, we continue discussing stand-alone hybrid nanostructures in the weak-coupling regime focusing, however, now on energy transfer in the opposite direction, that is, from an optically pumped organic material to an inorganic semiconductor component.

Nonradiative energy transfer into an inorganic semiconductor (perhaps nanostructured as quantum wells or quantum wires) can result in the production of electron−hole (e−h) pairs to be used for photovoltaic applications. One can envision hybrid structures of various configurations such as, for example, those shown in Figure 10 employed as energy-transfer-based hybrid solar cells. Solar light here would be predominantly absorbed in organic media (the absorbers used in the structure of Figure 10 are quantum dots instead) generating molecular excitons that would be diffusing toward interface(s) with inorganic semiconductors.

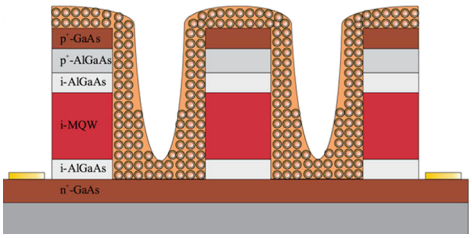

Figure 10. A schematic of the hybrid patterned device where the channels are partially filled with nanocrystal quantum dots; the structure is discussed in more detail below. Reprinted with permission from ref 71. Copyright 2009 American Physical Society.

In the vicinity of the interface, nonradiative energy transfer takes place, with the molecular exciton disappearing and an electron−hole pair created in the semiconductor. This e−h pair is then efficiently separated by built-in electric fields, and individual charge carriers are further transported to collecting electrodes, all entirely within the inorganic component. This operation mode of a hybrid structure is very different from charge-transfer-based hybrids where the interface is used to split the molecular exciton into an electron and a hole on different sides of the interface.[2] The energy-transfer-based hybrids are expected to be more interface quality tolerant and not suffer from low charge carrier mobilities in the organic component. It is also important that in many cases the energy of incident light absorbed by the organic component can exceed the energy absorbed by inorganic nanostructures. It is clear that the strongly absorbing organic part in such hybrid structures can function also as an effective collector of the light energy.

The possibility of producing excitations in quantum wells by energy transfer from organics enabling thereby a novel type of hybrid solar cells was mentioned in refs 22,53,72. However, as we found recently, nearly the same idea was formulated in an earlier paper by Dexter[73] published in the *Journal of Luminescence* in 1979. It is surprising that, to our knowledge, in recent publications on the photovoltaic devices this paper does not seem to be quoted. V.M.A. regrets that his own publications[22,53,72] discussing this possibility to exploit energy transfer to a semiconductor layer for photovoltaics did not cite that Dexter's paper.

Dexter's paper was entitled "Two ideas on energy transfer phenomena: ion-pair effects involving the OH stretching mode, and sensitization of photovoltaic cells", and it is the second idea, on sensitization, that is of interest to us now. Dexter draws attention to the production of e−h pairs in a semiconductor by nonradiative energy transfer from molecules on the surface and writes: "Energy transfer can also produce e−h pairs in a semiconductor, although this effect seems not to have been considered heretofore. I shall argue that there are some large potential benefits from so sensitizing the photovoltaic effect". He considered a sample of a semiconductor as in Figure 11 with a metallic cathode as a base and a grid of wires on top providing Schottky barriers, enclosed in an organic coating suitably chosen to absorb the incident light, for example, the solar spectrum, in the strong singlet absorption bands. Dexter concentrates his hopes on the triplet excitons. He argues that "The absorption depth is typically much less than the diffusion length of the triplet excitons which are usually produced by inter-system crossing or by exciton fission in one species (e.g. tetracene or a mixture of two (like pentacene and tetracene)". In his paper, Dexter stressed potential benefits of proposed structure in Figure 11 and also

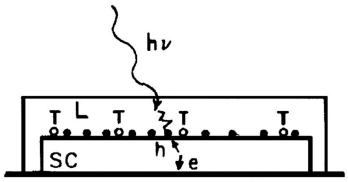

Figure 11. Sketch of a photovoltaic cell consisting of a semiconductor SC and an organic layer L with some surface traps. The solid circles denote a metallic grid of hole collector. Reprinted with permission from ref 73. Copyright 1979 Elsevier BV.

Table 1. Transition Matrix Element M for the First Excitonic Transitions, Due to a Dipole with $d = 10$ D, $\theta_d = 0$, Placed at a Distance $r_0 = 6$ nm from the Center of a Quantum Dot of Radius $R = 3.9$ nm[a]

transitions in NC (VB → CB)	transition energy (eV)	M (meV) (E^d)	M (meV) (E_0)
$1S_{1/2} \rightarrow 1S_{1/2}$	0.627	0.181	0.184
$1S_{1/2} \rightarrow 1P_{3/2}$	0.744	0.0869	0
$1S_{1/2} \rightarrow 1P_{1/2}$	0.768	0.0569	0
$1P_{3/2} \rightarrow 1S_{1/2}$	0.804	0.0798	0
$1P_{1/2} \rightarrow 1S_{1/2}$	0.843	0.0520	0
$1S_{1/2} \rightarrow 1D_{5/2}$	0.877	0.0476	0
$1S_{1/2} \rightarrow 1D_{3/2}$	0.917	0.0303	0
$1P_{3/2} \rightarrow 1P_{3/2}$	0.921	0.133	0.134
$1P_{1/2} \rightarrow 1P_{1/2}$	0.984	0.0327	0.0511

[a] Single particle states for conduction (CB) and valence (VB) band are indicated by the notation nl_j. In the last column, we report the values obtained with a uniform electric field having the same intensity as the intensity produced by the dipole at the NC center.

discussed some practical problems. He also mentions that in the process of energy transfer from an organic molecule to a semiconductor, the momentum conservation may be relaxed.

As the electric fields involved in the process of energy transfer can be highly nonuniform, familiar optical transition selection rules can be also relaxed for transfer from organic molecules to nanocrystals (NCs). A discussion of this effect for the hybrid structures in which a semiconductor slab is replaced by a layer of semiconductor quantum dots was provided in ref 74. Table 1 illustrates the effect quantitatively for the case of a PbSe quantum dot acceptor of radius $R = 3.9$ nm and a molecular donor of the transition dipole moment $d = 10$ D placed at a distance $r_0 = 6$ nm from the center of the NC with orientation $\theta_d = 0$. Such a dipole produces, at the center of the NC, an electric field $E^d(0,0,0) = 2875$ V/cm. In the last column of the table, the transitions are evaluated that would be excited by a uniform electric field of the same magnitude $E_0 = 2875$ V/cm.

It is interesting to evaluate characteristic magnitudes of the electric field, which can be created in a semiconductor layer of the hybrid structure by a nearby excited organic molecule. In the case of a pure system of NCs, the operator M describes a coupling between the dipole interband (single-exciton channel) or intraband (biexciton channel) transitions and the light field. On the other hand, in a hybrid nanocomposite system, as we mentioned, the light field is replaced by the Coulomb field produced by the electronic dipole transition in a neighboring organic molecule. For a typical magnitude $d \approx 5 \times 10^{-18}$ esu (or 5 D) of the dipole moment of an optical transition in organics, the strength of the electric field, $E = d/R^3$, created by this dipole at distance $R \approx 5$ nm is estimated to be quite strong, about 12 kV/cm.

Charge carrier generation in inorganic semiconductors by energy transfer from organics, as compared to the direct pumping by the sunlight, can also have additional benefits and special features. The absorption coefficient of light by an organic material in the region of its resonances can be quite large. Accordingly, relatively small amounts of organics would be able to absorb the sunlight in the resonant region of its spectrum to further transfer this energy to the inorganic semiconductor component. In some cases, perhaps even layers thinner than the exciton diffusion length might be sufficient. Otherwise, judicious designs of the geometry of hybrid structures can be employed; see, for example, Figure 10. Overall, the organic component of the hybrid structure can be considered as a special type of the concentrator of the solar energy made available to its inorganic component. We reiterate that both the magnitude and the spatial distribution of the electric field involved in energy transfer from nearby organic molecules are quite different from the field involved in the direct absorption of the sunlight in the inorganic semiconductor. The former field can be very nonuniform making thereby some previously forbidden electronic transitions allowed. In the case of a NC layer, for example, these states become populated and can contribute to the processes of phosphorescence.

2.2.2. Nonradiative Energy Transfer into an Inorganic Semiconductor. The subject of nonradiative energy transfer from small molecular species (and molecular crystalline layers) into bulk solids has a long history and was particularly extensively researched in the context of modification of lifetimes and quenching of molecular excitations in the vicinity of metallic surfaces (see, e.g., references to numerous studies in refs 29,75−79). It is well established that at large spatial separations from the surface the radiative lifetimes exhibit an oscillating dependence on the distance as caused by the interference of the primary and reflected radiation fields. At smaller separations, however, the lifetimes drastically shorten as nonradiative energy transfer into the metallic substrate becomes very efficient thanks to the strong dipole near-zone field. (Note that if charge transfer takes place at the interface as a result of the interaction between organic and inorganic layers, the resulting double electric layer may constitute a barrier, preventing the exciton from approaching the interface. In this case, exciton energy transfer depends on the barrier height and width.[80,81]) Fundamental understanding of these phenomena can be achieved already within a classical macroscopic electrodynamics picture of the fields of an oscillating electric dipole in the media characterized by their frequency-dependent complex dielectric functions $\varepsilon(\omega) = \varepsilon'(\omega) + i\varepsilon''(\omega)$. Stemming from Sommerfeld's treatment[82] of an oscillating dipole above a half-space and encompassing developments related to nonradiative energy transfer,[83] a very comprehensive macroscopic picture of this kind has been worked out for dipoles in different environments; for succinct summarizing reviews, see refs 76,79. Being a generic macroscopic description, the picture can be applied not only to metals but to various media, including semiconductors of our interest.

The efficiency of nonradiative energy transfer can be clearly illustrated in the simplest geometry of an oscillating dipole embedded in medium 1 (dielectric function ε_1) at distance d from the planar interface with medium 2 (dielectric function ε_2). If compared to the dipole vacuum radiative rate w_r^0, the rate of nonradiative energy transfer w_{nr} into

dx.doi.org/10.1021/cr100156x |Chem. Rev. 2011, 111, 5179–5214

medium 2 would be given[29,76] as

$$\frac{w_{nr}}{w_r^0} \approx \left(\frac{\lambda}{2\pi d}\right)^3 \frac{\varepsilon''_2}{|\varepsilon_1 + \varepsilon_2|^2} \quad (12)$$

where $\lambda = 2\pi c/\omega$ is the vacuum photon wavelength at the dipole frequency ω. Expression 12 features a power-law distance d dependence of the type

$$w_{nr}/w_r = (R_0/d)^n \quad (13)$$

commonly considered for the nonradiative energy transfer rate from a point-like donor dipole to an array of dipole acceptors. Here, R_0 is the effective Förster radius, and power n depends on the dimensionality of the array. The standard nonradiative Förster transfer rate between two point-like molecules, eq 3, corresponds to $n = 6$, integrating which over a half-space of acceptors results in $n = 3$ exhibited in eq 12. A thin planar layer of acceptors would yield $n = 4$.[83]

The relative effectiveness of energy transfer at small distances d is largely predicated by the first factor in eq 12: for a $\hbar\omega = 2$ eV excitation, for example, the wavelength λ is about 600 nm, and for the distance $d = 1$ nm, the factor is on the order of 10^6. This enhancement is diminished but cannot be overcome by the dielectric screening: typically $|\varepsilon_1 + \varepsilon_2|^2$ is on the order of 10^2–10^3. The absorptive strength ε''_2 in the semiconductor is also frequency-dependent and varies greatly between direct and indirect transitions. Importantly, even in the latter case, nonradiative energy transfer can be quite effective. So for Si ambient ε''_2 at 2 eV is about 0.17;[84] hence, the rate of nonradiative energy transfer to Si is expected to be about 2 orders of magnitude larger than the vacuum radiative rate. This crude estimate is very much consistent with results of more detailed calculations on the basis of theory of ref 76 shown in Figure 3 of ref 85 for different excitation energies $\hbar\omega$. The onset of direct transitions in Si is clearly seen in that figure via a further sharp increase of the energy transfer rate at higher $\hbar\omega$ between 3 and 3.5 eV. For GaAs with its direct transitions, ε''_2 already at 2 eV is about 1.6,[84] and the energy transfer rate is roughly 3 orders of magnitude larger than the vacuum radiative rate. These estimates based on the macroscopic $\varepsilon(\omega)$-description clearly indicate the potential efficacy of nonradiative energy transfer from neighboring molecular excitons into "classical" semiconductor materials as a mechanism of electron–hole pair production in the latter.

While providing guidance to understanding the efficiency of nonradiative energy transfer, a simplified picture based on a point-like dipole molecular sensitizer in the vicinity of the $\varepsilon(\omega)$-characterized medium substrate needs more accuracy for a quantitative assessment of the transfer at small spatial separations, where deviations from results like eq 12 may be expected. One particularly notes that $\varepsilon(\omega)$ can successfully describe the medium response for nearly uniform plane electromagnetic fields (wave vectors $\mathbf{k} \simeq 0$), but the near-zone dipolar electric field is highly nonuniform and may contain a multitude of planar $\mathbf{k}$-components. At very small distances d from the substrate, the range of relevant wave numbers $k \approx 1/d$ may constitute a substantial part of the Brillouin zone of the substrate material. In other words, a proper macroscopic description of the medium response would be by means of the $\mathbf{k}$-dependent dielectric (tensor) $\varepsilon(\omega,\mathbf{k})$.[35,86] In the traditional language of the electronic transitions in semiconductors, the optical response $\varepsilon(\omega)$ is determined by the "vertical" valence-to-conduction-band transitions, while the dipolar field can excite electron–hole pairs "non-vertically".

To address this issue for a semiconducting half-space, the authors of a theoretical paper ref 87 retained the picture of a point-like dipole but explicitly considered electronic transitions excited by the dipolar field near band edges of semiconductors in the effective mass approximation. Their analysis yields the classical theory result eq 12 ("optical limit"[87]) at large enough sensitizer–semiconductor separations but shows deviations at smaller distances. In addition to the distance, the magnitude of deviations and their character depend on whether the semiconductor is a direct- or indirect-gap, and on the excess energy $\Delta = \hbar\omega - E_g$ for transitions above the band gap E_g. For direct-gap semiconductor transitions near the threshold, the simultaneous conservation of the energy and momentum results in limitations on the "participating" $\mathbf{k}$-components of the dipolar field, leading to the overall decrease of the energy transfer rate in comparison with the classical optical limit rate. As a crude estimate, ref 87 offers the following expression for distance d beyond which the optical limit result eq 12 is valid:

$$d^2 > 5\hbar^2/(m_c + m_v)\Delta$$

where m_c and m_v are effective masses in conduction and valence bands. This estimate is useful to see the essential parametric dependences; it, for example, would require d to be larger than 7 semiconductor lattice spacings for $\Delta = 0.1$ eV and $m_c + m_v = 0.5m_e$. Their numerical results for such effective masses show practically no difference with the optical limit rate for $\Delta = 0.3$ eV when d is beyond 5 lattice spacings. We note here that at such small separations, the very representation of the molecular exciton as a point-dipole would likely be itself inaccurate, and the rates need to be recalculated for realistic molecular transition charge densities.

While limitations on participating $\mathbf{k}$-components are also operative at very small dipole–semiconductor separations for indirect-gap semiconductors, the very fact that the dipolar field contains substantial nonzero $\mathbf{k}$ contributions leads here to a qualitatively new consideration. This is the possibility of excitation of indirect electronic transitions without phonon assistance, the latter required for ordinary optical transitions and reflected in ε''_2. Coined as a "proximity effect" by the authors of ref 87, it was found most pronounced for indirect near-threshold transitions along the direction perpendicular to the semiconductor surface. Interestingly, this effect also exhibits a different larger-distance dependence, $\propto \Delta/d^4$, for energy transfer probability than revealed in classical result eq 12. Numerical results show that the phonon-assisted mechanism of indirect transitions can be less efficient than the phonon-less excitation by the dipolar field of the nearby molecular exciton. This effect may make prospects of nonradiative energy transfer into Si substrates even better.

Experimental studies of nonradiative energy transfer from molecular excitons into semiconductors are relatively few, particularly with regard to highly desirable detailed quantitative assessments of the distance and frequency dependence. A good coverage of the distance dependence for d between 20 and 400 Å was reported in ref 88, which studied the phosphorescence lifetime of the triplet $n\pi^*$ excitation of pyrazine (emission at $\hbar\omega \simeq 3.3$ eV) in the vicinity of the intrinsic GaAs surface. The observed lifetime dependence on separation d was generally found in good quantitative agreement with the predictions of the classical macroscopic theory,[76] yet with some discrepancies at

short distances possibly displaying the distance dependence slightly greater than in eq 12. Overall, the lifetime was observed to decrease by more than 2 orders of magnitude when moving to smaller separations, indicating that the dominant decay mechanism becomes the transfer of energy to electron−hole pair excitations in GaAs via the high-wave-vector components of the dipolar field.[88]

In the study of ref 85, the fluorescence decay of submonolayer pyrene films (emission wavelengths ∼390−480 nm) was measured at distances d from 20 to 200 Å from the surface of intrinsic Si. The observed dynamics and dependences were determined by both energy transfer and trapping within pyrene layers as well as by energy transfer into the Si substrate. The data clearly show that as the distance to the substrate decreases, the fluorescence decay becomes faster and its quantum yield is reduced, thus confirming that nonradiative energy transfer from pyrene to Si becomes an efficient decay channel for above the band gap molecular excitations.

Another kind of a hybrid organic−inorganic system was studied recently[89] on the basis of amorphous silicon (band gap ∼1.6 eV) and semiconducting conjugated polymers MEH-PPV (energy gap ∼2.3 eV) and P3HT (∼2 eV). Both bilayer planar and nanostructured (ordered arrays of silicon nanopillars) geometries have been explored. In this system, both charge and energy transfer can occur as excitons excited in the polymer migrate toward the polymer−inorganic−semiconductor interface, and the presence of the oxide layer can especially significantly affect the charge transfer. In studying the photoluminescence quenching of the polymer excitons, the authors of ref 89 found that in the case of MEH-PPV at least 80% of quenched excitons undergo energy transfer and estimated that this number becomes 30% in the case of P3HT. While apparently confirming the efficacy of nonradiative energy transfer, the principle of solar cell operation of this system is still ultimately in the eventual charge separation at the interface with electrons and holes residing on its different sides.

Hybrid organic/inorganic nanocomposites have been studied in ref 90 composed of alternating monolayers of *J*-aggregates of the cyanine dye and crystalline semiconductor quantum dots grown by a layer-by-layer self-assembly technique. Energy transfer from *J*-aggregates to inorganic quantum dots has been reported to achieve efficiencies of up to 98% at room temperature.

Direct illustrations of viability of true energy-transfer based photovoltaic operational principle came recently from experimental studies[71,90−92] of a different type of hybrid systems in which the role of efficient light absorbers and energy-transfer donors is played not by organic molecules but by nanocrystal semiconducting quantum dots (QDs).

Studied in ref 71 was a patterned p−i−n structure consisting of multiple periods of GaAs quantum wells with AlGaAs barriers in which channels were fabricated that then would be filled with colloidal CdSe/CdS QDs (see Figure 10). Lateral energy transfer from QDs to the patterned structure was demonstrated to be a new nonradiative decay channel for the photoexcited QDs. Comparing the fluorescence decay of QDs on glass and in the patterned structure, the authors estimated the nonradiative energy transfer efficiency from QDs in the patterned configuration at 79% (QDs in the vicinity of the exposed patterned semiconductor surface). Furthermore, a dramatic 6-fold enhancement of the photocurrent was found in the patterned hybrid devices in comparison with the bare p−i−n structure. By studying and modeling the photoluminescence decay of the quantum wells, the authors estimated that about 89% of the energy is injected into the wells through nonradiative energy transfer from the QDs. They also noted that the studied configuration is not limited to QDs but should be applicable to other solution-based highly absorbing semiconductor materials.

The feasibility of nonradiative energy transfer from QDs to buried quantum wells was also demonstrated in ref 91 for the case of PbS QDs (emission at ∼965 nm) and InGaAs wells (energy gap ∼1100 nm) in the GaAs substrate (∼ 873 nm). The near surface quantum well in this study was a short period superlattice buried about 3 nm below the sulfur-passivated GaAs surface on which submonolayer coverages of QDs were deposited (the distance from the monolayer to the well about 8 nm). To eliminate feeding of the quantum well by electron−hole pairs generated in the substrate, the authors in particular used the excitation at wavelength of 910 nm. Comparison of the QD photoluminescence intensity in the absence and in the presence of the buried quantum well yielded about a 35% reduction in the latter case. Accompanying this reduction was the observed faster (by about 40%) decay rate of the luminescence: the mean luminescence decay time changed from 298 ns on GaAs to 208 ns on the buried well. From these measurements, the authors estimated the nonradiative transfer time of about 690 ns, which is to be compared to the radiative decay time of QDs of 960 ns. That translates into ∼30% nonradiative transfer efficiency to the quantum wells from these QDs with a 30% quantum yield. The transfer efficiency would increase to 60% for near-unity quantum yield quantum dots. Applying eq 13 with $n = 4$ to their results, the authors extracted a surprisingly substantial size $R_0 \approx 8.9$ nm for the Förster radius.

One more illustration to support the potential feasibility of the solar cell paradigm based on nonradiative energy transfer from highly absorbing QDs to adjacent high-carrier-mobility channels came in ref 92 studying the system where PbS nanocrystals were deposited on the top of a planar array of Si nanowires. In this work, the time-resolved measurements of the photocurrent in nanowires were performed and comparisons made of systems with and without deposited QDs. On the basis of their previous study,[91] the expectation was that nonradiative energy transfer time would be on the order of hundreds of nanoseconds, while the direct absorption in quantum wires should result in a much faster response. The expected separation of time scales was indeed observed in reported measurements, showing a clear enhancement of the photocurrent at delay times of tens to hundreds of nanoseconds. The integrated photocurrent in the sample with QDs was wound to be enhanced by a factor of 1.8. In estimations of the authors, the efficiency of energy transfer was in the range of 15−40%.

Experimental demonstrations of nonradiative energy transfer into Si-based nanostructures should be particularly noteworthy given the maturity of Si technologies. Further evidence of the practical potential of such processes for photovoltaic devices was provided recently in ref 93 that studied hybrid structures consisting of a monolayer of colloidal CdSe nanocrystals grafted on hydrogenated Si surfaces. Comparative spectroscopic measurements of QD photoluminescence lifetime were quantitatively analyzed revealing a 65% efficiency of nonradiative energy transfer from QDs centered about 4.4 nm away from the Si surface.

2.3. Strong-Coupling Regime

2.3.1. Hybrid 2D Frenkel−Wannier−Mott Excitons at the Interface of Organic and Inorganic Quantum Wells.

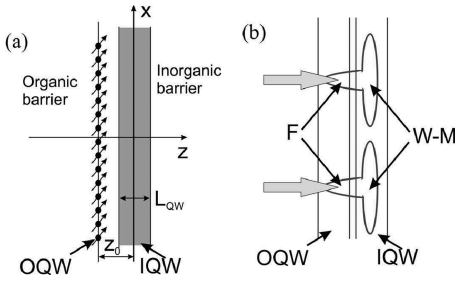

Figure 12. (a) Schematically, a planar structure consisting of inorganic (IQW) and organic (OQW) quantum wells. (b) The Frenkel and W−M excitons in this nanostructure interact to form hybrid excitons.

The interaction of Frenkel and W−M excitons at the interface of a hybrid nanostructure can be strong. In this so-called strong-coupling regime, new eigenstates (hybrid excitons) would result as appropriate coherent linear combinations of large-radius exciton states in the inorganic material and small-radius exciton states in the organic medium. In contrast to the hybridization of excited states of two resonant molecules, for instance, in liquids, in the hybrid structure the interacting are two resonance excitations whose energies and wave functions depend on continuous quantum numbers (such as the 2D in-plane wave vector $\mathbf{k}$ in planar structures). The hybrid electronic excitations are characterized by a radius dominated by their 2D W−M component and by an oscillator strength dominated by their Frenkel component. One of the most natural choices to implement this idea is a layered structure with an interface between a covalent semiconductor and a crystalline molecular semiconductor (Figure 12a). We can say that a hybrid exciton will interact with light through its Frenkel component and interact with other hybrid excitons through its large-radius W−M component (Figure 12b). Following ref 6, we now describe this situation in more detail.

The total Hamiltonian $\tilde{H}$ of this system can be written as

$$\tilde{H} = \hat{H}_{\mathrm{F}} + \hat{H}_{\mathrm{W}} + \hat{H}_{int} \tag{14}$$

where the Frenkel-exciton Hamiltonian is

$$\hat{H}_{\mathrm{F}} = \sum_{l\mathbf{k}} E_l^{\mathrm{F}}(k) A_l^{\dagger}(\mathbf{k}) A_l(\mathbf{k})$$

and, analogously, the Wannier−Mott exciton Hamiltonian is

$$\hat{H}_{\mathrm{W}} = \sum_{l\mathbf{k}} E_l^{\mathrm{W}}(k) B_l^{\dagger}(\mathbf{k}) B_l(\mathbf{k})$$

Here, index l labels the space-quantized molecular excitons in $\tilde{H}_{\mathrm{F}}$, and the WM excltons in $\tilde{H}_{\mathrm{W}}$. Their respective creation operators are denoted as $A_l^{\dagger}(\mathbf{k})$ and $B_l^{\dagger}(\mathbf{k})$, and the energies are written as dependent only on the wavenumber $k = |\mathbf{k}|$. Characterization of the exciton states by the 2D wave vector $\mathbf{k}$ (in the first Brillouin zone) assumes perfect 2D translational symmetry. The interaction $\tilde{H}_{\mathrm{int}}$ in eq 14 mixes organic and inorganic excitons:

$$\hat{H}_{int} = \sum_{l,l',k} \langle F, l, \mathbf{k} | \hat{H}_{int} | W, l', \mathbf{k} \rangle A_l^{\dagger}(\mathbf{k}) B_{l'}(\mathbf{k}) + \mathrm{h.c.}$$

(The diagonal terms are included in the exciton energies $E_l(k)$.) Consider now the case when for some fixed band indices l and l', the difference $|E_l^{\mathrm{F}} - E_{l'}^{\mathrm{W}}|$ is small in comparison with the energy separation from other exciton bands. One then can look for solutions of the Schrödinger equation $\hat{H}\mathbf{\Psi} = E\mathbf{\Psi}$, which are combinations of the resonating exciton bands only. Next

$$\Psi(\mathbf{k}) = A_l \Psi_l^{\mathrm{F}}(\mathbf{k}) \Phi_{\mathrm{IQW}} + B_l \Psi_{l'}^{\mathrm{W}}(\mathbf{k}) \Phi_{\mathrm{OQW}}$$

where Φ_{OQW} ($\mathbf{\Psi}_l^{\mathrm{F}}(\mathbf{k})$) and Φ_{IQW} ($\mathbf{\Psi}_{l'}^{\mathrm{W}}(\mathbf{k})$) are the respective ground (excited) state wave functions of organic and inorganic layers. For thin organic and inorganic layers, we consider the mixing between the lowest exciton states only and, correspondingly, omit indices l and l' in the following. The Schrödinger equation is now written as a system of two equations for the amplitudes A and B:

$$\begin{aligned} A(E^{\mathrm{F}}(k) - E) + B\langle F, \mathbf{k} | \hat{H}_{int} | W, \mathbf{k} \rangle &= 0 \\ A\langle W, \mathbf{k} | \hat{H}_{int} | F, \mathbf{k} \rangle + B(E^{\mathrm{W}}(k) - E) &= 0 \end{aligned} \tag{15}$$

Eigenvalues of the system eq 15 determine energies $E(k)$, eq 18, of two hybrid Frenkel−W−M excitations as functions of the wavenumber k. In a hybrid state, the excitation could be in the Frenkel state or in the W−M state with the corresponding probability equal to the weight coefficients. The latter are evaluated from solutions of eq 15 under the normalization condition $|A|^2 + |B|^2 = 1$. One thus obtains

$$|A(k)|^2 = \frac{\Gamma^2(k)}{[E^{\mathrm{F}}(k) - E(k)]^2 + \Gamma^2(k)} \tag{16}$$

$$|B(k)|^2 = \frac{[E^{\mathrm{F}}(k) - E(k)]^2}{[E^{\mathrm{F}}(k) - E(k)]^2 + \Gamma^2(k)}$$

where parameter

$$\Gamma(k) = |\langle F, \mathbf{k} | \hat{H}_{int} | W, \mathbf{k} \rangle| \tag{17}$$

determines the strength of the interaction between Frenkel and W−M excitons.

In the effective mass approximation, the W−M exciton energy is represented as $E^{\mathrm{W}}(k) = E^{\mathrm{W}}(0) + \hbar^2 k^2/2M$, where $M = m_{\mathrm{e}} + m_{\mathrm{h}}$ is the exciton effective mass in the plane of the semiconductor QW. The effective mass of Frenkel excitons is usually much larger than the effective mass of Wannier−Mott excitons, and one can neglect the k-dispersion of the Frenkel exciton energy E^{F}. In such an approximation, the hybrid exciton dispersion curves for the upper (u) and lower (l) branches are given as

$$E_{\mathrm{u,l}}(k) = E^{\mathrm{W}}(0) + \frac{\delta}{2} + \frac{\hbar^2 k^2}{4M} \pm \left[\left(\frac{\delta}{2} - \frac{\hbar^2 k^2}{4M} \right)^2 + \Gamma^2(k) \right]^{1/2} \tag{18}$$

where the detuning $\delta = E_{\mathrm{F}}(0) - E_{\mathrm{W}}(0)$.

It is worthwhile to note that the k-dispersion of exciton energies $E_{\mathrm{u,l}}(k)$ may be substantially affected by the dispersion of the interaction parameter $\Gamma(k)$ in eq 17. The origin of its dependence on k is clarified below where we indicate main steps in its calculation while referring the reader to refs 6,20 for more detail. For simplicity, a heterostructure shown in Figure 12 is considered. It consists of an inorganic QW of width L_{W} and an organic monolayer placed at distance $z_0 > 0$. The generalization to the case of several molecular monolayers is straightforward and does not change the essence of the main results.

2.3.1.1. Interaction Parameter Γ(k). Parameter Γ of eq 17 determines the mixing of resonating Frenkel and Wannier−Mott excitons and depends on the relevant distribution of the transition

dx.doi.org/10.1021/cr100156x |*Chem. Rev.* 2011, 111, 5179–5214

charge densities. In the electric dipole approximation, the interaction Hamiltonian in eq 14 can be written as

$$\hat{H}_{int} = -\sum_{\mathbf{n}} \hat{\mathbf{P}}_{\mathbf{n}} \cdot \hat{\mathbf{E}}(\mathbf{n}) \tag{19}$$

where

$$\hat{\mathbf{P}}_{\mathbf{n}} = \mathbf{P}^{0f}(A_{\mathbf{n}}^{\dagger} + A_{\mathbf{n}})$$

is the electric dipole operator for a molecule at site $\mathbf{n}$, $\mathbf{P}^{0f}$ being the transition dipole moment of a single molecule (we assumed that organic molecules have a center of symmetry) and $A_{\mathbf{n}}^{\dagger}$ the exciton creation operator. $\tilde{\mathbf{E}}(\mathbf{n})$, on the other hand, is the operator of the electric field produced by the inorganic QW polarization.

The Frenkel exciton wave function in state f and with the wave vector $\mathbf{k}$ can be presented in the form:

$$\Psi^{F}(\mathbf{k}) = \frac{1}{\sqrt{N}} \sum_{\mathbf{n}} \chi_n^f \, exp(i\mathbf{k}\cdot\mathbf{n}) \tag{20}$$

where $\chi_{\mathbf{n}}^{f} = \phi_{\mathbf{n}}^{f} \Pi_{\mathbf{m}\neq\mathbf{n}} \phi_{\mathbf{m}}^{0}$ is the wave function of the molecule $\mathbf{n}$ in an excited nondegenerate state f (N is the total number of molecules). As the hybrid exciton wave functions are given as the products of the organic and inorganic quantum wells wave functions, the transition matrix elements of eq 19 between resonating states may be written in the form:

$$\langle F, \mathbf{k}|\hat{H}_{int}|W, \mathbf{k}\rangle = -\sum_{\mathbf{n}} \langle F, \mathbf{k}|\hat{\mathbf{P}}_{\mathbf{n}}|0\rangle \cdot \langle 0|\hat{\mathbf{E}}(\mathbf{n})|W, \mathbf{k}\rangle \tag{21}$$

One factor in the sum in eq 21 follows from eq 20 as

$$\langle F, \mathbf{k}|\hat{P}_{\mathbf{n}}|0\rangle = \frac{\mathbf{P}^{0f}}{\sqrt{N}} \, exp(-i\mathbf{k}\cdot\mathbf{n})$$

The other factor corresponds to the matrix element of the electric field produced by the IQW polarization whose calculation we discussed in section 2.1. For this reason, here we will outline only final results for the same simplified microscopic quantum mechanical model of a 2D W−M exciton, in which the polarization vanishes for $|z| > L_w/2$ and in the approximation of the infinitely deep well. As in the calculations of section 2.1, one finds that the interaction of the excitations in the organic and inorganic layers is finite only for two of the W−M exciton polarizations, the corresponding interaction parameters denoted as $\Gamma_Z(k)$ and $\Gamma_L(k)$. Here, we quote the result only for the L-modes where vector $\mathbf{d}^{vc}$ is parallel to vector $\mathbf{k}$ (see refs 6,20). Without loss of generality, one can take vector $\mathbf{k}$ along the x-axis, then

$$\Gamma_L(k) = \frac{4d_x^{vc}(k)\sqrt{(P_x^{0f})^2 + (P_z^{0f})^2}}{a_F a_B L_W} \frac{q^2}{k^2 + q^2} K(\varepsilon, k) \, exp(-kz_0) \tag{22}$$

where $q = 2\pi/L_W$ and function

$$K(\varepsilon, k) = \frac{1 - exp(-kL_W)}{(\varepsilon + 1)/2}$$

This interaction parameter does not depend on the orientation of $\mathbf{P}^{0f}$ in the xz-plane and has its maximum when $\mathbf{P}^{0f}$ is parallel to the plane of the well. The behavior of eq 22 as a function of wavenumber k is illustrated in Figure 13; it clearly exhibits a nonmonotonic behavior vanishing in the limits of both very small and very large k.

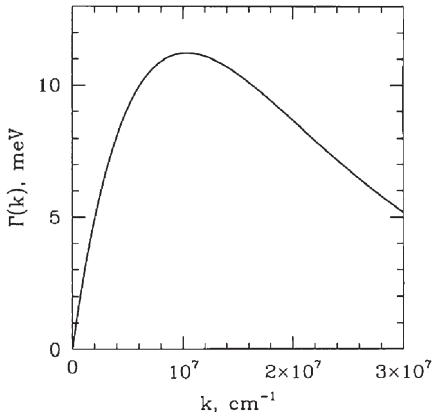

Figure 13. The interaction parameter $\Gamma(k)$ for $d^{vc} = 12$ D, the transition dipole moment in organic molecule $d^{F} = 5$ D, $a_B = 2.5$ nm, $a_F = 0.5$ nm, $L_W = 1$ nm, $z_0 = 1$ nm, and the dielectric constant in QW and in organics $\varepsilon_\infty = 6$, $\tilde{\varepsilon}_\infty = 4$.

Panels of Figure 14 demonstrate the resulting dispersion eq 18 of new hybrid exciton states as well as the weight eq 16 of the Frenkel component in the lower-branch exciton. Both Figures 13 and 14 illustrate calculations for an inorganic QW of the II−VI type semiconductor ($ZnSe/Zn_{0,69}Cd_{0,31}Se$) exploiting numerical values of $\varepsilon = \varepsilon_\infty = 5.4$, $d^{vc}/a_B 0.1e$ (which corresponds to d^{vc}12 D and a Bohr radius of 4 nm), the exciton mass $M_W = 0.32m_0$, $E^{W} = 2700$ meV, and the well width $L_w = 1$ nm. For the organic part of the structure, typical parameters for such media were used: $\tilde{\varepsilon} = \tilde{\varepsilon}_\infty = 4$, the transition dipole for the molecules in the monolayer $d^{F} = 5$ D, and $z_0 = 1$ nm. The dispersion curves of upper and lower braches $E_{u,l}(k)$ are plotted in Figure 14 for three different values of the energy detuning parameters: $\delta = 10$ meV, $\delta = 0$, and $\delta = -10$ meV. The interesting feature of the lower branch is the appearance of the negative group velocity region at small wave vectors and energy minima at some value of wave vector $k \neq 0$. At low temperatures, such minima will be populated, and the intensity of the luminescence along the normal to the QW can be expected to increase with the increased temperature.

One can see that the characteristic energy of the interaction of Frenkel and W−M excitons varies within a region on the order of 10 meV for considered values of the system parameters. It determines the value of the splitting at the resonance and the typical times of interconversion between Frenkel and W−M excitons. The latter time, as estimated from the uncertainty principle, then turns out to be on the order of 0.1 ps. This is much shorter than the radiative lifetime of Frenkel or W−M excitons. Qualitatively this conclusion can be rationalized when one recalls that the resonant exciton−photon interaction energy, which determines the exciton radiative lifetime, is roughly a product of the exciton transition dipole moment and the amplitude of the electric field of the photon. As the photon is spatially distributed, its electric field at the point of the exciton dipole moment location is much weaker than the electric field produced by a nearby Frenkel exciton large transition dipole moment. Relatively shorter times for energy transfer explain why Frenkel excitons can effectively diffuse in organic solids. The same of course also applies in the weak coupling regime (section 2.1) where we found nonradiative energy transfer times in hybrid structures shorter than radiative times.

One should note, however, that the fabrication of strongly coupled hybrid QW structures would demandingly require a nearly

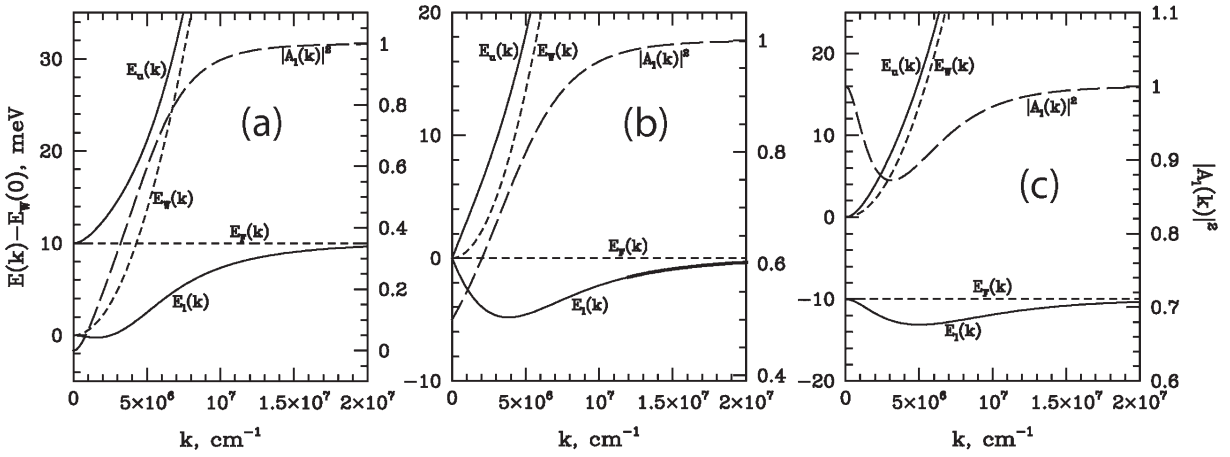

Figure 14. (a) The dispersion $E_{u,l}(k)$ of the upper and lower hybrid exciton branches (−) and that of the unperturbed Frenkel and Wannier excitons (- - -). The "weight" of the FE component in the lower branch $|A_l(k)|^2$ is shown by "− − −". The interaction parameters are the electric transition dipole between the conduction and valence band $d^{vc} = 12$ D, the transition dipole moment in organic molecule $d^F = 5$ D, $a_B = 2.5$ nm, $a_F = 0.5$ nm, $L_W = 1$ nm, $z_0 = 1$ nm, the effective mass of Wannier exciton $m_W = 0.7m_0$, dielectric constant in QW and in organics $\varepsilon_\infty = 6$, $\tilde{\varepsilon}_\infty = 4$, and the detuning $\delta = E_F(0) - E_W = 10$ meV. (b) Same as in (a) but for $\delta = 0$. (c) Same as in (a) but for $\delta = -10$ meV. Reprinted with permission from ref 6. Copyright 1994 Pergamon.

perfect interfacing of crystalline inorganic and organic components. Perhaps even more difficult is to find appropriate crystalline organic materials with strong and narrow exciton transitions. In our consideration of the hybrid excitons above, we completely neglected the dissipation. The W−M excitons, at least at low temperatures, can indeed have very small dissipation widths on the order of few meV. In the majority of organic solids, on the other hand, the dissipation width of the lowest energy Frenkel excitons even at low temperature is larger than or comparable to 10 meV. Still, attempts at making such organic−inorganic nanostructures are in place; one example of such an effort can be found in ref 94. Another example corresponds to 2D Frenkel excitons in the outermost monolayer of anthracene crystals, where the line width at low temperature is smaller than 1 meV (for more on the theory and experiments for the outermost monolayers in anthracene, see papers by Philpott and Turlet[95,96]). Many organic materials have a layered structure, and it is tempting to wonder if methods similar to those used for the production of graphene sheets could be applied to derive perfect organic monolayers with large oscillator strengths and narrow absorption and luminescence spectra.

2.3.2. Optical Nonlinearities. Calculations[11] of the figure of merit for the resonant $\chi^{(3)}$ nonlinearity showed that ratio η of the figure of merit of the hybrid organic−inorganic nanostructure M_{hybr} and the figure of merit of the semiconductor component alone M_{semQW} is determined as

$$\eta \simeq \left(\frac{a_B}{a_F}\right)^2 \tag{23}$$

where a_B and a_F are the radii, respectively, of the W−M and Frenkel excitons in the hybrid structure. The enhancement factor eq 23 can be large whenever the Bohr radius of the exciton in the semiconductor QW is large in comparison with the size of the organic molecule. For instance, if a_B is about 5 nm while the size of the molecular exciton is about 0.5 nm, the enhancement of the resonant nonlinearity in the hybrid structure in the strong-coupling regime (for a given pump intensity) can be about 2 orders of magnitude in comparison with a stand-alone typical inorganic semiconductor QW.

Qualitatively, relation eq 23 can be derived using simple estimates for the hybrid excitons analogous to those made at the end of section 1.2 for the resonance nonlinearity in the stand-alone QW. In a hybrid structure, the concentration n_{hybr} (per unit area) of hybrid excitations is determined by the absorption of the incident radiation by the organic component of the hybrid excitons and therefore proportional to $n_{hybr} \propto FI_P$, where $F \propto a_F^{-2}$ is the oscillator strength of the organic layer per unit area and I_P the intensity of pumping. At the same time, the saturation density in the hybrid structure is nearly the same as in the stand-alone semiconductor QW. As discussed in section 1.2, the generic figure of merit for all optical nonlinearities for such QWs scales as $I_P^{-1}(\Delta\chi/\chi)$, where $\Delta\chi$ is the nonlinear part of the susceptibility in the presence of the pump of intensity I_P. In the hybrid structure, the ratio is still of the same form $\Delta\chi/\chi \approx n/n_S$; now, however, n and n_S are the concentration and saturation density of the hybrid excitons (per unit area). The concentration of W−M excitons in the stand-alone QW would be $n_{semQW} \propto fI_P$, where $f \propto a_B^{-2}$ is the oscillator strength of W−M excitons per unit area. Hence, the ratio of the figures of merit of the hybrid structure and the stand-alone QW, eq 23, follows as largely determined by the ratio n_{hybr}/n_{semQW} of the concentrations of the radiation-produced excitons. The high nonlinearity of semiconductor QWs is used in many applications.[5,23] It is important for hybrid structures that semiconductor QWs can be effectively pumped not only optically but also electrically.

While we have specifically discussed above hybrid excitons at the interface of organic and inorganic materials, it should be clear that, in a sense, similar hybrid states can arise at interfaces between other ordered media with resonating excitations. For instance, hybrid states can be created at the interface of two inorganic quantum wells with resonating Wannier−Mott excitons. If the Bohr radius of the exciton in one of the QWs is much smaller than the Bohr radius of the exciton in the second QW, one can expect effects of the strong coupling analogous to what we just considered for organic−inorganic hybrids.

2.3.3. Second-Order Susceptibility. Hybrid structures in the regime of strong coupling can also have a nonvanishing second-order susceptibility $\chi^{(2)}$ even if the organic and inorganic quantum wells separately possess central symmetry (so that the

second-order processes in each of them are forbidden by the parity conservation). This phenomenon can take place in the hybrid structure because the resonant dipole−dipole-type coupling breaks the symmetry along the growth direction. Of course, any interaction between the organic and inorganic QWs can be responsible for the symmetry breaking. However, the resonant dipole−dipole coupling we are concerned with is likely the strongest among different possibilities. Geometrically, such a system is analogous to an asymmetric semiconductor QW. Calculations of $\chi^{(2)}$ for an asymmetric semiconductor QW can be found in ref 97; evaluations of $\chi^{(2)}$ for hybrid systems may be performed along the lines of their consideration. A detailed analysis of the second-order nonlinear susceptibility of hybrid structures will be discussed elsewhere. A theory of the enhanced second harmonic generation by the quadrupole-dipole hybrid exciton at the interface of cuprous oxide crystals, resonantly hybridized with an organic material, was developed by Roslyak and Birman.[70]

This and other predicted effects could be tested once the strong-coupling regime in hybrid systems is realized experimentally.

3. ORGANIC AND HYBRID NANOSTRUCTURES IN A MICROCAVITY

3.1. Strong Exciton−Photon Coupling and Polaritons

Our discussion of the properties of excitons in previous sections assumed the weak interaction of excitons and photons. When the exciton−photon interaction is a weak perturbation, it does not modify the nature of quasiparticles in a very substantial way. A typical example of the weak-coupling regime effect is the appearance of the radiative width of excitons (or excited states in molecules and atoms), which can be calculated using Fermi's Golden Rule. We will now turn to the discussion of the effects associated with the strong interaction between excitons and photons.

The separation into limiting cases of weak- and strong-coupling regimes here is based on considerations similar to the discussion in section 1.1. The broadening of excitonic states γ_{exc} is determined by their interaction with phonons (so-called homogeneous broadening) and by crystal defects (inhomogeneous broadening). The photonic dephasing rate γ_{phot} depends on the excitation source and the geometry; in the microcavity configuration, it is determined by the photon's finite lifetime within microcavity. The exciton−photon interaction is considered strong when the exciton−photon interaction strength W is substantially larger than the broadenings of the bare exciton and photon states: $W \gg \gamma_{exc}, \gamma_{phot}$. In the strong exciton−photon coupling regime, new quasiparticles are formed, which are called in modern literature polaritons. Depending on the origin of the excitations, various realizations are frequently specified as exciton-polaritons, plasmon-polaritons, phonon-polaritons, etc. In many experimental situations under the strong exciton−photon coupling regime (where the strong coupling takes place at relatively small wave vectors), it is in fact polaritons, and not excitons, that determine the optical response of solids.

In ideal crystals, excitonic states are derived as solutions of the Schrödinger equation that takes into account the instantaneous Coulomb interaction between all charged particles. Because of the translational symmetry of the crystal, the states of excitons are characterized by the wave vector $\mathbf{k}$, which is a continuous quantum number. Different excitonic states can also be specified by discrete quantum numbers. We denote energies of these so-called Coulomb excitons[86] as $E_s(\mathbf{k})$, where s is a discrete quantum number.

In organic molecular crystals, at least for the lowest excited states, the intermolecular interaction is rather weak, and molecules do not completely lose their individuality. In the simplest case of a single excited state (no mixing of molecular configurations), the wave function of the crystal with one exciton is given by eq 20. The energy $E_f(\mathbf{k})$ of this plane-wave exciton state, eq 20, generally depends on its wave vector $\mathbf{k}$.

The total electromagnetic interaction between charged particles, however, also contains its retarded part. One can incorporate the latter by introducing the coupling between Coulomb excitons and transverse photons. In ideal 3D crystals, this coupling takes place only between exciton and photon states with the same wave vector $\mathbf{k}$. The total Hamiltonian of the exciton−photon system can then be simply diagonalized with proper linear combinations of the bare exciton and transverse photon operators. These linear combinations correspond to polariton operators. As a result of the exciton−photon interaction, two polaritonic states appear for each $\mathbf{k}$ as discussed in detail in ref 98 for semiconductors and in ref 99 for molecular crystals. In a quantum-mechanical description, polaritons are linear superpositions of bare Coulomb excitons and bare photons; in this sense, polaritons can be regarded as hybrid quasiparticles.

The microscopic quantum-mechanical picture discussed above allows one to establish the correspondence between the site and the wave vector representations. The long-wavelength (small wave numbers $|\mathbf{k}|$) polaritonic states can, however, be derived already within the framework of the macroscopic classical electrodynamics of the condensed medium characterized by the dielectric tensor[35,86] $\varepsilon_{ij}(\omega,\mathbf{k})$ featuring an excitonic resonance. The dependence of the dielectric tensor on $\mathbf{k}$ (spatial dispersion) results mainly from the dependence of exciton energies $E_s(\mathbf{k})$ on the wave vector. In many cases, the quantum theory of polaritons turns out to be more convenient, particularly in the consideration of nonlinear optical and scattering processes, where the role of states with large wave numbers can be substantial. We will be using both quantum and classical descriptions of polaritons in what follows.

If the hybridization of only one exciton state and one transverse photon is taking place, the polaritonic spectrum consists of two branches of single quasiparticle hybrid states, known as the upper- and the lower-branch polaritons; see Figure 15. Far from the resonance (crossing of the excitonic and photonic dispersion curves), polaritons tend to the respective behavior the bare excitations. Near the resonance, however, the fractions of the exciton and photon content in polaritonic states are comparable. As is typical for two coupled resonating systems, the new states exhibit the avoided crossing behavior, and a gap opens in the spectrum between the two resulting branches. This gap is sometimes referred to as polariton splitting. As discussed below, the number of mixing states of qusiparticles (excitons and photons) depends on the geometry of the problem and on the material supporting excitonic states. This may result in a variety of different polaritonic spectra.

Since the theoretical work in the late 1950s,[98,99] where the microscopic theory of polaritons in optically isotropic and anisotropic crystals was developed, a series of experiments demonstrated the polaritonic effects in different solids and for different geometries. Here, we refer to optical properties of solids that would be not explainable within the picture of pure Coulomb excitons. A polaritonic effect was, for example, found in the

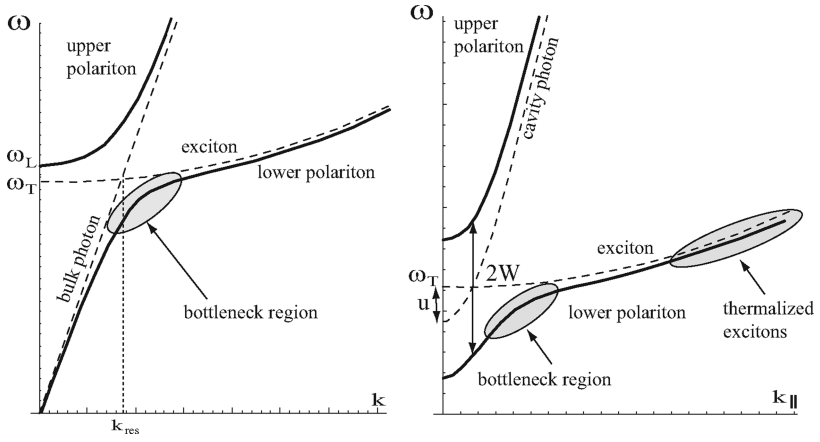

Figure 15. A not-to-scale sketch of the dispersion of the polariton in a bulk medium (left panel) and in a microcavity configuration (right panel) for an isotropic material with one excitonic resonance. Frequencies ω_L and ω_T correspond to, respectively, the zero and the pole of the dielectric function $\varepsilon(\omega,k)$ at $k = 0$. The wave-vector dependence of the exciton energy seen in the figure accounts for the mobility of excitons.

studies of the exciton diffusion in layers of anthracene crystals at low temperatures.[100] The resonance of excitons and transverse photons takes place at small **k**. The strong light−matter interaction in this region of spectrum produces a splitting and strong hybridization of the exciton and photon states. At nonresonant pumping and low temperatures, the relaxing excitations mainly populate the so-called "bottleneck" region of the lower branch of the polariton spectrum (Figure 15). It was found in ref 100 that these hybrid excitations can have a diffusion constant larger than the diffusion constant of the same sample at high temperatures by 2−3 orders of magnitude: the diffusion constant D of excitations in the anthracene crystal at room temperature is[101] $\simeq 5 \times 10^{-3}$ cm^2/s, while at low temperatures (1−30 K) the values of 1−10 cm^2/s were measured.[100] The polaritonic effects were also detected in the absorption and fluorescence in thin flakes of anthracene,[102] in measurements of group velocity in time-of-flight experiments,[103] in observations of exciton−polariton fluorescence,[104−106] and in the resonant Brillouin-scattering of exciton-polaritons.[107] We can also mention the early optical experiments in semiconductors including the sum and difference frequency generation in GaP,[108] the near-forward Raman scattering in anisotropic ZnO,[109] and in many other materials (see, e.g., the review in ref 110).

The structure of the polariton as a hybrid excited state can be qualitatively described by function $S(\omega)$ corresponding to the exciton component in the polariton. First calculations of this function can be found in the book by Born and Huang[111] within the classical theory of the electromagnetic waves in solids near the frequency of the optical dipole vibration. For polaritons in the vicinity of electronic excitations, function $S(\omega)$ was considered in refs 110,112. If the excitonic transition is strong, function $S(\omega)$ can be substantial both above and below the exciton frequency ω_{exc}. Polaritonic effects may take place at the low-frequency edge of the exciton absorption. At the surface of a solid, the incident photon transforms into a polariton propagating in the solid with the same frequency. Upon the neglect of retardation, the frequency $\omega_{exc}(\mathbf{k} = 0)$ would determine the low-frequency edge of the absorption (for excitons with a positive effective mass). With the retardation effects included, function $S(\omega) \neq 0$ even at $\omega < \omega_{exc}(\mathbf{k} = 0)$. Hence, polaritons with frequencies below $\omega_{exc}(\mathbf{k} = 0)$ would contain an exciton contribution, and the absorption of light occurs as the virtual exciton is scattered by phonons. The low-frequency edge of the absorption is thus red-shifted. The shift can be up to 100 wave numbers,[113] thereby contributing[114] to the well-known Urbach-rule behavior of the near-the-edge absorption. For a discussion of the role of retarded interactions in nonlinear optical susceptibilities, see ref 115. The light−matter interaction picture is valid also in the vicinity of plasmonic (plasmon-polaritons) and optical phonon (phonon-polaritons) resonances.

3.1.1. Surface Polaritons. Our main interest in this Review is on polaritons formed as a result of the exciton−photon interaction in organic and hybrid nanostructures of the reduced dimensionality (2D). Polaritons in a planar microcavity configuration (cavity polaritons) have been studied since the early 1990s, after the observation[116] of the polariton splitting in a microcavity with a GaAs quantum well.

The strong coupling of 2D-light and 2D-excitations and their hybridization in planar structures were first considered at interfaces. It was shown theoretically in ref 117 that the interaction of surface optical waves with a dipole-active excitation of a thin film attached to the surface produces the polaritonic splitting $\Delta_S \propto (d/\lambda)^{1/2}$, where $d \ll \lambda$ is the thickness of the film and λ is the surface polariton wavelength. As the absorption of the layer α is proportional to its thickness, $\Delta_S \propto (\alpha/\lambda)^{1/2}$. While the very fact of the appearance of the splitting in the excitation spectrum does not depend on the nature of the excitation in the layer (it can be an optical phonon, or a plasmon in a thin metallic film, or Frenkel or Wannier−Mott exciton in a thin dielectric), the nature of the excitation matters quantitatively: the larger is the oscillator strength of the excitation, the larger the splitting it produces. The splitting in the spectrum of the surface polariton waves has been now observed in infrared, visible, and ultraviolet regions of the spectrum (see refs 118,119 for a review).

The combinations of materials may also include both metallic films (supporting plasmons) and dielectric films (supporting excitons). The admixture of surface plasmon−polaritons may enhance the strength of the resonant coupling between light and an excitonic transition. Recently, a strong exciton−plasmon coupling for excitons in an organic layer of *J*-aggregates of cyanine dyes deposited on a silver film supporting a surface plasmon has been observed in ref 120. The splitting at the resonance between the Frenkel exciton and the surface plasmon was found equal to 180 meV at room temperature. This work was

already a second demonstration of the strong coupling of Frenkel excitons and surface plasmons, first observed in ref 121 for the Langmuir−Blodgett dye bimonolayer on silver, where, however, the observed splitting was much smaller. Nowadays, the strong coupling between surface plasmons and Frenkel excitons in thin films has been found in many studies (see, for instance, refs 122−126). For organic materials with a large oscillator strength of Frenkel excitons, the splitting can be even a few hundreds of meV. While the interaction of surface plasmons with electronic excitations in semiconductor GaAs/AlAs quantum wells results in a splitting of about 20 meV,[123] the giant splitting of 450 meV has been observed in ref 127 for exciton-plasmon states in a system with plasmons localized in nanodisks organized in arrays on the top of an organic semiconductor.

3.1.2. Cavity Polaritons. We now turn to the discussion of polaritons in a planar microcavity configuration, where quasiparticles are confined to the region of space between two planar mirrors. This is another case of quasi-2D polaritons in the sense that they are characterized by a 2D continuous wave vector (k_x,k_y).

It is instructive to first recall the properties of photons in such a microcavity. As is known from the Maxwell theory, in the uniform isotropic 3D medium the dispersion of photons, that is, the dependence of their frequency ω on the wavenumber $k = (k_x^2 + k_y^2 + k_z^2)^{1/2}$, is determined from the relation

$$\omega^2 = c^2k^2/\varepsilon_0 \tag{24}$$

where c is the speed of light in vacuum and ε_0 is the dielectric constant of the medium. Particularly simple is the case when the dielectric constant is frequency-independent resulting in the ordinary isotropic linear photon dispersion with frequency varying from zero to infinity. In a microcavity between two ideal planar mirrors, however, it is only the in-plane part of the wave vector, (k_x,k_y), that describes an unbounded motion and changes continuously. The z-component of the wave vector, k_z, can now acquire only discrete values that have to be found from the boundary conditions for the electromagnetic field in the microcavity. For the electric field vanishing at the mirrors (at $z = 0$ and at $z = L$), its spatial distribution between the mirrors would be given by

$$sin(k_z z)e^{i(k_x x + k_y y)}$$

if k_z satisfies $k_z L = \pi m$ with integer $m = 1, 2, ...$, yielding thus a discrete set of the allowed values. Let us discuss photons with the fixed smallest value of $k_z = \pi/L$. It then immediately follows from eq 24 that the corresponding 2D photons have now the frequency dispersion:

$$\omega_{cav}(k_x, k_y) = \omega_c[1 + L^2(k_x^2 + k_y^2)/\pi^2]^{1/2} \tag{25}$$

as a function of the two continuous wave vector components. Here:

$$\omega_c = \pi c/L\sqrt{\varepsilon_0} \tag{26}$$

is the so-called cutoff frequency, that is, the minimal possible frequency of the photon in the microcavity. It is important to note that, for instance, at $L \simeq 100$ nm and $\varepsilon_0 \simeq 3$, the cutoff frequency $\omega_c \approx 3 \times 10^{15}$ s^{-1}, which is on the order of the exciton frequencies in organic and inorganic solids. In the approximation of the ideal mirrors, the TE- and TM-polarized modes have the same dispersion eq 25.

If the medium, in addition, features an excitonic resonance at some frequency ω_T, its overall frequency-dependent dielectric function becomes

$$\varepsilon(\omega) = \varepsilon_0 + \frac{4W_1^2}{\omega_T^2 - \omega^2} \tag{27}$$

where W_1^2 is proportional to the oscillator strength of the resonance. Using this dielectric function instead of ε_0 in eq 24 for the same cavity-determined fixed value of k_z leads now to the following equation:

$$(\omega^2 - \omega_{cav}^2(k))(\omega^2 - \omega_T^2) = 4W^2\omega^2 \tag{28}$$

for the eigenfrequencies, where $W^2 = {W_1}^2/\varepsilon_0$, and we used k to denote the 2D wavenumber $k = (k_x^2 + k_y^2)^{1/2}$. Equation 28 determines the frequencies of the new eigenstates of the system. As the form of eq 28 indicates, they are superpositions of the cavity photons ($\omega = \omega_{cav}(k)$) and excitons ($\omega = \omega_T$); these states are called cavity polaritons. For each k, eq 28 yields two solutions for ω determining the dispersion of the two (upper and lower) branches of the polariton spectrum. In the resonance region $\omega \simeq \omega_T \simeq \omega_{cav}(k)$, eq 28 can be approximated quite accurately by a simpler equation:

$$(\omega - \omega_{cav}(k))(\omega - \omega_T) = W^2 \tag{29}$$

This approximation corresponds to what is usually referred to as a model of two coupled oscillators (the exciton and the photon). The solutions of eq 29 behave as shown in the right panel of Figure 15, with the resulting splitting in the polariton spectrum equal to $2W$ at resonance (the so-called Rabi splitting). The difference between the bottoms of the cavity photon and the exciton bands, so-called detuning $u = \omega_{cav}(k = 0) - \omega_T$, is determined by width L of the cavity. As will be discussed below, this simple model can be complicated by many factors, among which are the crystal anisotropy and the presence of several excitonic resonances or vibrational modes. All of those factors, however, can be understood on the same basis as the above model of two coupled oscillators. A complication of another kind, which does not fit into this model, comes from the so-called in-gap polaritons arising from the interaction of the excitonic polarization with higher order cavity photons (whose quantized values of k_z larger than π/L).) These modes can appear in the polariton gap, and in some cases they may change the measured value of the gap (see section 3.2.2).

As the electromagnetic field of a photon is confined in the small volume of a microcavity, its amplitude is much larger than for a photon in vacuum. As a result, the light−exciton interaction may become much larger than in the bulk. Therefore, resonance effects in microcavities are more pronounced, and the polariton picture becomes stable within a wider window of system parameters (in some materials, up to the room temperatures). Put another way, an exciton weakly interacting with light in a bulk crystal may demonstrate the strong coupling at the same temperature in the microcavity configuration. Also, unlike the bulk case, the ground state of cavity polaritons corresponds to finite energies (see Figure 15). This has been used to achieve a macroscopic population of the ground state leading to BEC-like phase transitions or lasing effects.[128,129]

An inorganic microcavity usually contains several quantum wells placed at the antinodes of the electric field to provide the strongest possible interaction between photons and quantum well excitons. An organic microcavity, as we actually assumed in

eq 27, is usually homogeneously filled by an organic material possessing an excitonic resonance with the (dispersionless) frequency ω_T close to the lowest ($m = 1$) cavity photon mode. The filling medium, in the simplest case of an isotropic material of a macroscopic width, can be characterized by its dielectric function with one or few resonances.

Since the first experimental observation[116] of the polariton splitting between a quantum well exciton and a cavity photon mode, the regime of strong light−matter coupling in planar microcavities has been examined extensively.[130,131] In widely used inorganic semiconductor quantum wells, the Rabi splitting typically varies between 4 and 10 meV. Recently, the interest in cavity polaritons has been revived due to the experimental observation of stimulated and self-stimulated polariton−polariton scattering. Numerous experiments have been carried out to exploit this property of cavity polaritons and to achieve their Bose−Einstein condensation or an associated phase transition.[128,129] The accumulation of lower branch polaritons in the lowest energy state was observed under different experimental conditions in inorganic microcavities, and the possibility of condensation of low-energy polaritons was extensively discussed.

Evidently, the same type of ideas and problems can be formulated also for organic microcavities with larger magnitudes of the Rabi splitting, which could provide the stability of the polaritonic picture at room temperatures and at higher pump densities. Below we review spectra of polaritons appearing in organic structures (sections 3.2, 3.3) and then the new physical processes typical for different organic microcavities (section 3.4). A discussion of the similarities and differences between inorganic and organic semiconductor microcavities operating within the strong coupling regime, as well as a discussion of the prospects for using organic−inorganic hybrid materials for optoelectronic devices, can be found in ref 9. Over the last several years, this area of research has quickly expanded.[19]

When a microcavity contains a hybrid structure, that is, both an organic and an inorganic quantum wells separated in space, one can expect that the resonant interaction between the states of Frenkel excitons in the organic layer and Wannier−Mott excitons in the semiconductor layer would also be taking place via the exchange with virtual cavity photons. If both inorganic and organic excitons have similar energies and are strongly coupled to the cavity photon mode, the hybrid states will now be superpositions of three states: a Frenkel exciton, a Wannier−Mott exciton, and a cavity photon, that hybridize to form new polaritons. These polaritonic states can be tailored to engineer the fluorescence efficiency and relaxation processes in the microcavity.[8,132] Hybrid microcavities are discussed in section 3.5.

3.1.3. Giant Rabi Splitting in Organic Microcavities. The value of the Rabi splitting energy $2W$ (see eq 29) is proportional to the square root of the oscillator strength of the excitonic transition. Estimates made in ref 8 show that an appropriately chosen organic material can produce the Rabi splitting about 2 orders of magnitude larger than the Rabi splitting in a microcavity containing a GaAs inorganic QW. Indeed, in experiments[133,134] with organic microcavities containing *J*-aggregates of cyanine dyes, the Rabi splitting magnitudes of 200−450 meV have been measured. Typical values of the gap observed in the microcavities containing organic crystals (such as anthracene and naphthalene) are 100−350 meV. Besides the possibility to exploit the strong coupling regime at room temperatures, which is potentially important for applications, the largeness of the Rabi splitting energy is also very important from the following considerations.

First, as discussed in sections 1.1 and 3.1, the strong coupling regime holds if the losses (characterized by the widths of the bare states) are smaller than the interaction-induced splitting (which is proportional to the interaction constant). The mirrors in typically used microcavities provide cavity photon lifetimes on the order of ∼100 fs, which corresponds to the bare photon line width ∼7 meV. A typical width of an excitonic transition in an organic material is, however, ∼50−100 meV, which in many cases is comparable to the light−matter interaction constant. That is why, before the first observation of the strong-coupling regime in ref 133, organic materials were usually associated with the weak coupling regime.

Second, the largeness of the Rabi splitting energy turns out to be quite important for energy relaxation in a microcavity. The strong mixing of excitons and cavity photons takes place only within a very small fraction of the wave-vector-space, close to the dispersion curve of light. Those wave numbers k are much smaller than the typical wave numbers of thermalized excitons (see Figure 15). The relaxation of nonresonantly pumped excitons in an inorganic semiconductor microcavity to these small-k states, being mediated by acoustic phonons, is a slow and inefficient process with a chracteristic time scale of nanoseconds and longer. The relaxation is slowed at the "knee" of the lower polariton branch near the strong coupling region, where the radiative losses increase due to the growth of the photonic fraction in the polaritonic state, and the relaxation itself is impeded due to the decrease of the excitonic fraction (the so-called "bottleneck effect").[135] Because of this bottleneck, the spontaneous emission from microcavities in the strong-coupling regime in many experimental situations remains dominated by uncoupled excitons, in contrast to the anticipations expressed in early studies.

The situation changes for organic microcavities as the large values of the Rabi splitting energies allow not only for acoustic-phonon-assisted relaxation, but also for relaxation via emission of optical phonons and intramolecular vibrations. The quanta of these excitations are on the order of 50−100 meV, comparable both with the Rabi splitting energy and with the energy distance to the "reservoir" of incoherent exciton states. This mechanism can thus provide a way for a one- or two-step relaxation. In addition, the restrictions of the wave vector conservation can be relaxed for such transitions (both for crystalline and for amorphous organic materials). Indeed, even if vibrational excitations form bands, as may happen in organic crystals, their bandwidths ∼5 meV remain very narrow in comparison with the polaritonic energy scales. The neglect of the wave vector of the vibrational excitation would correspond to the adiabatic approximation, where the vibronic excitations are treated as the slow subsystem while the polaritons as the fast one. The inelastic scattering of polaritons by vibronic excitations may provide an efficient (section 3.4.1) energy relaxation channel for polaritons in large-Rabi-splitting microcavities (organic as well as hybrid) and may thus assist in the creation of a macroscopic population in low-energy states. In recent studies[136] of the relaxation processes in organic microcavities with *J*-aggregates of a cyanine dye, the ultrafast polariton dynamics with times ∼50 fs was observed for transitions from the upper-branch polaritons to incoherent exciton states. This observation explains the relative weakness of the upper-branch luminescence determined from continuous-wave measurements.

As polaritons in organic microcavities are quite stable at room temperatures, one may hope to observe bosonic effects such as stimulated scattering or a BEC-like phase transition at unusually high temperatures. In some materials, vibronic resonances can also have large enough oscillator strengths to couple strongly with photon modes in the same way as the excitonic transition does. In this case, several low-energy polaritonic gaps may open, leading to a rather complicated energy spectrum of polaritons consisting of many branches. Such a picture was observed, for instance, in refs 137−139. A theoretical description of the linear response and photoluminescence for this case was worked out in refs 140,141.

3.2. Microcavities with Crystalline Organic Materials

Although the strong exciton−photon coupling in organic microcavities was first observed in disordered samples,[133] we will start here from a picture in crystalline microcavities unaffected by the presence of disorder. The strong-coupling regime in microcavities uniformly filled with single-crystal anthracene was observed in refs 137,142,143.

Besides large Rabi splitting energies, a distinctive feature of crystals such as anthracene, naphthalene, tetracene, or pentacene is their strong optical anisotropy. Below, we discuss two effects, which are typical for these structures: the smoothing of the anisotropy (section 3.2.1) and the appearance of the in-gap states (section 3.2.2). Another characteristic feature of these systems is the presence of exciton−vibron excitations with oscillator strengths large enough to produce additional Rabi splittings in the excitation spectra. In section 3.2.3, we describe experimental observations of the strong exciton−vibron−photon and exciton−photon coupling in organic monocrystalline microcavities.

3.2.1. Cavity Polaritons in Anthracene-type Crystals. As an example of an anisotropic organic crystal, consider the case of a layered anthracene-type structure. The unit cell of the crystal contains two molecules with the same electronic transition energies but different orientations of their transition dipole moments. The number of excitonic bands in a crystal produced by this transition is equal to the number of molecules in the unit cell of the crystal (the so-called Davydov splitting[144]). The excitonic bands in a crystal of the anthracene type form the so-called Davydov doublet, and the components of the doublet have mutually perpendicular polarizations. The dispersion of the bands is also anisotropic, and in the bulk materials it exhibits a nonanalytic behavior at small wave vectors $\mathbf{k}$.[145] This means that exciton energy $E(\mathbf{k})$ depends on the direction of wave vector even at small $\mathbf{k}$ when $k \to 0$.

The bulk anthracene-type crystal (assuming that the excitonic transitions have polarization along the plane of the layers) can be characterized by the following diagonal dielectric tensor:

$$\varepsilon_{ik}(\omega) = \begin{pmatrix} \varepsilon_c\left(1 - \dfrac{W_b^2}{\omega^2 - \omega_{Tb}^2}\right) & 0 & 0 \\ 0 & \varepsilon_c\left(1 - \dfrac{W_a^2}{\omega^2 - \omega_{Ta}^2}\right) & 0 \\ 0 & 0 & \varepsilon_c \end{pmatrix} \tag{30}$$

where $W_{a,b} \propto (F_{(a,b)})^{1/2}$ and $\omega_{Ta,Tb}$ are the exciton−photon coupling constants (proportional to the square root of the respective oscillator strengths) and the resonance frequencies of the components of the Davydov doublet. Here, x- and y-axes have been chosen along the polarization vectors of the doublet. In accordance with the widely used notation, $\omega_{Ta} > \omega_{Tb}$ is assumed. The dispersion relation for cavity polaritons in anisotropic crystalline microcavities has been discussed in ref 146 within the framework of a macroscopic approach for a given dielectric tensor of the crystal. Here, we follow that discussion and refer the reader to it for details of the derivation. The corresponding microscopic consideration is available in ref 147.

For an isotropic crystal with one exciton resonance, the polariton spectrum contains just two (upper and lower) branches. In the case of two close exciton resonances, a more complicated picture arises because of the interaction of resonances via exchange of virtual photons. Results are even more complicated for anisotropic crystals as different resonances have different directions of the transition dipoles. The dispersion equation for resulting cavity polaritons is derived by solving the system of Maxwell equations with the dielectric tensor in eq 30 accompanied by proper boundary conditions for the fields (for the ideal model mirrors, the tangential components of the fields vanish at the mirror surfaces). In this approach, both polarizations of the cavity photons in microcavity and both polarizations of excitonic resonances are automatically taken into account. In contrast to W−M excitons in semiconductors, Frenkel excitons have rather large effective masses. Neglecting in this case a weak dependence of the excitonic frequencies on the wave vector, the resulting dispersion equation for cavity polaritons reads

$$\left[\left(\frac{\omega^2}{c^2}\varepsilon_{zz} - k^2\right)\varepsilon_{xx} - k_m^2\varepsilon_{zz}\right]\left[\frac{\omega^2}{c^2}\varepsilon_{yy} - k^2 - k_m^2\right]\cos^2\varphi + \left[\left(\frac{\omega^2}{c^2}\varepsilon_{zz} - k^2\right)\varepsilon_{yy} - k_m^2\varepsilon_{zz}\right]\left[\frac{\omega^2}{c^2}\varepsilon_{xx} - k^2 - k_m^2\right]\sin^2\varphi = 0 \tag{31}$$

Here, φ is the angle between the x-axis and the direction of the in-plane wave vector $\mathbf{k}$, ε_{ii} shows the diagonal components of the dielectric tensor, and $k_m = \pi m/L$ is the z-component of the wave vector in the cavity modes. In this section, we consider only the lowest cavity photon modes with $m = 1$, $k_m \equiv k_c = \pi/L$ (as in eq 25) interacting resonantly with excitons. The nonresonant interaction with higher-m photon modes (that have substantially higher energy) is discussed in section 3.2.2.

Using ε_{ii} from eq 30, one can reduce the dispersion equation (eq 31) to the following form:

$$[\omega^2 - \omega_{La}^2(\mathbf{k})][\omega^2 - \omega_{Ua}^2(\mathbf{k})][\omega^2 - \omega_{Lb}^2(\mathbf{k})][\omega^2 - \omega_{Ub}^2(\mathbf{k})] = W_a^2 W_b^2 \frac{c^4 k_x^2 k_y^2}{\varepsilon_c^2} \tag{32}$$

Here, subscripts La,Lb and Ua,Ub denote the lower and upper polariton branches that would be created by the "non-interacting" a and b resonances, separately. The corresponding

dx.doi.org/10.1021/cr100156x |Chem. Rev. 2011, 111, 5179–5214

frequencies are given by

$$\omega^2_{\mathrm{La,\,Ua}}(\mathbf{k}) = \frac{1}{2}\left\{\omega^2_{\mathrm{cav}}(k) + \omega^2_{\mathrm{a}} + W^2_{\mathrm{a}} \mp \sqrt{(\omega^2_{\mathrm{cav}}(k) - \omega^2_{\mathrm{a}} - W^2_{\mathrm{a}})^2 + 4W^2_{\mathrm{a}}\left(\omega^2_{\mathrm{cav}}(k) - \frac{c^2k^2_y}{\varepsilon_{\mathrm{c}}}\right)}\right\},$$

$$\omega^2_{\mathrm{Lb,\,Ub}}(\mathbf{k}) = \frac{1}{2}\left\{\omega^2_{\mathrm{cav}}(k) + \omega^2_{\mathrm{b}} + W^2_{\mathrm{b}} \mp \sqrt{(\omega^2_{\mathrm{cav}}(k) - \omega^2_{\mathrm{b}} - W^2_{\mathrm{b}})^2 + 4W^2_{\mathrm{b}}\left(\omega^2_{\mathrm{cav}}(k) - \frac{c^2k^2_x}{\varepsilon_{\mathrm{c}}}\right)}\right\} \quad (33)$$

As the crystal is optically anisotropic in the cavity plane, the eigenmodes cannot be classified now as purely TE- or TM-polarized modes (except the waves propagating along the optical axes of the crystal). In the relation eq 32, the basic modes are represented as two doublets of polaritons, each doublet attributed to either a or b exciton, while the right-hand side of that equation (it would vanish along the optical axes of the crystal) determines the mixing between those modes.

Interestingly, despite the strong optical anisotropy of the crystal, the solutions of equations (eq 32) turn out[146] to be isotropic at small in-plane wave vectors; because $W^2/\omega_{\mathrm{T}} \ll 1$, an anisotropy appears at larger k only. This is a combined effect of special arrangements of the fields in the modes and of the reduced dimensionality of the problem. First, note that in the dipole approximation, the interaction between the electric field **E** and the excitonic polarization **P** is determined as $-\mathbf{P}\cdot\mathbf{E}$; hence the Rabi splitting energy depends on the mutual orientation of **E** and **P**. The electric field in the microcavity, however, is such a combination of the TE- and TM-polarized (empty) cavity photons that in a polariton mode, **E** is parallel to the excitonic transition dipole moment for each given direction of **k**. This circumstance removes the dependence of the Rabi splitting energy on the direction of **k**. Second, the energies $\omega^{\mathrm{Coul}}_{\mathrm{a,b}}(\mathbf{k})$ of Coulomb excitons that are determined from equation:

$$\varepsilon_{xx}(\omega)k^2_x + \varepsilon_{yy}(\omega)k^2_y + \varepsilon_{zz}(\omega)k^2_z = 0$$

would exhibit a nonanalytic dependence on the 3D wave vector in bulk anisotropic crystals, that is, for all three Cartesian components of the wave vector vanishing. In the case of a microcavity, however, the z-component of this vector is fixed at $k_z = \pi/L$, and at small in-plane wave vector components, the dependence on the direction of the in-plane 2D wave vector $\mathbf{k} \equiv (k_x,k_y)$ disappears. The anisotropy of Coulomb excitons in thin films becomes seen only at large **k**, where the exciton−cavity photon interaction already is not important. The combined effect of these two factors is a nearly isotropic in-plane dispersion of the polariton modes in a microcavity containing a strongly anisotropic medium. This effect could be observed in the studies of reflection or transmission of light waves with small in-plane components of the wave vector and different angles φ with the x-axis. An example of the dispersion of the four polaritonic modes is shown in Figure 16a for the parameters of the anthracene crystal and for $\varphi = 0$. Similar pictures can be obtained for other angles.

3.2.2. In-Gap Polaritons in Uniformly Filled Microcavities. As has been mentioned before, one of the differences between organic and inorganic microcavities is that the former are usually uniformly filled with a resonant material, while the latter contain a thin (∼10% of the cavity thickness) quantum well situated in the antinode of the electric field. This, insignificant at first sight, difference can result, however, in a qualitatively new additional feature in the spectra of organic microcavities.[148]

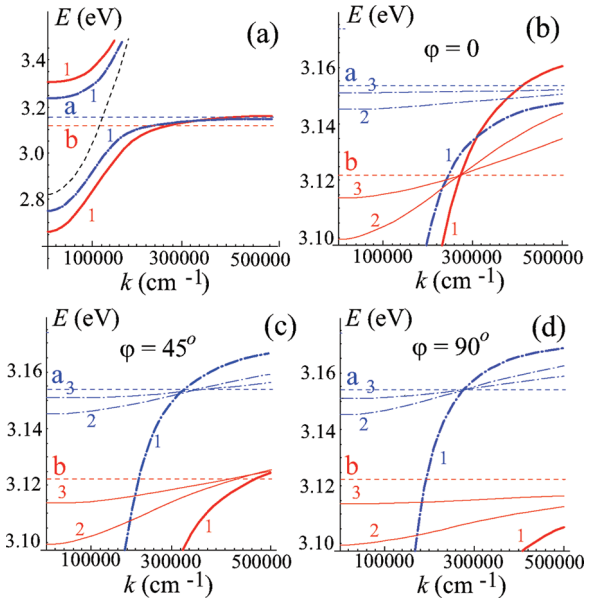

Figure 16. Dispersion of cavity polaritons in a microcavity containing a monocrystal with two molecules per unit cell. The modes with polarization along P_b (P_a) are shown as "−" (− · − · −) lines, while the horizontal dashed lines denote the resonance energies $\hbar\omega_a$ and $\hbar\omega_b$. The parameters are: ω_b = 3122 meV, ω_a = 3154 meV, $\hbar W_b$ = 570 meV, $\hbar W_a$ = 355 meV, ε_c = 3.[142,143] (a) Resonant polariton modes. (b,c,d) In-gap modes eq 34 for different values of the angle φ. Values of m are shown as numbers near each curve. Reprinted with permission from ref 148. Copyright 2009 IOP Publishing.

The excitonic polarization in a slab of a material with a macroscopic thickness can be quantized in a manner similar to the quantization of the photonic modes. Just as for the cavity photons, section 3.1.2, different excitonic modes are also characterized by integer number m determining the number of oscillations of the excitonic polarization along the growth direction. Photon modes with $m > 1$ are much higher in energy (the nearest energy separation is about 2 eV). The $m > 1$ excitonic modes, however, may have energies very close to ω_{T} (particularly for heavy Frenkel excitons, see below). Thus, the photonic and excitonic modes with the same $m > 1$ would experience only a weak nonresonant interaction resulting from the retardation effects. One might say that, just as in the case of $m = 1$ modes, a doublet is formed for each $m > 1$. The upper and lower components of those $m > 1$ doublets are, however, very close to the bare photons or excitons, respectively. The upper components of the doublets are well separated in energy from the resonance region and can in fact be disregarded (as it is usually done for the higher-m photon modes). The lower components of $m > 1$ polaritons can remain within the Rabi splitting energy and usually must be taken into account. For each $m > 1$ inside the Rabi splitting (produced by the $m = 1$ resonant modes), there are two lower polariton modes with mutually perpendicular polarizations, one mode attributed to

the a-exciton, the other to the b-exciton. Their dispersions are as follows:

$$\omega_A(m;\mathbf{k}) = \omega_a - \frac{W_a^2 A(\omega,\mathbf{k})}{2\omega_a[\omega_{cav}^2(m,k) - \omega_a^2]},$$
$$\omega_B(m;\mathbf{k}) = \omega_b - \frac{W_b^2 B(\omega,\mathbf{k})}{2\omega_b[\omega_{cav}^2(m,k) - \omega_b^2]} \quad (34)$$

Correction terms in eq 34 describe the nonresonant polaritonic effects, where $A(\omega,\mathbf{k})$ and $B(\omega,\mathbf{k})$ are some functions (see ref 148 for their explicit form). In Figure 16a, we show for reference the polariton modes with $m = 1$ for $\varphi = 0$ (φ is the angle between x-axis and the direction of the wave vector $\mathbf{k}$). In panels b−d of Figure 16, the resonance region is magnified to display modes with $m = 1$, 2, and 3 for the angles $\varphi = 0°$, 45°, and 90°. The parameters of anthracene have been utilized for this plot. The polaritonic modes with $m = 2$ form wide (∼40 meV) bands in the gap. Recently, multiple polariton modes in the vicinity of the resonance frequencies have been observed in anthracene[142,143] and correctly interpreted as higher-m modes. As the in-gap modes are located in the middle of the Rabi gap or are in resonance with the upper-branch polaritons, they may play an active role in all of the processes with the participation of polaritons. In particular, if the line width of the bare exciton modes is large, they can even wash out the Rabi splitting and prevent the strong coupling regime from being achieved. Also, they may play an important role in the energy relaxation processes: although the states with different symmetries are orthogonal, disorder unavoidably present in microcavities can lead to the mixing of the modes with different m. If the disorder-induced broadening of the in-gap modes exceeds the splitting between them, they cannot be resolved and would manifest themselves only via incoherent emission from the gap. Also, the in-gap polariton modes have small group velocities (their dispersion is flat), so that disorder can result in the appearance of the coexisting localized and delocalized states (see section 3.3.2). The effects related to disorder for in-gap modes require further analysis.

For W−M excitons in a microcavity uniformly filled with an inorganic semiconductor, the above consideration has to be modified to take into account the dependence of the excitonic resonance frequency on the wave vector (more information on the in-gap modes in semiconductor microcavities can be found in ref 148).

3.2.3. Crystalline Organic Microcavities: First Experiments. Experimental work on crystalline organic microcavities is now at a very early stage. Below, we review the results obtained by two groups, which have observed the strong coupling regime in a single crystal anthracene microcavity.[137,142,143]

The first observation of cavity polaritons with large (∼200 and ∼100 meV for the b- and a-polaritons, respectively) Rabi splitting energies in a single-crystal microcavity was reported in ref 137. The energies of cavity polaritons were measured as functions of the angle of incidence. The authors concluded that the observed polaritons arise from a coherent coupling of cavity modes with the lowest electronic (0−0) and two higher vibronic (0−1 and 0−2) transitions. This situation can be described analogously to eq 29 but with the account of eight coupled oscillators: two polarizations of cavity photons and three (0−0, 0−1 and 0−2) Davydov doublets of material resonances. The coupling constants were extracted by fitting solutions of the dispersion equation to the observed positions of polariton peaks. The resulting spectra consist of eight polariton branches: a-polarized 0−0, 0−1, and 0−2 transitions couple strongly to the linear combination of TE- and TM-cavity photons that has the polarization parallel to the a-axis and form four (one upper, one lower, and two middle) a-polarized branches, and the same for the b-components of the doublet. As the b-exciton has a larger oscillator strength, the b-polarized modes are easier to observe. In fact, only three b-polarized (the lower and two middle) and one a-polarized (the lower) modes have been observed in the experiment (see Figure 17a). In ref 149, the resonant Rayleigh scattering of polaritons has been observed in organic microcavities with crystalline anthracene.

Although the emission from the cavity was indeed found polarized along a- and b-axes in accordance with the results of ref 146, a visible anisotropy of the polariton dispersion was observed even at small wave vectors. Its existence had been attributed to nonideal microcavity mirrors: cavity photons with different polarizations penetrate differently into the microcavity mirrors constructed from DBRs. As a result, the TE- and TM-polarized bare cavity modes split. As polaritons involve combinations of the TE- and TM-photons matched in such a way that the electric field is directed along the excitonic transitions, the amount of the admixture of both bare photons in the polariton state depends on the propagation direction. Thus, surprisingly, cavity polaritons in organic crystalline structures with DBR mirrors demonstrate anisotropic behavior not as a result of the anisotropy of the crystal, which would be smoothed as discussed in section 3.2.1, but rather as a result of different transmissivity of the mirrors for the two bare photon polarizations.

The strong-coupling regime in a singe-crystal anthracene microcavity was also observed by another group.[142,143] There the energy of polaritons was measured at the normal incidence as a function of the detuning between the cutoff frequency of cavity photons and bare excitons (which is possible when the cavity is wedge-shaped). The Rabi splitting energies were found to be ∼340 and ∼140 meV for the b- and a-polaritons. This group did not observe the coupling between the cavity modes and higher-energy vibronic transitions but, instead, reported the observation of the in-gap polaritonic modes (see Figure 17b). Further research is needed to clarify the apparent discrepancy in the interpretation of the polaritonic spectra.

3.3. Microcavities with Disordered Organic Materials

3.3.1. First Observations of the Strong-Coupling Regime in Organic Materials. In earlier studies, the main obstacle for the organic materials to exhibit a strong photon−exciton coupling was the intrinsically large width of the excitonic resonances. Nevertheless, the first observation[133] of the strong-coupling regime in organic media in fact occurred in a material strongly disordered by its nature: a large Rabi splitting (160 meV at room temperature) was found in a microcavity containing a slab of porphyrin dyes. Shortly afterward, the strong-coupling regime was observed by the same group in a microcavity utilizing J-aggregates of cyanine dyes.[134,150,151] This material became the principal medium for organic cavity polaritons for the next 6 years until the first observation of polaritons in a single-crystal microcavity was reported.[137] Electronic excitations in J-aggregates have an inhomogeneous broadening of about 40 meV. In microcavities with various J-aggregates, the polaritonic branches were found to be separated by Rabi splittings ranging between 80 and 300 meV at room temperature. Since then, cavity polaritons have been also observed in σ-conjugated silane polymers,[9] NTCDA,[138] and in polycrystalline tetracene films.[139]

dx.doi.org/10.1021/cr100156x |Chem. Rev. 2011, 111, 5179–5214

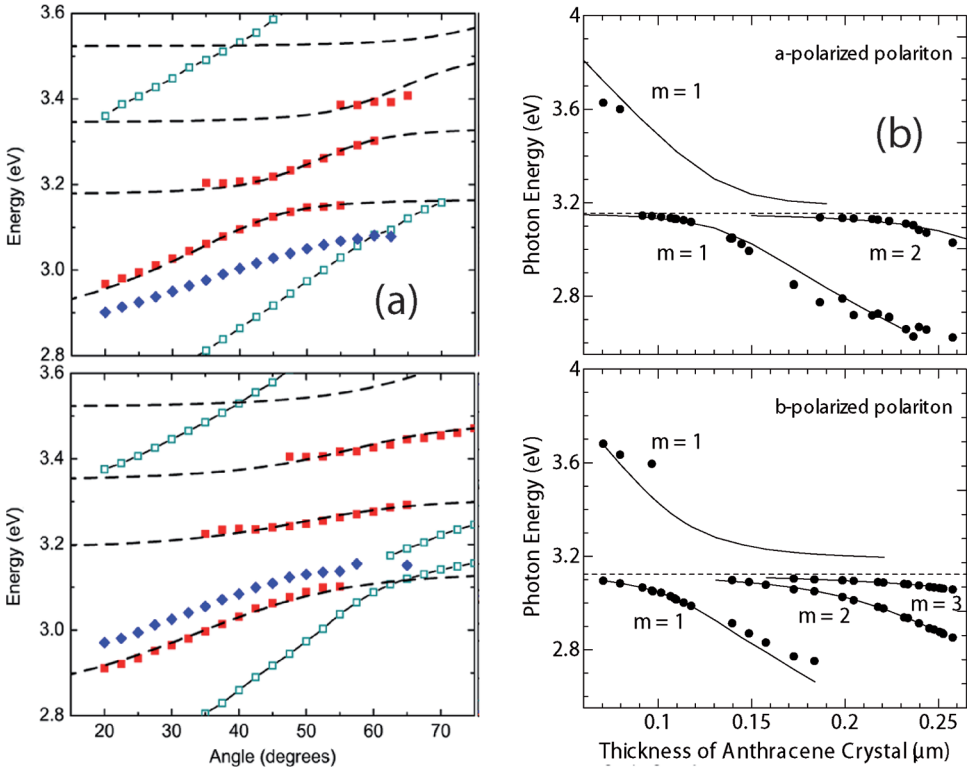

Figure 17. Measured dispersion of polaritons in an anthracene microcavity. (a) Two lower (a- and b-) and two middle (b-) polaritons. The b-/a-polaritons are shown by ■/◆; upper/lower panel is for electric field parallel to a-/b-exciton. Reprinted with permission from ref 137. Copyright 2008 American Physical Society. (b) Upper and lower polaritons ($m = 1$) and in-gap modes ($m = 2,3$). Upper/lower panel shows a-/b-polarized polaritons as adapted to the notation of this Review. Reprinted with permission from ref 142. Copyright 2008 Elsevier BV. Reprinted with permission from ref 143. Copyright 2009 Wiley-VCH Verlag GmbH & Co. KGaA.

In polar solvents, cyanine dye monomers self-organize to form one-dimension chains (so-called *J*-aggregates). The interaction between the monomers within a single chain results in the appearance of collective 1D excitonic states in each *J*-aggregate. The total oscillator strength in long *J*-aggregates is concentrated (up to 85%) in the lowest excitonic state.[152] The interaction between this "bright" state with other excitonic states can be neglected, and this "bright" state can be treated as a single dispersionless resonance. The total oscillator strength of the aggregate is enhanced as compared to the oscillator strength of a monomer in proportion to the number n of coupled monomers in the aggregate.[152] In addition, the inhomogeneous broadening of a *J*-aggregate scales as $n^{-1/2}$ as compared to the inhomogeneous broadening of a single monomer due to the process of motional narrowing.[153] Thus, the excitonic transition in long *J*-aggregates comprised of many molecules has both a relatively narrow line width and a large oscillator strength, allowing the strong-coupling regime to be reached.

As the mean size (~100 Å) of *J*-aggregates is much smaller that the wavelength of light in the strong-coupling region, they can be considered as point dipoles with transition dipole moments (directed along each chain) situated within the microcavity plane. The structure is strongly disordered, with two types of disorder: (i) structural (off-diagonal) disorder due to the fact that the positions of the *J*-aggregates are chaotically distributed within the cavity volume, and the directions of their dipole moments are homogeneously distributed in the plane of the microcavity; (ii) energy broadening of the electronic transition due to variations of the internal structure of individual *J*-aggregates and different surroundings (diagonal disorder). As the structure is homogeneous when averaged over larger scales, one may nevertheless try to characterize the states of polaritons in terms of wave vectors.

The mean distance between *J*-aggregates in these microcavities is rather large (about 200 Å). As the orientation of *J*-aggregates is random, the Coulomb interaction between them can be included into the inhomogeneous broadening of the excitonic resonance, while the *J*-aggregates can be treated as noninteracting. Thus, in disordered organic microcavities, a cavity photon with a given in-plane wave vector **k** interacts not with the exciton with the same wave vector, as it does in crystalline organic material or in inorganic microcavities, but rather with an incoherent set of noninteracting electronic transitions. As we discuss in the next subsection, the resulting excitation spectrum of polaritons consists of coexisting plane-wave-like and spatially localized states. This structure of the excitation spectrum may result in interesting and unusual relaxation dynamics (section 3.4.1).

3.3.1.1. Reversible Switching of Strong Light-Molecule Coupling in Microcavity. It was demonstrated recently[154] that photochromic molecules in microcavity open the possibility of switching from the weak to strong coupling regimes reversibly using all optical control. In this work, a low-*Q* metallic cavity was filled with photochromic spiropyran (SPI) molecules (1′,3′-dihydro-1′3′3′-trimethyl-6-nitrospiro[2*H*-1-benzopyran-2,2′-(2*H*)-indole]) in a polymer matrix (PMMA or polymethylmethacrylate). Under UV illumination, the molecules undergo photoisomerization into a colored merocyanine form (MC), and back to a transparent SPI form by visible illumination (or thermally). The switch is

dx.doi.org/10.1021/cr100156x |*Chem. Rev.* 2011, 111, 5179–5214

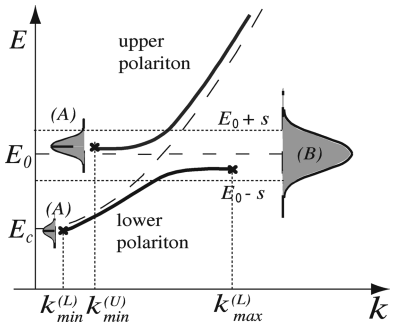

Figure 18. A sketch of the excited states in the disordered organic microcavity. States similar to plane waves exist only in restricted intervals of the wave vectors; the "×" are the end-points for the plane-wave-like part of the excitation spectrum. (A) and (B) denote the incoherent excited states. States (A) correspond to localized states with a large radius of localization. States (B) are more or less similar to electronic excitations localized near individual molecules.

achieved by photochemically inducing conformational changes in the molecule. This effect has been used before[155−157] in optical switching devices. Measured magnitudes of the Rabi splitting of up to 700 meV at room temperature, corresponding to 32% of the transition energy of the molecule resonance, demonstrate a very strong coupling of MC molecules with light. A similar coupling strength was also demonstrated[120] in the so-called plasmonic structure where the surface of metal is covered by a layer of organic molecules. In the case of MC molecules at the surface of Ag,[154] the value of splitting was found to be 650 meV, which is comparable to the value obtained in the microcavity. The structures considered in ref 154 present an interesting and maybe unique combination of the coupling strength and functional capabilities.

3.3.2. Coexistence of Coherent and Localized States in Microcavities with Disordered Organic Materials. The structure of the excitation spectrum of a disordered organic microcavity was analyzed in ref 158 within the macroscopic Maxwell-equations framework with the material described by a homogeneous dielectric function but containing an imaginary part. The resulting polaritonic states were then characterized by frequency ω and wave vector k (along any in-plane direction) containing both real and imaginary parts: $k = k' + i\delta k$, where δk determines the uncertainty of the wave vector. As usual, far away from the resonance the modes tend to the bare excitation energies (in this case, to coherent cavity photons and incoherent excitons). However, even in the region of the resonance between the exciton transitions and the cavity photon, one can roughly distinguish between "coherent" (characterized by a wave vector) and "incoherent" (spatially localized on a given *J*-aggregate or near a given group of *J*-aggregates) polariton states (see Figure 18). A "coherent" polaritonic state can form when the electric field of the cavity photon couples strongly with the electronic transitions of the ensemble of incoherent *J*-aggregates, and the scattering of polaritons by disorder is rather weak. Such a state could be approximately characterized by a wave vector. Inhomogeneities present in the system scatter such states, which may lead to their localization. As the inhomogeneity results in a broadening of the wave vector, $k \rightarrow \{k',\delta k\}$, one can say that the plane-wave picture applies as long as $\delta k \ll k'$. These plane-wave-like states are shown in Figure 18 as solid lines. If, however, $\delta k \geq k'$, then such states should be considered as localized. The localized states are shown as bell-shaped distributions in Figure 18 (they are located arbitrarily with respect to the wave vector axis, as they are characterized by their energy only). The states close in energy to the bottom of the polariton bands (marked as (A) in the figure) are still formed from cavity photons coupled with the electronic transitions of all the molecules, although they cannot be characterized in terms of wave vectors. The states marked as (B) are similar to electronic excitations of individual *J*-aggregates, because at large k the cavity photons are out of resonance with the electronic transitions and the interaction between them is not expected to change visibly the excitation spectrum. In fact, the large-k end-point at the lower polariton branch marks the crossover to the regime in which light and electronic excitations of *J*-aggregates are weakly coupled.

Although the distinction between the "coherent" and "incoherent" states in the region of exciton resonances is only a convenient approximation (in reality, the excited states of the cavity are something intermediate, being more similar to plane waves or to spatially localized excitations), it is useful (in particular, for the understanding of the processes of energy relaxation and for the interpretation of experiments) to know the location of the end-points of the coherent part of the spectrum. In ref 158, it was proposed to consider the values of the wave vector at which $\delta k \approx k'$ as the end-points of the plane-wave like part of the spectrum. From Figure 18, it is seen that the end-points appear when the polariton dispersion curves get flat. The plateaus of the dispersion curves correspond to strongly diminished group velocities of polaritons:

$$v_g(k) \simeq \frac{E_c L^2 k}{\pi^2 \hbar} \frac{(E_0 - E_{pol})^2}{(E_0 - E_{pol})^2 + W^2}$$

where $2W$ is the Rabi splitting energy, and E_0 and E_c are denoted in the figure. However, the notion of the group velocity in this form is valid only if the dissipation in the system is very small, so that this approach needs further improvements. Nevertheless, it clearly illustrates that the vanishing of the group velocity results in a growth of the wave vector broadening $\delta k = \delta E/\hbar v_g(k)$, where δE is the polariton energy broadening, consequently, to the violation of the requirement $\delta k \ll k$. The estimates of the end-points in ref 158 indicated that the plane-wave-like lower-branch polaritonic states constitute about 5−10% of the total number of excitations. The majority of the excited states of the system below the electronic transition energy E_0 thus correspond to the localized states, which significantly influences the energy relaxation (section 3.4.1).

The origin of polariton localization in disordered microcavities was later examined in the framework of a microscopic model[159] considering the scattering of cavity polaritons by disorder. This approach enables one to determine explicitly the physical reason of the polariton localization. It was shown that in most experimental cases polaritons get localized due to their resonant scattering by exciton states from the tail of their inhomogeneous distribution. In other words, with exceptions of rather small inhomogeneous broadening of the electronic transition or extremely large negative detuning $u = E_c - E_0$ (see Figure 18), the diagonal disorder always dominates, while off-diagonal-disorder scattering is washed out due to the motional narrowing effects. The low-energy localized states (marked as (A) in Figure 18) were also examined numerically in refs 160,161 for a model one-dimensional microcavity with diagonal disorder. Wave functions of polariton states were calculated for a given energy disorder

dx.doi.org/10.1021/cr100156x |*Chem. Rev.* 2011, 111, 5179–5214

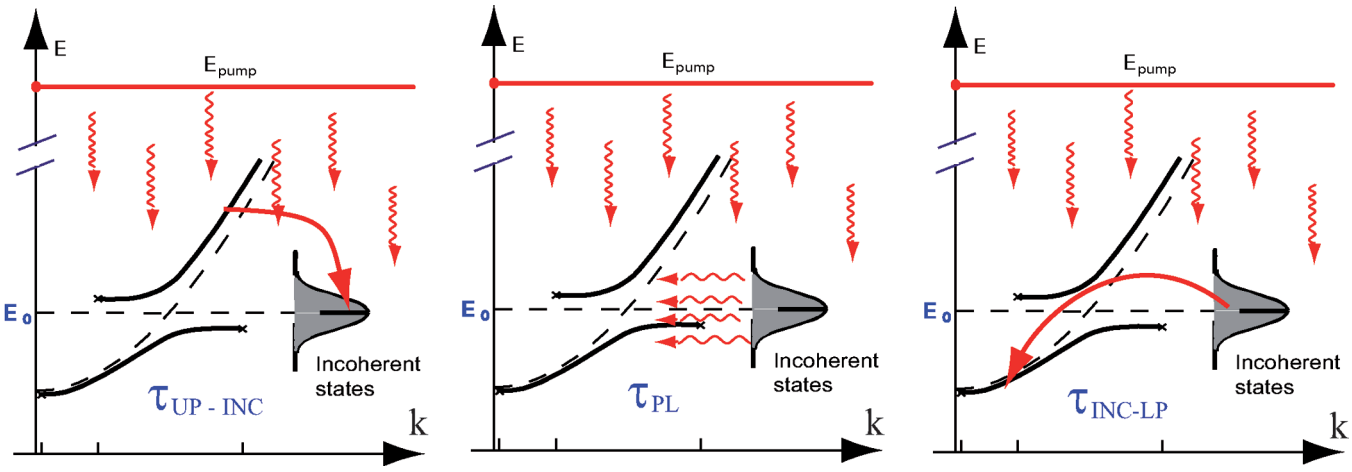

Figure 19. A sketch of possible relaxation processes in a disordered microcavity. Left: Decay of upper polaritons into incoherent excited states with the emission of a vibration quantum. Middle: Radiation from the incoherent excited states pumps coherent polaritonic states. Right: Nonradiative decay of the incoherent excited states into lower branch coherent polaritonic states due to emission of a vibrational quantum.

realization, and the spatial structure of the photon and exciton parts of the eigenstates was examined. It was found that indeed the eigenstates are mixtures of photonic and excitonic states (so that they retain their hybrid polaritonic character). The spectrum of polaritons contains states with different degrees of localization (weakly and strongly localized states). In ref 161, the time evolution of wave packets formed from low-energy polaritons in a microcavity with a diagonal disorder was studied. Disorder was demonstrated to drastically change the character of the propagation of the wave packets. At a time scale shorter than a fraction of picosecond, the initial packet is transformed into a lumpy structure, reflecting the multitude of localized polaritonic states within the spatial region of the initial excitation. This lumpy structure shows some internal dynamics (likely resulting from the overlap between different localized states), but does not propagate well beyond the initial excitation region. In contrast, an identical wave packet in a disorder-free microcavity exhibits both the broadening and the translational motion in the microcavity plane. In ref 162, different regimes of exciton−polariton propagation and localization (including weak and strong localization) in disordered organic microcavities were discussed. It was shown that, by varying the angle of incidence of light and the detuning between the photon mode and the excitonic resonance, those regimes can be achieved in the same sample at room temperature.

3.4. Relaxation and Dynamics of Exciton−Polaritons in Organic Microcavities

Quite often the microcavities are excited nonresonantly to observe the relaxation of the excitations toward the lowest energy states. The large Rabi splitting energies in organic microcavities allow for a new (with respect to inorganic materials) relaxation channel, which may lead to qualitatively different energy relaxation picture. Besides that, the majority of excited states in disordered organic microcavities are localized states with the energies close to energy E_0 of the electronic transition in an organic molecule. These two factors result in some peculiarities of the relaxation dynamics, which we address in this section. A complete and comprehensive picture of energy relaxation in organic microcavities has not been developed yet. For this reason, our exposition is limited to a discussion of several processes, which may be important for the consideration of the energy relaxation in disordered microcavities (section 3.4.1). We will also discuss effects arising at higher excitation densities, among which there are statistical effects, related to the appearance of a specific nonlinear interaction between polaritons (the so-called kinematic interaction, section 3.4.2), and the suppression of bimolecular quenching (section 3.4.3).

3.4.1. Different Scenarios of the Energy Relaxation. An important ingredient for the relaxation dynamics is that organic molecules possess a variety of intramolecular vibrations having energies E_{vib} of the order of tens of meV.[150,163] Such vibrations are typical for complex organic molecules, *J*-aggregates of cyanine dyes, and other organic complexes. The energy of a vibration can be on the order of the Rabi splitting energy, and thus the emission of such quanta of energy might serve as an effective channel for the transitions from the higher-energy states (both coherent upper polariton states and incoherent states with the energies close to E_0) down to the lower energy states (either to coherent lower polariton states or to the lowest energy localized states). In a microcavity with a disordered organic material featuring coexisting coherent and incoherent excited states, many different transitions between various kinds of states would appear. We now summarize some estimates for various transition rates.

Resonant Decay of the Upper Branch Polaritons into Incoherent States with Energies $\sim E_0$. The rate of the resonant decay of the upper branch polaritonic states into a dense set of incoherent excited states with energies $\sim E_0$ was calculated in ref 158. In such transitions (see Figure 19, left panel), the initial state is a coherent UP state with wave vector **k**, and the final state is an excited state in which the electronic and vibrational quanta are localized on the same organic molecule. The corresponding transition rate is

$$W_{\mathrm{UP}\rightarrow\mathrm{INC}}(\mathbf{k}) = \frac{2\pi g^2 E_{\mathrm{vib}}^2}{\hbar\sqrt{\pi}\gamma}\frac{W^2}{(E_0 - E_{\mathrm{U}}(k))^2 + W^2}\, e^{-[E_0 - (E_{\mathrm{U}}(k) - E_{\mathrm{vib}})]^2/\gamma^2}$$

where $2W$ is the Rabi splitting energy, $E_{\mathrm{U}}(k)$ the upper polariton energy, E_{vib} is the intramolecular vibration energy, g is the electron−vibron coupling constant, and γ is the width of the electronic transition (taken to be Gaussian distributed). The respective transition times are estimated as $\tau_{\mathrm{UP}\rightarrow\mathrm{INC}} \approx 50$ fs. This relaxation is very fast due to a very large amount of final

dx.doi.org/10.1021/cr100156x |*Chem. Rev.* 2011, 111, 5179–5214

incoherent excited states (we recall that about 95% of the eigenstates of the system are incoherent excited states with the energies $\sim E_0$). For comparison, the transition rate of the upper polaritons to the lower energy coherent polaritonic states with the emission of an intramolecular phonon was estimated to be in the picosecond range.[8]

Recently, the influence of molecular vibrations on the polaritonic spectra in a disordered microcavity was examined experimentally.[163] Photoluminescence from both the upper and the lower polaritonic branches was measured in samples with the same vibrational spectra, but with different Rabi splitting energy (the Rabi splitting was tuned by changing the dye concentration in the solvent). The measurements showed the decrease of the relative upper-to-lower branch polariton photoluminescence with the increased Rabi splitting at negative detuning. The observed effect can be understood as follows. If upper polaritons are resonant with the exciton−vibron excited states, the decay into these states is expected to dominate over the decay into the lower branch states, as the number of available final states in the former case is much larger than in the latter. When the Rabi splitting energy is smaller than the energy of the vibrational quantum, the exciton−vibron is resonant with the photon-like part of the upper polariton branch. Even if the temperature is not low and the considered upper branch polariton state is populated, the decay is suppressed due to a small excitonic fraction in the polariton state. With the growth of the Rabi splitting energy, the exciton−vibron becomes resonant with the more exciton-like part of the upper branch dispersion curve, and the described above upper polariton decay into incoherent excited states becomes favored. In the simple qualitative discussion of the experimental observations, we took into account only one intramolecular vibration. In organic microcavities with several vibrational modes (with energies close to the Rabi splitting energy), the quantitative interpretation of experimental observations needs a more careful analysis.[163]

Decay of Incoherent (Localized) States into the Lowest Energy Coherent States. After nonresonant high-energy optical excitation of a microcavity, the energy relaxes (on a picosecond time scale) mainly to the lowest energy electronic incoherent states (having energies around E_0; states (B) in Figure 18). These incoherent states can either decay radiatively and pump the coherent states of the upper and lower polaritonic branches (Figure 19, middle panel) or relax nonradiatively downward with the emission of intramolecular vibrations (Figure 19, right panel). It is thus important to know the ratio between the radiative lifetime τ_{PL} of the electronic transition and its lifetime $\tau_{INC\rightarrow LP}$ with respect to its decay into the lower-branch coherent states. Typically, τ_{PL} is on the order of tens of picoseconds for *J*-aggregates, depending on the properties of the particular material; for some complex molecules, it can reach hundreds of picoseconds and even much longer. The lifetime τ_{INC} was calculated in ref 164 considering the transition in which the initial state is an incoherent excited state, and the final state consists of a lower polariton with the wave vector $\mathbf{k}$ and a vibrational quantum localized on one of the molecules. The corresponding transition rate is

$$W_{INC\rightarrow LP} \simeq \left(\frac{a}{L}\right)\frac{\pi^2 g^2 \Delta^2}{\hbar E_c^2} E_{cav}(k_*)$$

where L is the cavity width, a is the mean distance between *J*-aggregates, $E_c = E_{cav}(k = 0)$, $E_L(k)$ is the lower polariton energy, and k_* is determined from the condition $E_0 - E_{vib} = E_L(k_*)$. Numerical estimates yield time scales $\tau_{INC\rightarrow LP} \approx 10-25$ ps (the larger is the Rabi splitting, the faster is the nonradiative relaxation). Thus, this process may be faster than the radiative decay of electronic excitations and can therefore be used for a fast one-step relaxation toward the bottom of the polariton band.

As was already mentioned, if the vibronic replica (exciton−vibron state) has a large enough oscillator strength, the strong-coupling regime can be achieved between the cavity photon and the exciton−vibron state, and two (or more) Rabi splittings can be observed in the spectrum of polaritons. The photoluminescence from a microcavity in this regime was studied theoretically in ref 141 where the coupling of a cavity photon to $|10\rangle$ and $|11\rangle$ states was considered (here, $|nm\rangle$ denotes the nth electronic and mth vibronic excited state of the molecule). The state $|01\rangle$ turns out not to be strongly coupled to light due to its short lifetime, but could serve as a final state in the polariton relaxation. The master equation for the polariton population was solved showing that the lower polariton photoluminescence indeed exhibits a peak corresponding to an efficient decay of reservoir (exciton-like) lower polaritons into lower-energy (below the "knee") polaritonic states, it is accompanied by emission of an incoherent vibrational quantum (a molecular $|01\rangle$ excitation). This process is similar to the one depicted in the right panel of Figure 19, if the incoherent states are replaced by the excitonic reservoir.

To conclude this section, we can say that it is the density of available final states that makes the main impact on the rates of different relaxation processes. Those relaxation processes in which the final states are coherent occur on the time scale of tens of picoseconds. If incoherent excited states with energy $\sim E_0$ are the final states of a relaxation process, its time scale shortens to a hundred of femtoseconds. This difference is a consequence of different (by 2 orders of magnitude) amounts of the excited states of both types (section 3.3.2).

3.4.2. Kinematic and Dynamic Interactions of Cavity Polaritons. During the past decade, a keen interest was taken in nonlinear experiments with cavity polaritons. It is now recognized that cavity polaritons in crystalline inorganic structures behave as interacting bosons. In the vicinity of cutoff frequency, they have a very small effective mass, leading to BEC-like phase transitions.[128,129] However, studies of nonlinear effects in organic microcavities are only in the very beginning. One of the important current objectives is to study nonlinear interactions of polaritons in crystalline organic microcavities. Their bosonic properties can lead to the same type of effects as found in inorganic microcavities, but polaritons in organic microcavities are more stable due to a much larger value of the Rabi splitting energy. We will discuss below the main features of nonlinear interactions typical for crystalline systems supporting Frenkel excitons. One of them is the dynamic nonlinear interaction, which is determined by matrix elements of the intermolecular interaction operators (such as the quadrupole interaction), or it can stem from the coupling between Frenkel excitons via exchange of lattice phonons. The second is the so-called kinematic interaction. It is a purely statistical effect, resulting from the mixed statistics of Frenkel excitons. We now briefly introduce these two types of interactions and give an outlook for future work.

3.4.2.1. Dynamic Interaction. The dynamic interaction can be long-range. One can show[22,165] that the operator of the exciton−exciton interaction has the form of

$$\hat{H}_{int}^{IV} = \frac{1}{2}\sum_{\mathbf{n}\neq\mathbf{n}'} M_{\mathbf{n}\mathbf{n}'}^{IV} P_{\mathbf{n}}^{\dagger} P_{\mathbf{n}'}^{\dagger} P_{\mathbf{n}} P_{\mathbf{n}'} \qquad (35)$$

where $P_{\mathbf{n}}$ and $P_{\mathbf{n}}^{\dagger}$ are, respectively, the site-specific exciton destruction and creation operators:

$$M_{\mathbf{nn}'}^{\mathrm{IV}} = \langle \mathrm{ff}|\hat{V}_{\mathbf{nn}'}|\mathrm{ff}\rangle + \langle 00|\hat{V}_{\mathbf{nn}'}|00\rangle - 2\langle 0\mathrm{f}|\hat{V}_{\mathbf{nn}'}|0\mathrm{f}\rangle \quad (36)$$

and $\hat{V}_{\mathbf{nn}'}$ is the operator of the interaction between molecules $\mathbf{n}$ and $\mathbf{n}'$. The first term in eq 36 represents the interaction energy of molecules $\mathbf{n}$ and $\mathbf{n}'$ being in the excited state f, the second term gives the interaction energy of these molecules when both are in the ground state, and the third term gives the interaction energy when only one molecule is in the excited state f. The terms in eq 36 can be evaluated when the wave functions of an isolated molecule in the ground state and in the excited state f are known.

The quantity $M_{\mathbf{nn}'}^{\mathrm{IV}}$ in crystals having an inversion center decreases with increasing distance $|\mathbf{n} - \mathbf{n}'|$ between them as $|\mathbf{n} - \mathbf{n}'|^{-5}$ or faster. If molecules of the crystal have no inversion center, the static dipole moments of a molecule in the ground and in the excited states are usually not equal to zero. In this case, the matrix element eq 36 in the dipole−dipole approximation for $\hat{V}_{\mathbf{nn}'}$ can be reduced to the interaction energy of the dipoles $\mathscr{P}_n$ and $\mathscr{P}_{\mathbf{n}'}$, where

$$\mathscr{P}_{\mathbf{n}} = \mathscr{P}_{\mathbf{n}}^{\mathrm{ff}} - \mathscr{P}_{\mathbf{n}}^{00}$$

equals the change of the dipole moment of the molecule upon its excitation. In this approximation:

$$M_{\mathbf{nn}'}^{\mathrm{IV}} = \frac{\mathscr{P}_{\mathbf{n}}\mathscr{P}_{\mathbf{n}'} - 3(\mathscr{P}_{\mathbf{n}}\mathbf{l}_{\mathbf{nn}'})(\mathscr{P}_{\mathbf{n}'}\mathbf{l}_{\mathbf{nn}'})}{|\mathbf{n} - \mathbf{n}'|^3}$$

where the unit vector

$$\mathbf{l}_{\mathbf{nn}'} = \frac{\mathbf{n} - \mathbf{n}'}{|\mathbf{n} - \mathbf{n}'|}$$

For dipole moments on the order of 5 D and the nearest distance between the molecules on the order of 5 Å, the nearest-neighbor energy $M_{\mathbf{nn}'}^{\mathrm{IV}}$ is on the order of 1000 cm^{-1}, which can be larger or of the same order as the exciton bandwidth. In such crystals, biexciton states can form, if the interaction between excitons is attractive.

3.4.2.2. Kinematic Interaction. Frenkel excitons are known to be paulions; that is, their operators $P_{\mathbf{n}}$ and $P_{\mathbf{n}}^{\dagger}$ obey Fermi commutation rules when the excitations reside on the same lattice site $\mathbf{n}$ and Bose commutation rules when on different lattice sites.[22] To facilitate the description, one can use the transformation,[166] which allows one to replace Pauli exciton operators by Bose operators at the cost of extra terms appearing in the Hamiltonian. These terms describe an effective nonlinear interaction between the bosons (kinematic interaction), which compensates the difference between Bose and Pauli statistics. Application of this transformation to the leading term in the exciton Hamiltonian in the pair-interaction approximation yields the following extra term:

$$H_{\mathrm{kin}} = -E_0 \sum_{\mathbf{n}} B_{\mathbf{n}}^{\dagger} B_{\mathbf{n}}^{\dagger} B_{\mathbf{n}} B_{\mathbf{n}} \quad (37)$$

where the exciton operators $B_{\mathbf{n}}^{\dagger}$, $B_{\mathbf{n}}$ obey Bose statistics, and $E_0 \approx 2$ eV is the excitation energy of the molecule. If excitons are strongly coupled with light, one can form polariton operators from exciton and photon operators and obtain the corresponding polariton Hamiltonian (see, for instance, ref 167). Equation 37 implies that the kinematic interaction of two excitons (or polaritons) is short-range, described by a contact delta-like interaction potential, and thus the possibility to treat it as a perturbation is questionable. However, in some cases, one can replace the true interaction potential by an effective potential $V_{\mathrm{eff}}(\mathbf{r})$ with the same scattering amplitude $f(\mathbf{k})$, which allows for the use of the perturbation theory. Such a procedure does not influence the scattering properties of the quasiparticles and is known as renormalization (see, e.g., section 6 of ref 168).

The exciton−exciton and polariton−polariton kimenatic interactions in an ideal crystalline organic monolayer placed into a microcavity were discussed in refs 167,169. In ref 167, the transformation from paulions to bosons was performed for two-dimensional cavity polaritons. Using the effective mass approximation for excitons, the exciton−exciton scattering amplitude was calculated. As the scattering amplitude has a nonnegligible imaginary part, the kinematic interaction of excitons can never be treated as a perturbation. From the calculated exciton−exciton scattering cross section, it was found that the kinematic scattering of excitons can be described as the scattering between hard disks. It was shown that, as in the case of a two-dimensional trapped gas of ultracold atoms, excitons in a confined monolayer may behave as a dilute degenerate boson gas at low temperatures.

The kinematic interaction of cavity polaritons is influenced by, first, the intricate (nonparabolic) shape of the lower polariton dispersion curve, and, second, by the two-branch structure of their excitation spectrum, which opens a way for additional (interbranch) scattering channels. The scattering amplitudes describing the polariton−polariton kinematic interaction for different channels were calculated in ref 169. When the scattering of two incoming polaritons into exciton-like states is allowed by the energy and momentum conservation laws, this process will strongly dominate over any other scattering channel, and the corresponding scattering is nonperturbative (the scattering amplitude has a large imaginary part, and thus the Born approximation cannot be used to describe such scattering). On the contrary, when the scattering into the exciton-like part of the spectrum is not possible, the polariton−polariton scattering amplitude is real, and an effective potential describing the kinematic interaction can be introduced and used for calculations in the framework of the perturbation theory. It was shown in ref 169 that this potential is always repulsive, and its energy scale is on the order of the exciton bandwidth.

In summary, we note that in a comprehensive discussion of nonlinear polariton−polariton interactions and polariton relaxation, both the long-range dynamic and the short-range kinematic interactions should be taken into account simultaneously. Experimental information on the strength of the dynamic interaction between Frenkel excitons in organic crystals is needed, which could clarify its relative importance. For comparison, in inorganic microcavities an effective interaction between polaritons similar to the kinematic interaction also appears when the true (Fermi) statistics of the constituents of the W−M excitons is taken into account.[170,171] However, its effect was found[171] to be smaller in magnitude than the nonlinear term originating from the Coulomb interaction of excitons (dominated by the electron−electron and hole−hole exchange terms). The kinematic interaction has been therefore usually omitted when dealing with nonlinear processes in inorganic microcavities. Having in mind that the kinematic interaction between Frenkel excitons differs in nature from the nonlinear interactions between W−M excitons caused by nonbosonic corrections, one can expect that collective properties of polaritons in organic and in the hybrid

organic−inorganic microcavities as well as their nonlinear properties[172] may have many peculiarities reflected in their dynamics and condensation.

3.4.3. Suppression of Bimolecular Quenching of Polaritons in Microcavities. Nonlinear dynamics and deviations from the bosonic behavior of excitons can be observed at relatively high excitation densities. It is known, however, that it may be difficult to create large concentrations of Frenkel excitons in organic materials because of the so-called bimolecular quenching, the process that results from resonant intermolecular energy transfer. In this process, the energy of two excited molecules (with the excitation energies E_0 each) becomes accumulated on only one of them in a higher-energy state with the excitation energy $E_1 \simeq 2E_0$. As the higher-energy state then relaxes irreversibly into the lowest electronic excited state, only one (instead of two) excitation of energy E_0 remains.

In the microcavity, the process of bimolecular quenching acquires new interesting features. Of particular interest are disordered microcavities, where the specifics of bimolecular quenching is determined by the complex (coherent−incoherent) structure of the polariton spectrum (section 3.3.2). A given polariton can take part in the annihilation processes with either another polariton or with an incoherent excited state. At nonresonant pumping, the main part of the excitations are incoherent states (with the energy close to E_0). Thus, the main contribution to the bimolecular quenching of a given polariton stems from these incoherent excited states. In contrast, for resonant pumping of lowest energy polaritons, the role of incoherent excited states with energies close to E_0 is insubstantial.

Let two polaritons with wave vectors $\mathbf{k}_1$ and $\mathbf{k}_2$ and branch indices $\rho_{1,2} = U,L$ interact to form a higher-energy excitation. The resulting rate of the polariton−polariton annihilation will be smaller than the rate of the exciton−exciton annihilation by the factor of $\Gamma(k_1,\rho_1;k_2,\rho_2) = |X_{\rho 1}(k_1)|^2|X_{\rho 2}(k_2)|^2$, where $|X_\rho(k)|^2$ denotes the weight of the excitonic component in the polariton. This factor is on the order of unity if both polaritons are excitonic-like (for instance, this can be for excitons localized in the "reservoir" of local states (B) in Figure 18), but it can become very small (of the order of 0.01 or less if one of of both excitons are localized with a large localization length among states (A)) in the case of negative detuning. This observation[173] could be particularly important for nonlinear effects, because strong bimolecular quenching can destroy the polariton population. The decrease of bimolecular quenching for strongly delocalized polariton states reflects the decrease of the probability for such excitons to be found at neighboring molecules. This possibility, for instance, is likely for polaritonic states in the vicinity of the cutoff frequency. To create a high population of these states, resonant pumping of polaritons has to be used. At nonresonant pumping, such organic microcavities need to be explored, where the probability of bimolecular quenching in the reservoir is less than the probability of polariton transitions from the reservoir to one of the states in the vicinity of the cutoff frequency. The room-temperature polariton lasing in an organic single-crystal microcavity[174] at frequencies close to the cutoff frequency of the microcavity may be useful to estimate the role of bimolecular quenching in such type of devices. Also interesting are recent investigations of the exciton−exciton annihilation and diffusion of excitons in organic microcavities with disordered *J*-aggregate cyanine dyes having a very high, 10^6 cm^{-1}, absorption coefficient.[175] It is clear, however, that further experimental and theoretical studies of the discussed processes need to be in place to evaluate bimolecular polariton quenching in the nonlinear dynamics of excitations in disordered, single-crystal, and hybrid organic microcavities.

3.5. Cavity Polaritons in Hybrid Microcavities: First Experiments

As we discussed at length, hybrid organic−inorganic microcavities are expected to combine the merits of both components in the same system. It is worthwhile, however, to also mention several studies in which the hybridization has been realized of inorganic−inorganic and organic−organic excitons in a microcavity. In ref 176, the strong coupling of heavy- and light-hole excitons to one cavity mode was reported in an inorganic GaAs microcavity. Another example of cooperative hybridization of excitations from the same (organic) material can be found in ref 138, where a Frenkel exciton and higher energy vibrons are strongly coupled to the cavity mode. The coupling of two W−M excitons from different quantum wells and of two Frenkel excitons from two separated organic layers with microcavity photons has been observed, respectively, in refs 177 and 178. As one should expect, three cavity polariton branches have been detected in those studies, with the middle branch containing a significant component of the cavity photon as well as both excitonic states, while the upper (lower) branch corresponds mainly to an admixture of the cavity photon with the higher (lower) energy exciton.

A theoretical study of hybrid organic−inorganic cavity polaritons composed of two (one Frenkel and one W-M) quasi-2D excitons strongly coupled to the same cavity photon mode was performed in ref 8. In the strong-coupling regime, this system can be described as three coupled oscillators whose eigenstates are determined from equation:

$$\begin{pmatrix} E_{\mathrm{cav}}(k) - E & W_{\mathrm{F}} & W_{\mathrm{WM}} \\ W_{\mathrm{F}} & E_{\mathrm{F}} - E & 0 \\ W_{\mathrm{WM}} & 0 & E_{\mathrm{WM}} - E \end{pmatrix} \begin{pmatrix} C(k) \\ X_{\mathrm{F}}(k) \\ X_{\mathrm{WM}}(k) \end{pmatrix} = 0 \tag{38}$$

Here, subscripts clearly identify each of the involved states. It was suggested that a large oscillator strength of the Frenkel exciton could lead to a large Rabi splitting energy, which in turn would allow for the one-step energy relaxation with the emission of a higher-energy optical phonon, as illustrated in Figure 20. The corresponding transition time was calculated to be ∼10 ps, so that such transitions could be operational in accessing the bottom of the lower polariton branch despite the bottleneck knee (section 3.1.3). Also suggested in ref 8 was the possibility to combine in these structures the electrical pumping of the inorganic component with the fast relaxation and fluorescence of excitons in organic materials.

First experimental observations[179,180] (two papers submitted with a three-day difference) of the hybridization of Frenkel and W−M excitons in microcavities appeared only recently. In ref 179, the hybridization between the excitons in a polycrystalline tetraphenylporphyrin layer (Frenkel exciton) and in nine $In_{0.52}Ga_{0.48}P$ quantum wells (W−M exciton) with a single cavity photon was observed. The compounds were separated by a barrier of 75 nm to prevent the direct coupling between excitons.

dx.doi.org/10.1021/cr100156x |*Chem. Rev.* 2011, 111, 5179–5214

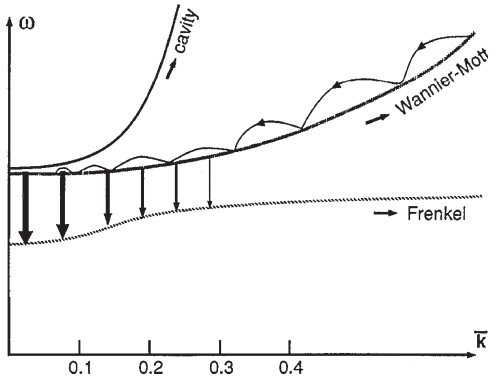

Figure 20. In a hybrid organic−inorganic microcavity, the energy relaxation via emission of small-energy acoustical phonons along the Wannier−Mott-like branch is followed by a one-step optical phonon-assisted relaxation to the lowest energy state. Reprinted with permission from ref 8. Copyright 1997 Pergamon.

The angularly resolved reflectivity spectra were taken under white light excitation for temperatures of 100 and 4 K. As a reference, the 4 K measurements were also performed in a purely inorganic microcavity with the identical structure. The anticrossing giving rise to the three hybrid modes (upper, middle, and lower polaritons) was observed, and the dispersion curves fitted with a model of three coupled oscillators. The bare excitons were found separated by the energy difference of 40 meV. The lower (upper) branch was basically a mixture of the cavity photon with Frenkel (W−M) exciton, while the middle branch was a hybrid state with significant fractions of all three components. At the angle of the strongest Frenkel−W−M exciton coupling (which was defined as an angle at which both excitons have the same fraction in the middle polariton state), the hybrid middle state consisted of 10% of excitons of each type and 80% of the cavity photon. At significantly lower temperatures, the excitonic fraction was observed to decrease due to the blue shift of the higher-energy W−M exciton. At higher temperatures, the strong-coupling regime was destroyed because of the growth of the W−M exciton line width. The following coupling constants (the half of the Rabi splitting energy; see eq 38) were extracted from the fit: W_F = 10 meV (at T = 100 K) and 11 meV (at T = 4 K), W_{WM} = 4 meV (T = 100 K and T = 4 K). The observed coupling strength W_{WM} was approximately one-half of the coupling strength found for the purely inorganic microcavity: W_{in} = 10 meV at T = 4 K.

In ref 180, the hybridized polaritons are formed in the system of organic dyes zinc tetraphenyl-porphyrin supporting Frenkel-type excitons, and layered perovskites of phenylethylamine tetrabromoplumbate $[(C_6H_5C_2H_4NH_3)_2PbBr_4]$ as the inorganic semiconductor material supporting W−M-type excitons. The materials were chosen so that they have similar oscillator strengths and absorption linewidths. Two layers placed in the wage-shaped microcavity exhibited the strong coupling, despite the presence of the lower-lying state for the organic component of the hybrid system (in the uncoupled regime, the Frenkel exciton of the organic compound would undergo a rapid relaxation into this lower energy state from the so-called Soret band, which was used for hybridization). The position-resolved reflectivity measurements were made at a fixed oblique angle of incidence under white light excitation, and the results were again fitted with the three coupled oscillator model eq 38. The extracted coupling constants were W_F = 54 meV, W_{WM} = 81 meV (the linewidths of both excitons were of the order of 100 meV). The weight coefficients at the point of the largest mixing between excitons of the both type were measured as $|X_F|^2 = |X_{WM}|^2 = 0.3$, $|C|^2 = 0.4$.

The photoluminescence measurements performed in ref 180 exhibited only one peak, which overlapped with the middle branch for large photon fraction and small Frenkel exciton fraction, and corresponded to the uncoupled emission from the perovskite layer otherwise. On the basis of this observation, the following picture of the energy relaxation in these structures was proposed. The energy of the W−M exciton in the sample was larger than the energy of the Frenkel-type exciton. The middle branch polaritonic states were populated from the perovskite W−M-type states (most likely, from the reservoir of the uncoupled exciton-like states), as the population of polaritons from the Frenkel-type Soret band excitons was anticipated to be negligible due to their fast decay into the lower-lying organic dye state. Because of this decay, when the Frenkel-type exciton fraction was large, the polaritonic regime was destroyed, the Frenkel-type state decayed nonradiatively, and the photoluminescence from the microcavity was dominated by the uncoupled W−M-type exciton emission. When X_F was small and C was large (so as to provide the effective hybridization), fast nonradiative relaxation was suppressed, the polaritonic regime was recovered, and the photoluminescence came from the middle branch polariton states. The upper and lower branch polaritonic states were not observed in the photoluminescence due to their negligible overlap with the perovskite excitons.

The field of hybrid organic−inorganic microcavities appears ripe for further development, both experimentally and theoretically.

A. APPENDIX

A.1. Excitonic Polarization in the Semiconductor Quantum Well

The Cartesian components d_i^{vc} of the electric dipole transition moment $\mathbf{d}^{vc}$ between the conduction and valence bands of the semiconductor material can be expressed in terms of the Kane's energy E_{Kane} and the exciton transition energy by the the relation:[26]

$$|d_i^{vc}|^2 = \frac{e^2\hbar^2 C_i^2 E_{Kane}}{2m_0(E_g)^2} \quad (39)$$

where index i labels the coordinate axes ($i = x, y, z$), m_0 is the free electron mass, and E_g is the bandgap energy. In semiconductors of the zink-blende structure for the heavy-hole (hh) or light-hole (lh) valence bands, the coefficients C_i are given as follows: $C_{xhh} = C_{yhh} = 1/\sqrt{2}$ and $C_{zhh} = 0$, $C_{xlh} = C_{ylh} = 1/\sqrt{6}$, $C_{zlh} = (2/3)^{1/2}$. In ZnSe/ZnCdSe quantum wells, which we consider here as an example, vector $\mathbf{d}$ could be along the growth direction z (Z-modes), in which case only light-hole states contribute, or in the QW plane (x,y). If vector $\mathbf{d}$ is parallel to the wave vector $\mathbf{k}$, the corresponding transitions are called L-modes. If vector $\mathbf{d}$ is perpendicular to $\mathbf{k}$ and parallel to the quantum well plane, the corresponding transitions are called T-modes.

One can adopt a simplified microscopic quantum-mechanical model of a two-dimensional W−M exciton, in which the

dx.doi.org/10.1021/cr100156x |Chem. Rev. 2011, 111, 5179–5214

polarization $\mathbf{P}$ vanishes for $|z| > L_w/2$. Inside the well, on the other hand, it is determined by the product of the 1s lowest sub-band envelope wave function of the relative motion of the electron and hole at the origin and the wave function of the center-of-mass motion:

$$\mathbf{P}(\mathbf{r}) = \mathbf{d}^{vc}\sqrt{\frac{2}{\pi a_B^2}}\frac{2}{L_w}cos^2\left(\frac{\pi z}{L_w}\right)\frac{e^{i\mathbf{k}\mathbf{r}_\parallel}}{\sqrt{S}} \quad (40)$$

Here, S is the in-plane normalization area, $\mathbf{k}$ is the in-plane wave vector of the center-of-mass motion, $\mathbf{r} = (x;y)$ is the in-plane component of $\mathbf{r}$, and a_B is the 2D 1s-exciton Bohr radius.[26] Let us choose the x-axis along the direction of the in-plane component of the exciton dipole moment $\mathbf{d}^{vc}$. Consider two cases of $\mathbf{d}^{vc}$ being parallel or perpendicular to the quantum well plane, we would then refer to them as X- and Z-polarizations, respectively. When dealing with free excitons, three modes of different symmetry can be identified: longitudinal (L), transverse (T), and perpendicular (Z). The L- and Z-modes correspond to the X and Z polarizations above. The T-mode does not contribute to transitional charge density and energy transfer.[6] Leaving out the common dependence on $\exp(i\mathbf{k}\mathbf{r}_\parallel)$, the Poisson equation can now be written as

$$\left[\frac{d^2}{dz^2} - k^2\right]\varphi(z) = \begin{cases} 4\pi\rho(z)/\varepsilon_b, & |z| < L_w/2, \\ 0, & |z| > L_w/2, \end{cases} \quad (41)$$

The charge density $\rho(z)$ in eq 41, as discussed, depends on the exciton polarization:

$$\rho_X(z) = ik_xL_w\rho_0(1 + cos\ qz),\ \rho_Z(z) = -qL_w\rho_0\ sin\ qz \quad (42)$$

$$\rho_0 = \sqrt{\frac{2}{\pi a_B^2}}\frac{d^{vc}}{L_w^2\sqrt{S}},\ q = 2\pi/L_w$$

The boundary conditions to be used in the solution of eq 41 are that $\varphi(z)$ and $\varepsilon(z)\ d\varphi\ (z)/dz$ should be continuous at the four interfaces of the structure. The corresponding solution in the overlayer (organic) material (for $|z| > L_w/2 + L_b$) is given by

$$\varphi(z) = \rho_0 C_k e^{-k(|z| - L_w/2 - L_b)} \quad (43)$$

where the function C_k is different for X- and Z-polarizations:

$$C_k^X = -\frac{ik_x}{k}\frac{8\pi^2 q}{k(k^2+q^2)}\frac{sinh(kL_w/2)}{\varepsilon_b\ sinh(kL_b + kL_w/2) + \tilde{\varepsilon}\ cosh(kL_b + kL_w/2)}$$

and

$$C_k^Z = \frac{8\pi^2 q}{k(k^2+q^2)}\frac{sinh(kL_w/2)}{\varepsilon_b\ cosh(kL_b + kL_w/2) + \tilde{\varepsilon}\ sinh(kL_b + kL_w/2)}$$

AUTHOR INFORMATION

Corresponding Author

*E-mail: vladimir.agranovich@utdallas.edu.

BIOGRAPHIES

Vladimir M. Agranovich, currently a Research Scientist Fellow of Chemistry at The University of Texas at Dallas and a Principal Investigator at the Institute for Spectroscopy of the Russian Academy of Sciences (RAS), received his Ph.D. in 1955 from Kiev State University and Dr.Sci. in 1961 from the RAS Institute of Chemical Physics. For over 40 years, he was a head of the Theoretical Department of Institute for Spectroscopy. He is the recipient of the Humboldt Research Prize (Alexander von Humboldt Foundation, Germany), the Kapitsa Award (UK), and the Mandelstam Prize (the Russian Academy of Science). He is an elected Fellow of Institute of Physics (UK) and of the American Physical Society, and he has a title of Doctor Honoris Causa from Blaise Pascal University (Clermont-Ferrand, France). His recent interests focus on electronic excitations (Frenkel and charge-transfer excitons, plasmons, polaritons) in nanostructures, microcavities, and at interfaces, on hybrid organic−inorganic nanostructures for light emitting devices and solar cells, and on linear and nonlinear optical properties of natural materials with negative refraction. He authored or coauthored several monographs including "Theory of Excitons", "Crystal Optics with Spatial Dispersion, and Excitons" (with V. L. Ginzburg), "Electronic Excitation Energy Transfer in Condensed Matter" (with M. D. Galanin), and "Electronic Excitations in Organic Solids". He currently serves as an editor of the journal "Physics Letters A".

Yuri Gartstein received his Ph.D. in 1988 from the Institute for Spectroscopy of the Soviet Academy of Sciences. He worked as a research physicist at the Uzbekistan Academy of Sciences, at the NSF Center for Photoinduced Charge Transfer at the University of Rochester, and as a Member of the Research and Technology

Staff of Xerox Corp. In 2003, he joined the faculty of the Department of Physics at The University of Texas at Dallas, where he resides now. His research interests cover various aspects of theory and modeling of electronic, optical, transport, and mechanical properties of advanced materials and nanostructures including carbon nanotubes, organic solids, conjugated polymers, organic−inorganic hybrids, and unconventional superconductors. He is also interested in physics of devices on the basis of such materials, examples being light-emitting diodes, solar cells, and electromechanical actuators.

Marina Litinskaya received her Ph.D. in 2001 from Scuola Normale Superiore in Pisa. Since then, she worked as a researcher in the Theoretical department of the Institute for Spectroscopy in Troitsk, Moscow Region. She spent 2 years at the University of Ulm as a Humboldt fellow. During this time, her research interests were focused mainly on physics of exciton-polaritons in low dimensional organic and inorganic materials. Currently, she is a research associate at the University of British Columbia in Vancouver, where she studies excitonic effects in optical lattices with ultracold polar molecules.

ACKNOWLEDGMENT

V.M.A. acknowledges partial support from the Russian Foundation of Basic Research.

REFERENCES

(1) Shinar, J., Ed. *Organic Light-Emitting Devices*; Springer: New York, 2004.
(2) Sun, S. S., Sariciftci, N. S., Eds. *Organic Photovoltaics: Mechanisms, Materials, and Devices*; CRC Press: Boca Raton, FL, 2005.
(3) Vardeny, Z. V., Ed. *Ultrafast Dynamics and Laser Action of Organic Semiconductors*; CRC Press: Boca Raton, FL, 2009.
(4) Pope, M.; Kalmann, H.; Magnante, P. *J. Chem. Phys.* **1963**, *38*, 2042.
(5) Weisbuch, C.; Vinter, B. *Quantum Semiconductor Structures. Fundamentals and Applications*; Academic Press: Boston, 1991.
(6) Agranovich, V. M.; Atanasov, R.; Bassani, G. F. *Solid State Commun.* **1994**, *92*, 295.
(7) Agranovich, V. M.; La Rocca, G. C.; Bassani, F. *JETP Lett.* **1997**, *66*, 748.
(8) Agranovich, V. M.; Benisty, H.; Weisbuch, C. *Solid State Commun.* **1997**, *102*, 631.
(9) Oulton, R. F.; Takada, N.; Koe, J.; Stavrinou, P. N.; Bradley, D. D. C. *Semicond. Sci. Technol.* **2003**, *18*, S419.
(10) Green, B. I.; Orenstein, J.; Schmitt-Rink, S. *Science* **1990**, *247*, 679.
(11) La Rocca, G. C.; Bassani, F.; Agranovich, V. M. *Nuovo Cimento* **1995**, *17D*, 1555.
(12) Basko, D.; La Rocca, G. C.; Bassani, F.; Agranovich, V. M. *Eur. Phys. J. B* **1999**, *8*, 353.
(13) Agranovich, V. M.; Basko, D. M.; La Rocca, G. C.; Bassani, F. *Synth. Met.* **2001**, *116*, 349.
(14) Naher, D. *Macromol. Rapid Commun.* **2001**, *22*, 1365.
(15) Hide, F.; Kozodoy, P.; DenBaars, S. P.; Heeger, A. J. *Appl. Phys. Lett.* **1997**, *70*, 2664.
(16) Guha, S.; Haight, R. A.; Bojarczuk, N. A.; Kisker, D. *Appl. Phys. Lett.* **1997**, *82*, 4126.
(17) Belton, C. R.; et al. *J. Phys. D: Appl. Phys.* **2008**, *41*, 094006.
(18) Heliotis, G.; Itskos, G.; Murray, R.; Dawson, M. D.; Watson, I. M.; Bradley, D. D. C. *Adv. Mater.* **2006**, *18*, 334–338.
(19) Holmes, R. J.; Forrest, S. R. *Org. Electron.* **2006**, *8*, 77.
(20) Agranovich, V. M.; Basko, D. M.; La Rocca, G. C.; Bassani, F. *J. Phys.: Condens. Matter* **1998**, *10*, 9369.
(21) Agranovich, V. M. In *Problems of Condensed Matter*; Ivanov, A. L., Tikhodeev, S. G., Eds.; Clarendon Press: Oxford, 2008; p 24.
(22) Agranovich, V. M. *Excitations in Organic Solids*; Oxford University Press: Oxford, 2009; Chapter 13.
(23) Schmitt-Rink, S.; Chemla, D. S.; Miller, D. A. B. *Adv. Phys.* **1989**, *38*, 89.
(24) Boyd, R. W. *Nonlinear Optics*; Elsevier: Amsterdam, 2003.
(25) Chemla, D. S.; Zyss, J. *Nonlinear Optical Properties of Organic Molecules and Crystals*; Academic Press: New York, 1987.
(26) Bastard, G. *Wave Mechanics Applied to Semiconductor Heterostructures*; Les ed.s de Physique: Les Ulis, 1988.
(27) Haug, H.; Koch, S. W. *Quantum Theory of the Optical and Electronic Properties of Semiconductors*; World Scientific: NJ, 2004.
(28) Dodabalapur, A. *Solid State Commun.* **1997**, *102*, 259.
(29) Agranovich, V. M.; Galanin, M. D. *Electronic Excitation Energy Transfer in Condensed Matter*; Elsevier: Amsterdam, 1982.
(30) Agranovich, V. M.; Basko, D. M. *JETP Lett.* **1999**, *69*, 250.
(31) Basko, D. M.; Agranovich, V. M.; Bassani, F.; La Rocca, G. C. *Eur. Phys. J. B* **2000**, *13*, 653.
(32) Javier, A.; Yun, C. S.; Sorena, J.; Strouse, G. F. *J. Phys. Chem. B* **2003**, *107*, 435.
(33) Jing, P.; X, Y.; Ji, W.; Ikezawa, M.; Wang, Y. A.; Liu, X.; Zhang, L.; Zhao, J.; Masumoto, Y. *J. Phys. Chem.* **2010**, *114*, 19256.
(34) Basko, D. M. *Thin Films Nanostruct.* **2003**, *31*, 447.
(35) Landau, L. D.; Lifshitz, E. M. *Electrodynamics of Continuous Media*; Butterworth-Heinemann: Oxford, 1984.
(36) Cingolani, R. *Semicond. Semimetals* **1997**, *44*, 163.
(37) Yamada, T.; Hoshi, H.; Monaka, T.; Ishikawa, K.; Takezoe, H.; Fukuda, A. *Phys. Rev. B* **1966**, *53*, R13314.
(38) Umlauff, M.; et al. *Phys. Rev. B* **1998**, *57*, 1390.
(39) Shah, J. *Ultrafast Spectroscopy of Semiconductors and Semiconductor Nanostructures*; Springer-Verlag: Berlin, 1996.
(40) Blumstengel, S.; Sadofev, S.; Xu, C.; Puls, J.; Henneberger, F. *Phys. Rev. Lett.* **2006**, *97*, 237401.
(41) Achermann, M.; Petruska, M. A.; Kos, S.; Smith, D. L.; Koleske, D. D.; Klimov, V. I. *Nature* **2004**, *429*, 642.
(42) Rohmoser, S.; Baldauf, J.; Harley, R. T.; Lagoudakis, P. G.; Sapra, S.; Eychmuller, A.; Watson, I. M. *Appl. Phys. Lett.* **2007**, *91*, 092126.
(43) Deveaud, B.; Kappei, L.; Berney, J.; Morier-Genoud, F.; Portella-Oberli, M. T.; Szczytko, J.; Piermarocchi, C. *Chem. Phys.* **2005**, *318*, 104.
(44) Kaindl, R. A.; Hagele, D.; Carnaham, M. A.; Chemla, D. S. *Phys. Rev. B* **2009**, *79*, 045320.
(45) Sooklal, K.; Hanus, L. H.; Ploehn, H. J.; Murphy, C. J. *Adv. Mater.* **1998**, *10*, 1083.
(46) Huong, N. Q.; Birman, J. L. *Phys. Rev. B* **1999**, *61*, 13131.
(47) Lemon, B. I.; Crooks, R. M. *J. Am. Chem. Soc.* **2000**, *122*, 12886.
(48) Gayen, S. K.; Brito, M.; Das, B. B.; Comanescu, G.; Liang, X. C.; Alrubaiee, M.; Alfano, R. R.; Gonzalez, C.; Byro, A. H.; Bauer, D. L. V.; Balogh-Nair, V. *J. Opt. Soc. Am. B* **2007**, *24*, 3064.

(49) Blumstengel, S.; Sadofev, S.; Puls, J.; Henneberger, F. *Adv. Mater.* **2009**, *21*, 4850.
(50) Itskos, G.; Heliotis, G.; Lagoudakis, P. G.; Lupton, J.; Barradas, N. P.; Alves, E.; Pereira, S.; Watson, I. M.; Dawson, M. D.; Feldmann, J.; Murray, R.; Bradley, D. D. C. *Phys. Rev. B* **2007**, *76*, 035344.
(51) Rohrmoser, S.; Baldauf, J.; Harley, R. T.; Lagoudakis, P. G.; Sarpa, S.; Eychmuller, A.; Watson, I. M. *Appl. Phys. Lett.* **2007**, *91*, 092126.
(52) Zhang, Q.; Atay, T.; Tischler, J. R.; Bradley, M. S.; Bulović, V.; Nurmikko, A. V. *Nat. Nanotechnol.* **2007**, *2*, 555.
(53) Agranovich, V. M.; Czajkowski, G. arXiv:0801.3794, 2008.
(54) Sirota, M.; Minkin, E.; Lifshitz, E.; Hensel, V.; Lahav, M. *J. Phys. Chem. B* **2001**, *105*, 6792.
(55) Golubov, S. I.; Konobeev, Y. V. *Phys. Status Solidi B* **1977**, *79*, 79.
(56) Dexter, D. L. *J. Chem. Phys.* **1953**, *21*, 836.
(57) Lima, P. P.; et al. *J. Phys. Chem. C* **2007**, *111*, 17627.
(58) Ema, K.; Inomata, M.; Kato, Y.; Kunugita, H.; Era, M. *Phys. Rev. Lett.* **2008**, *100*, 257401.
(59) Tanaka, K.; Takahashi, T.; Kondo, T.; Umeda, K.; Ema, K.; Umebayashi, T.; Asai, K.; Uchida, K.; Miura, N. *Jpn. J. Appl. Phys.* **2005**, *44*, 5923.
(60) Ema, K.; Umeda, K.; Toda, M.; Yajima, C.; Arai, Y.; Kunugita, H.; Wolverson, D.; Davies, J. J. *Phys. Rev. B* **2006**, *73*, 241310(R).
(61) Ishihara, T.; Takahashi, J.; Goto, T. *Phys. Rev. B* **1990**, *42*, 11099.
(62) Tanaka, K.; Takahashi, T.; Kondo, T.; Umebayashi, T.; Asai, K.; Ema, K. *Phys. Rev. B* **2005**, *71*, 045312.
(63) Kato, Y.; Ichii, D.; Ohashi, K.; Kunugita, H.; Ema, K.; Tanaka, K.; Takahashi, T.; Kondo, T. *Solid State Commun.* **2003**, *128*, 15.
(64) Achermann, M.; Petrushka, M. A.; Koleske, D.; Crawford, M. H.; Klimov, V. I. *Nano Lett.* **2006**, *6*, 1396.
(65) Chanyawadee, S.; Lagoudakis, P. G.; Harley, R. T.; Charlton, M. D. B.; Talapin, D. V.; Huang, H. W.; Lin, C. H. *Adv. Mater.* **2009**, *21*, 1.
(66) La Rocca, G. C.; Gartstein, Y. N.; Henneberger, F.; Agranovich, V. M., in preparation.
(67) Shen, R. *The Principles of Nonlinear Optics*; Wiley: New York, 1984.
(68) Gao, Y.; Tonizzo, A.; Walser, A.; Potasek, M.; Dorsinville, R. *Appl. Phys. Lett.* **2008**, *92*, 033106.
(69) Gao, Y.; Huang, N. Q.; Birman, J. L.; Potasek, M. J. *J. Appl. Phys.* **2004**, *96*, 4839.
(70) Roslyak, O.; Birman, J. *J. Phys.: Condens. Matter* **2008**, *20*, 235238.
(71) Chanyawadee, S.; Harley, R. T.; Henini, M.; Talapin, D. V.; Lagoudakis, P. G. *Phys. Rev. Lett.* **2009**, *102*, 077402.
(72) Basko, D. M.; La Rocca, G. C.; Bassani, F.; Agranovich, V. M. *Phys. Rev. B* **2005**, *71*, 165330.
(73) Dexter, D. L. *J. Lumin.* **1979**, *18/19*, 779.
(74) Agranovich, V. M.; Rupasov, V. I.; Silvestry, L. *Phys. Status Solidi* **2010**, 111.
(75) Pope, M.; Swenberg, C. E. *Electronic Processes in Organic Crystals and Polymers*; Oxford: New York, 1999.
(76) Chance, R. R.; Prock, A.; Silbey, R. In *Advances in Chemical Physics*; Rice, S. A., Prigogine, I., Eds.; Wiley: New York, 1978; Vol. 37, p 1.
(77) Agranovich, V. M.; Malshukov, A. G.; Mekhtiev, M. *Sov. Phys. JETP* **1973**, *36*, 1203.
(78) Waldeck, D. H.; Alivisatos, A. P.; Harris, C. B. *Surf. Sci.* **1985**, *158*, 103.
(79) Novotny, L.; Hecht, B. *Principles of Nano-Optics*; Cambridge University Press: Cambridge, 2006.
(80) Agranovich, V. M. *Sov. Phys.-Solid State* **1973**, *14*, 3085.
(81) Agranovich, V. M.; Malshukov, A. G. *Chem. Phys. Lett.* **1976**, *43*, 221.
(82) Sommerfeld, A. *Partial Differential Equations in Physics*; Academic Press: New York, 1964.
(83) Kuhn, H. *J. Chem. Phys.* **1970**, *53*, 101.
(84) Aspnes, D. E.; Studna, A. A. *Phys. Rev. B* **1983**, *27*, 985.
(85) Alivisatos, A. P.; Arndt, M. F.; Efrima, S.; Waldeck, D. H.; Harris, C. B. *J. Chem. Phys.* **1987**, *86*, 6540.
(86) Agranovich, V. M.; Ginzburg, V. L. *Crystal Optics with Spatial Dispersion, and Excitons*; Springer-Verlag: Berlin, 1984.
(87) Stavola, M.; Dexter, D. L.; Knox, R. S. *Phys. Rev. B* **1985**, *31*, 2277.
(88) Whitmore, P. M.; Alivisatos, A. P.; Harris, C. B. *Phys. Rev. Lett.* **1983**, *50*, 1092.
(89) Gowrishankar, V.; Scully, S. R.; Chan, A. T.; McGehee, M. D.; Wang, Q.; Branz, H. M. *J. Appl. Phys.* **2008**, *103*, 064511.
(90) Zhang, Q.; Atay, T.; Tischler, J. R.; Bradley, M. S.; Bulovic, V.; Nurmikko, A. V. *Nat. Nanotechnol.* **2007**, *2*, 555.
(91) Lu, S.; Madhukar, A. *Nano Lett.* **2007**, *7*, 3443.
(92) Lu, S.; Lingley, Z.; Asano, T.; Harris, D.; Barwicz, T.; Guha, S.; Madhukar, A. *Nano Lett.* **2009**, *9*, 4548.
(93) Nguyen, H. M.; Seitz, O.; Aureau, D.; Sra, A.; Nijem, N.; Gartstein, Y. N.; Chabal, Y. J.; Malko, A. V. *Appl. Phys. Lett.* **2011**, *98*, 161904.
(94) Braun, M.; Tuffentsammer, W.; Wachtel, H.; Wolf, H. C. *Chem. Phys. Lett.* **1999**, *303*, 157.
(95) Turlet, J. M.; Kottis, P.; Philpott, M. R. *Adv. Chem. Phys.* **1983**, *54*, 303.
(96) Philpott, M. R.; Turlet, J. M. *J. Chem. Phys.* **1976**, *64*, 3852.
(97) Atanasov, R.; Bassani, G. F.; Agranovich, V. M. *Phys. Rev. B* **1994**, *50*, 7809.
(98) Hopfield, J. J. *Phys. Rev. B* **1958**, *112*, 1555.
(99) Agranovich, V. M. *Sov. Phys. JETP* **1959**, *10*, 307.
(100) Rose, T. S.; Nevel, V. J.; Meth, J. S.; Fayer, M. D. *Chem. Phys. Lett.* **1988**, *145*, 475.
(101) Simpson, O. *Proc. R. Soc. London, Ser. A* **1957**, *238*, 402.
(102) Ferguson, J. *Chem. Phys. Lett.* **1975**, *36*, 316.
(103) Vidmont, N. A.; Maksimov, A. A.; Tartakovskii, I. I. *ZhETP Lett.* **1983**, *37*, 689.
(104) Toyozawa, Y. *Suppl. Prog. Theor. Phys.* **1959**, *12*, 111.
(105) Agranovich, V. M. *Usp. Fiz. Nauk* **1960**, *71*, 141.
(106) Weisbuch, C.; Ulrich, R. G. *Phys. Rev. Lett.* **1977**, *39*, 654.
(107) Weisbuch, C.; Ulrich, R. G. *Phys. Rev. Lett.* **1977**, *38*, 865.
(108) Faust, W. L.; Henry, C. H. *Phys. Rev. Lett.* **1966**, *17*, 1265.
(109) Porto, S. P. S.; Tell, B.; Damen, T. C. *Phys. Rev. Lett.* **1966**, *16*, 450.
(110) Burstein, E. *Comments Solid State Phys.* **1969**, *1*, 202.
(111) Born, M.; Huang, K. *Dynamical Theory of Crystal Lattices*; Clarendon Press: Oxford, 1954.
(112) Burstein, E.; Mills, D. L. *Comments Solid State Phys.* **1970**, *3*, 12.
(113) Agranovich, V. M.; Konobeev, Y. V. *Sov. Phys. Solid State* **1961**, *3*, 260.
(114) Knox, R. S. *Solid State Phys. Suppl.* **1963**, *5*, x.
(115) Knoester, J.; Mukamel, S. *J. Chem. Phys.* **1989**, *91*, 989.
(116) Weisbuch, C.; Nishioka, M.; Ishikawa, A.; Arakawa, Y. *Phys. Rev. Lett.* **1992**, *69*, 3314.
(117) Agranovich, V. M.; Malshukov, A. G. *Opt. Commun.* **1974**, *11*, 169.
(118) Agranovich, V. M.; La Rocca, G. C. *Solid State Commun.* **2005**, *135*, 544.
(119) Vinogradov, E. A.; Leskova, T. A. *Phys. Rep.* **1990**, *194*, 271.
(120) Bellessa, J.; Bonnand, C.; Plenet, J. C. *Phys. Rev. Lett.* **2004**, *93*, 036402.
(121) Pockrand, I.; Brillante, A.; Mobius, D. *J. Chem. Phys.* **1982**, *77*, 6289.
(122) Dintinger, J.; Klein, S.; Bustos, F.; Barns, W. L.; Ebbesen, T. *Phys. Rev. B* **2005**, *71*, 035424.
(123) Bellessa, J.; Symonds, C.; Meynaud, C.; Plenet, J. C.; Cambri, E.; Miard, A.; Ferlazzo, L.; Lemaistre, A. *Phys. Rev. B* **2008**, *78*, 205326.
(124) Symonds, C.; Bonnand, C.; Plenet, J. C.; Brehier, A.; Parashkov, R.; Lauret, J. S.; Deleporte, E.; Bellessa, J. *New J. Phys.* **2008**, *10*, 065017.
(125) Symonds, C.; Bellessa, J.; Plenet, J. C. *Appl. Phys. Lett.* **2007**, *90*, 091107.

(126) Hakala, T. K.; Toppari, J. J.; Kuzyk, A.; Pettersson, M.; Tikkanen, H.; Kunttu, H.; Torma, A. *Phys. Rev. Lett.* **2009**, *103*, 053602.
(127) Bellessa, J.; Symonds, C.; Vynck, K.; Lemaistre, A.; Brioude, A.; Plenet, J. C.; Viste, P.; Felbacq, D.; Cambri, E.; Valvin, P. *Phys. Rev. B* **2009**, *80*, 033303.
(128) Kasprzak, J.; Richard, M.; Kundermann, S.; Baas, A.; Jeambrun, P.; Keeling, J. M. J.; Marchetti, F. M.; Szymańska, M. H.; André, R.; Staehli, J. L.; Savona, V.; Littlewood, P. B.; Deveaud, B.; Dang, L. S. *Nature* **2006**, *443*, 409.
(129) Deng, H.; Haug, H.; Yamamoto, Y. *Rev. Mod. Phys.* **2010**, *82*, 1489.
(130) Kavokin, A.; Malpuech, G. *Cavity Polaritons*; Elsevier: Amsterdam, 2003.
(131) Khitrova, G.; Gibbs, H. M.; Jahnke, F.; Kira, M.; Koch, S. W. *Rev. Mod. Phys.* **1999**, *71*, 1591.
(132) Benisty, H.; Weisbuch, C.; Agranovich, V. M. *Physica E* **1998**, *2*, 909.
(133) Lidzey, D. G.; Bradley, D. D. C.; Skolnick, M. S.; Virgili, T.; Walker, S.; Whittaker, D. M. *Nature* **1998**, *395*, 53.
(134) Lidzey, D. G.; Bradley, D. D. C.; Skolnick, M. S.; Virgili, T.; Walker, S.; Whittaker, D. M. *Phys. Rev. Lett.* **1999**, *82*, 3316.
(135) Sumi, H. *J. Phys. Soc. Jpn.* **1976**, *41*, 526.
(136) Virgili, T.; Coles, D.; Adawi, A. M.; Clark, C.; Michetti, P.; Rajendran, S. K.; Brida, D.; Polli, D.; Cerullo, G.; Lidzey, D. G. *Phys. Rev. B* **2011**, *83*, 245309.
(137) Kéna-Cohen, S.; Davanco, M.; Forrest, S. R. *Phys. Rev. Lett.* **2008**, *101*, 116401.
(138) Holmes, R. J.; Forrest, S. R. *Phys. Rev. Lett.* **2004**, *93*, 186404.
(139) Kéna-Cohen, S.; Forrest, S. R. *Phys. Rev. B* **2008**, *77*, 073205.
(140) Fontanezi, L.; Mazza, L.; La Rocca, G. C. *Phys. Rev. B* **2009**, *78*, 235313.
(141) Mazza, L.; Fontanezi, L.; La Rocca, G. C. *Phys. Rev. B* **2009**, *78*, 235314.
(142) Kondo, H.; Tongu, K.; Yamamoto, Y.; Takedo, A.; Yamamoto, S.; Kurisu, H. *J. Lumin.* **2008**, *128*, 777.
(143) Kondo, H.; Tongu, K.; Yamamoto, Y.; Yamamoto, S.; Kurisu, H. *Phys. Status Solidi C* **2009**, *6*, 284.
(144) Davydov, A. S. *Theory of Molecular Excitons*; Plenum: New York, 1971.
(145) Born, M.; Huang, K. *Dynamical Theory of Crystal Lattices*; Clarendon Press: Oxford, 1954.
(146) Litinskaya, M. L.; Reineker, P.; Agranovich, V. M. *Phys. Status Solidi A* **2004**, *201*, 646.
(147) Zoubi, H.; La Rocca, G. C. *Phys. Rev. B* **2005**, *71*, 235316.
(148) Litinskaya, M. L.; Agranovich, V. M. *J. Phys.: Condens. Matter* **2009**, *21*, 415301.
(149) Kéna-Cohen, S.; Davanco, M.; Forrest, S. R. *Phys. Rev. B* **2008**, *78*, 153102.
(150) Tartakovskii, A. I.; Emam-Ismail, M.; Lidzey, D. G.; Skolnik, M. S.; Bradley, D. D. C.; Walker, S.; Agranovich, V. M. *Phys. Rev. B* **2001**, *63*, 121302(R).
(151) Hobson, P. A.; Barnes, W. L.; Lidzey, D. G.; Gehring, G. A.; Whittaker, D. M.; Skolnick, M. S.; Walker, S. *Appl. Phys. Lett.* **2002**, *81*, 3519.
(152) Hochstrasser, R. M.; Whiteman, J. D. *J. Chem. Phys.* **1972**, *56*, 5945.
(153) Knapp, E. W. *Chem. Phys.* **1984**, *85*, 73.
(154) Schwartz, T.; Hutchison, J. A.; Genet, C.; Ebbesen, T. W. *Phys. Rev. Lett.* **2011**, *106*, 196405.
(155) Sasaki, K.; Nagamura, T. *J. Appl. Phys.* **1998**, *83*, 2894.
(156) Dintinger, J.; Klein, S.; Ebbesen, T. W. *Adv. Mater.* **2006**, *18*, 1267.
(157) Sridharan, D.; et al. *Appl. Phys. Lett.* **2010**, *96*, 153303.
(158) Agranovich, V. M.; Litinskaia, M.; Lidzey, D. G. *Phys. Rev. B* **2003**, *67*, 085311.
(159) Litinskaya, M.; Reineker, P. *Phys. Rev. B* **2006**, *74*, 165320.
(160) Michetti, P.; La Rocca, G. C. *Phys. Rev. B* **2005**, *71*, 115320.
(161) Agranovich, V. M.; Gartstein, Y. N. *Phys. Rev. B* **2007**, *75*, 075302.
(162) Litinskaya, M. *Phys. Lett. A* **2008**, *372*, 3898.
(163) Chovan, J.; Perakis, I. E.; Ceccarelli, S.; Lidzey, D. G. *Phys. Rev. B* **2008**, *78*, 045320.
(164) Litinskaya, M.; Reineker, P.; Agranovich, V. M. *J. Lumin.* **2004**, *110*, 364.
(165) Agranovich, V. M. *Theory of Excitons*; Nauka: Moscow, 1968.
(166) Agranovich, V. M.; Toshich, B. S. *Sov. Phys. JETP* **1968**, *26*, 104.
(167) Zoubi, H.; La Rocca, G. C. *Phys. Rev. B* **2005**, *72*, 125306.
(168) Lifshitz, E. M.; Pitaevskii, L. P. *Statistical Physics. Part 2*; Butterworth-Heinemann: Oxford, 1980.
(169) Litinskaya, M. *Phys. Rev. B* **2008**, *77*, 155325.
(170) Ciuti, C.; Savona, V.; Piermarocchi, C.; Quattropani, A.; Schwendimann, P. *Phys. Rev. B* **1998**, *58*, 7926.
(171) Rochat, G.; Ciuti, C.; Savona, V.; Piermarocchi, C.; Quattropani, A.; Schwendimann, P. *Phys. Rev. B* **2000**, *61*, 13856.
(172) Zoubi, H.; La Rocca, G. C. *Phys. Rev. B* **2007**, *76*, 035325.
(173) Agranovich, V. M.; Litinskaia, M.; La Rocca, G. C.; Lidzey, D. G. In *Organic Nanophotonics*; Charra, F., Agranovich, V. M., Kajzar, F., Eds.; Kluwer: Dordrecht, 2003; p 291.
(174) Kena-Cohen, S.; Forrest, S. R. *Nat. Photonics* **2010**, Advance online publication, April 18, 1.
(175) Akselrod, G. M.; Tischler, Y. R.; Young, E. R.; Nocera, D. G.; Bulovic, V. *Phys. Rev. B* **2010**, *82*, 113106.
(176) Goobar, E.; Ram, R. J.; Ko, J.; Björk, G.; Oestreich, M.; Imamoglu, A. *Appl. Phys. Lett.* **1996**, *69*, 3465.
(177) Wainstain, J.; Delalande, C.; Gendt, D.; Voos, M.; Bloch, J.; Thierry-Mieg, V.; Planel, R. *Phys. Rev. B* **1998**, *58*, 7269.
(178) Lidzey, D. G.; Bradley, D. D. C.; Armitage, A.; Walker, S.; Skolnick, M. S. *Science* **2000**, *288*, 1620.
(179) Holmes, R. J.; Kéna-Cohen, S.; Menon, V. M.; Forrest, S. R. *Phys. Rev. B* **2006**, *74*, 235211.
(180) Wenus, J.; Parashkov, R.; Ceccarelli, S.; Brehier, A.; Lauret, J. S.; Skolnick, M. S.; Deleporte, E.; Lidzey, D. G. *Phys. Rev. B* **2006**, *74*, 235212.